UNIVERSITAT POLITÈCNICA DE CATALUNYA BARCELONATECH

Experimental study and numerical modelling of soil-roots hydro-mechanical interaction

Alessandro Fraccica

UNIVERSITAT POLITÈCNICA DE CATALUNYA

Doctoral Thesis

Experimental Study and Numerical Modelling of Soil-Roots Hydro-Mechanical Interactions

Author:

Alessandro Fraccica

Directors:

Enrique Edgar Romero Morales

Thierry Fourcaud

Doctoral programme: Geotechnical Engineering

Department of Civil and Environmental Engineering

December 2019

THÈSE POUR OBTENIR LE GRADE DE DOCTEUR
DE L'UNIVERSITÉ DE MONTPELLIER

En Ecologie fonctionelle

École doctorale GAIA

Unité de recherche AMAP

En partenariat international avec Universitat Politècnica de Catalunya, SPAIN

Experimental Study and Numerical Modelling of Soil-Roots Hydro-Mechanical Interactions

Présentée par Alessandro FRACCICA
Le 09 Décembre 2019

Sous la direction de Thierry FOURCAUD
et Enrique Edgar ROMERO MORALES

Devant le jury composé de

Loïc BRANCHERIAU, Directeur de recherche, Université de Montpellier	Examinateur
Cristina JOMMI, Full professor, TU Delft – Politecnico di Milano	Rapporteur/Examinateur
Evelyne KOLB, Maître de conférences, Sorbonne Université	Examinateur
Alberto LEDESMA VILLALBA, Full professor, Universitat Politècnica de Catalunya	Examinateur
Slobodan MICKOVSKI, Full professor, Glasgow Caledonian University	Rapporteur/Examinateur

UNIVERSITÉ
DE MONTPELLIER

Abstract

The thesis is aimed at characterising the multi-scale and hydro-mechanical behaviour of lightly compacted silty sand penetrated by a turf-grass (Cynodon Dactilon). The study will allow better assessing the impact of vegetation on this compacted soil that has been used in an experimental and fully-instrumented embankment.

The literature agrees that roots are enhancing soil shear strength properties while contrasting results have been found in terms of soil hydraulic behaviour. Moreover, there is a lack of information on how roots affect soil microstructure and its consequences at the macroscopic scale (soil hydraulic behaviour, volume change and shear strength properties).

A protocol for soil compaction and roots growth was followed for preparing all the tested samples. The soil was lightly compacted, wetted under unconfined conditions to favour plant growth, and then dried up to different hydraulic states. The same soil, plant and seeding density used in the monitored embankment were adopted. Several techniques were exploited to characterise roots geometrical and mechanical features.

Large cell triaxial and direct shear tests were performed under saturated and partially saturated conditions. Different stress-strain responses were observed in the vegetated soil at different hydraulic states, due to different roots failure mechanisms and to the combination of water availability and the suction within the soil. Results were interpreted with several constitutive stress expressions for partially saturated soils to consider these state and stress variables. Larger compression deformations on shearing were systematically observed on rooted samples. Roots slightly affected the friction angle but generated an increase in soil cohesion. These observations were confirmed by direct tensile tests performed at different roots growth stages and hydraulic states. A constitutive expression was proposed to predict the increase in cohesion knowing the properties of roots and the soil hydraulic state.

Concerning the hydraulic behaviour, roots induced a systematic increase in soil water-saturated permeability. Water retention properties were also affected, with a decrease in the retention capacity as roots volume increased. Micro-CT tomography and mercury intrusion porosimetry were carried out at different soil hydraulic states on samples including plant individuals to obtain information about changes in soil microstructure. Reconstructed information from the two techniques showed that roots were generally increasing macropores (larger than 100 micrometres) due to fissuring and soil-

root interface phenomena while reducing smaller pores (below 5 micrometres) due to mucilage clogging. The opening of fissures was enhanced on concurrent soil and roots shrinkage upon drying. The alterations generated by roots growth on the soil structure allowed explaining not only the different soil hydraulic responses but also the soil volume change behaviour. A good agreement between the volume of fissures and the volume of roots was found and allowed calibrating and validating a model able to predict the soil water retention properties and permeability values based on the microstructural changes observed.

Results were used to simulate the effect of different periods of plants growth on the hydro-mechanical behaviour of the monitored embankment during a rainfall event. The vegetated slopes remained stable throughout the simulation, even when completely saturated, thanks to the mechanical reinforcement of the roots. Nevertheless, the higher permeability within the vegetated soil had a negative consequence, which was evidenced by a drastic drop in the slope stability safety factor at the early stages of the hydraulic event.

Resumen

La tesis tiene como objetivo caracterizar el comportamiento hidromecánico de una arena limosa compactada y con raíces (*Cynodon Dactilon*). El estudio ha permitido evaluar el impacto de la vegetación en este suelo, que ha sido utilizado en un terraplén experimental.

El estado de arte indica que las raíces mejoran las propiedades de resistencia al corte de un suelo, mientras que hay resultados contrastantes en términos del comportamiento hidráulico. Además, se carece de información sobre cómo las raíces afectan a la microestructura del suelo y sus consecuencias a escala macroscópica.

Se siguió un protocolo para la compactación del suelo y el crecimiento de las raíces para la preparación de todas las muestras estudiadas. El suelo se compactó ligeramente, se humedeció en condiciones no confinadas para favorecer el crecimiento de la planta, y luego se secó a diferentes estados hidráulicos. Se utilizaron varias técnicas para caracterizar las propiedades geométricas y mecánicas de las raíces.

Se realizaron ensayos de corte directo, edométricos y triaxiales con equipos de grandes dimensiones. Se observaron diferentes respuestas de tensión-deformación en el suelo con vegetación debido a los diferentes mecanismos de rotura de las raíces y a la combinación de humedad y de succión en el suelo. Los resultados se interpretaron con leyes constitutivas en términos de tensiones efectivas para suelos parcialmente saturados. En las muestras con raíces se observaron sistemáticamente deformaciones mayores de compresión durante el desarrollo del corte. Las raíces afectaron ligeramente el ángulo de fricción y desarrollaron un aumento en la cohesión del suelo. Estas observaciones también se confirmaron mediante ensayos de tracción, que se realizaron a diferentes estados de crecimiento de las raíces. Se propuso una expresión constitutiva para predecir el aumento de la cohesión en función de las propiedades de las raíces y el estado hidráulico del suelo.

En cuanto al comportamiento hidráulico, las raíces inducen un aumento de la permeabilidad saturada del suelo y una disminución en la capacidad de retención al agua a medida que aumenta el volumen de las raíces en el suelo. Se realizaron ensayos de micro-tomografía de rayos X y de porosimetría de intrusión de mercurio sobre muestras con raíces. La información reconstruida de las dos técnicas ha indicado que las raíces han inducido el aumento de los poros de más de 100 μm debido a la generación de fisuras y a fenómenos de interfase suelo-raíz, a la vez que han ocluido los poros más pequeños (menores de 5 μm) debido a la producción de mucílago. Las fisuras también se han abierto por la

retracción simultánea del suelo y de las raíces durante el secado. Estas alteraciones inducidas sobre la microestructura han permitido explicar mejor los cambios en las propiedades hidráulicas y de cambio de volumen del suelo. Se ha encontrado una relación entre el volumen de fisuras y el volumen de raíces, lo que ha permitido desarrollar y calibrar un modelo capaz de predecir las propiedades de retención al agua y los valores de permeabilidad del suelo.

Los resultados experimentales se han utilizado para simular el efecto que tiene los diferentes crecimientos de las plantas sobre el comportamiento hidromecánico del terraplén instrumentado durante un episodio de lluvia. Los taludes con raíces se mantuvieron estables a lo largo de la simulación, incluso cuando estaban completamente saturados, gracias al refuerzo mecánico de las raíces. Sin embargo, la mayor permeabilidad del suelo vegetado tuvo una consecuencia negativa, que se evidenció con una drástica caída en el factor de seguridad del talud en las primeras etapas del episodio de lluvia.

Resumé

La thèse vise à caractériser le comportement multi-échelles et hydro-mécanique du sable silteux pénétré par des racines de Cynodon Dactilon. L'étude permettra d'évaluer l'impact de la végétation sur ce sol compacté utilisé dans un remblai expérimental en extérieur.

La littérature s'accorde à dire que les racines améliorent les propriétés de résistance au cisaillement du sol, tandis que des résultats contrastés ont été obtenus en ce qui concerne leur effet sur le comportement hydraulique. De plus il existe peu d'information sur la façon dont les racines affectent la microstructure du sol et leurs conséquences à l'échelle macroscopique.

Un protocole de compactage du sol et de croissance de racines a été suivi pour la préparation de tous les échantillons testés. Le sol a été légèrement compacté, mouillé pour favoriser la croissance des plantes, puis séché jusqu'à différents états hydrauliques. Les plantes et la densité d'ensemencement ont été les mêmes que ceux utilisés dans le remblai. Plusieurs techniques ont été exploitées pour évaluer les caractéristiques géométriques et mécaniques des racines.

Des essais de cisaillement triaxial et direct ont été effectués avec des équipements de grande dimension dans des conditions saturées et partiellement saturées. Différentes réponses de contrainte-déformation ont été observées pour le sol végétalisé à différents états hydrauliques, en raison de différents mécanismes de rupture des racines. Les résultats ont été interprétés à l'aide de plusieurs lois de comportement pour les sols partiellement saturés afin de tenir compte des variables d'état et de stress. Des déformations de compression plus importantes lors du cisaillement ont été observées sur des échantillons avec racines. Les racines ont généré une augmentation de la cohésion du sol. Ces observations ont été confirmées par des essais de traction directe effectués à différents stades de croissance des racines. Une loi de comportement a été proposée pour prédire l'augmentation de la cohésion en connaissant les propriétés des racines et l'état hydraulique du sol.

En ce qui concerne le comportement hydraulique, les racines ont induit une augmentation de la perméabilité saturée en eau du sol et une diminution de la capacité de rétention à mesure que le volume des racines augmentait. La tomographie microCT et la porosimétrie par intrusion de mercure ont été effectuées à différents états hydrauliques du sol sur des échantillons avec racines pour obtenir des informations sur les changements de la microstructure du sol. L'information reconstruite à partir des deux techniques a montré que les racines augmentaient généralement les macropores (plus de 100 micromètres) en raison de phénomènes de fissuration et des interfaces sol-racine tout en réduisant les

pores plus petits (moins de 5 micromètres) en raison du colmatage dû au mucilage. L'ouverture des fissures a été augmentée par le retrait simultané du sol et des racines lors du séchage. Les altérations générées par la croissance des racines sur la structure du sol ont permis d'expliquer les différentes réponses hydrauliques du sol et aussi son changement de volume. Un bon accord entre le volume des fissures et le volume des racines a été trouvé et a permis de calibrer et de valider un modèle capable de prédire les propriétés de rétention d'eau et les valeurs de perméabilité du sol à partir des changements microstructurels observés.

Les résultats ont été utilisés pour simuler l'effet de différentes périodes de croissance des plantes sur le comportement hydro-mécanique du remblai lors d'une chute de pluie. Les pentes végétalisées sont restées stables tout au long de la simulation, même complètement saturées, grâce au renforcement mécanique des racines. Néanmoins, la perméabilité plus élevée dans le sol végétalisé a eu une conséquence négative, qui a été mise en évidence par une baisse drastique du facteur de sécurité de stabilité de la pente aux premiers stades de l'événement hydraulique.

Acknowledgments

I want to express my thankfulness to my thesis directors, Enrique Romero and Thierry Fourcaud, for the great chance they gave me to collaborate with them on this fascinating project.

I thank Enrique, for patiently guiding me through the proactive and exciting world of UPC's geotechnical laboratory, for listening to and discussing ideas anywhere or during a walk, to strengthen my knowledge on soil mechanics and all equipment made and to be invented for carrying out experiments. I thank him also to always give me support (*No pasa nada, tranquilo!*), to get me involved in his countless projects and presentations, and for making me indirectly learn and love Spanish (*Ya me dirás!*).

I thank Thierry for encouraging me to give the best of myself, even at a distance, to inspire me with his enthusiasm in the discovery and deepening of phenomena involving the growth and development of plants, to give me valuable observations on the work done and on the ideas to develop to meet the thesis objectives. I thank him also for his patience in “waiting for me” and for his welcome in Montpellier, for his greetings at the end of the day and for his humour (*Ton article est nul! Non, je rigole!*).

It was an honour to collaborate and discuss ideas and results with all the members of SMuCPhy Project: Raul Oorthuis, Marcel Hurlimann, Antonio Lloret, Jean Vaunat, Jose Moya and Càrol Puig-Polo. I have been given the opportunity to experience in the field what has been observed in the laboratory, to have other points of view on my results, to have support and awareness of the applicability of my thesis work.

A special mention should be made to my office colleagues: Agustín Cuadrado, Stefano Collico, Lluís Monforte and Erdem Toprak. All hard-working people, who don't waste time looking at what's outside the window.

It was a pleasure to interact with the other researchers and staff in the TERRE Project. The critical eye of numerous international experts in the geotechnical field, together with the friendship of the other doctoral students has made this experience unforgettable.

I thank all my colleagues and friends at the UPC for the short but intense moments of break and for sharing their ideas and knowledge: Oriol, Arisleidy, Núria, Rodrigo, Luis, Clara, Fernando, Alejandra, Michela, Riccardo, Gaia, Ferran, Ningning, Gerard, Fabiola, Christina, Miky, Lu, Laura, Jattna, Jackson, Saeed, David. I also thank Luis Gandarillas, with whom I've had the opportunity to

collaborate on lab tests included in this thesis and Vito Tagarelli, with whom there have been many fruitful discussions

I thank my friends and colleagues in AMAP, for their time to discuss about funny and useful stuff about plants, trips, food, culture, bureaucracy: Sofia, Roberta, Lorenzo, Jean-François, Hervé, Mao, Nora, Nathalie, Miléna, Nicolas, Gilles, Ghislain.

I acknowledge the precious work of the technicians, from Barcelona and Montpellier's lab: Rodrigo Gómez, José Alvarez, Tomás Perez, Mercedes Sondon, Markos Dueñas, Stéphane Fourtier.

Both in Barcelona and Montpellier, I've met a lot of people who haven't made me feel alone: Christian, Marc, Jack, James, Joan, Pol, Pau, David, John, Gerard, Claudia, Jordi, Nico, Lucia, Bea, Valeria, Francesca, Fadel, Giulio, Mattia, Sara, Carolina, Steve, Martina. Thanks for the laughter, the adventures, the football games and the evenings spent together: they were my energy to continue working on this thesis.

I want to thank my family at this point, for having always been close to me, even at a distance, with a video call, a message. For all the "welcome back" and "goodbye" received in these years. For soccer matches organized by the brothers or the best dishes prepared by grandmothers or mother when I came home.

Finally, I want to thank my girlfriend Lucy, for giving me support and understanding my moods even via messages, for enduring my absences and postponed returns because of complicated work periods or tests to do.

All mentioned people contributed to keep my mood up, to carry out a job that sometimes requires a huge psychological effort.

Table of contents

1. Introduction and objectives

This thesis has received support by the European Commission via the Marie Skłodowska-Curie Innovative Training Networks (ITN-ETN) project TERRE 'Training Engineers and Researchers to Rethink geotechnical Engineering for a low carbon future' (H2020-MSCA-ITN-2015-675762).

1.1 Introduction

Global warming and the approach of many countries towards ways of environmentally sustainable development are bringing new challenges to engineers. In the field of geotechnical engineering, for example, global warming and climate change are contributing to increase landslides and erosion phenomena, stemming from isolated and very intense rainfall events followed by long periods of drought. A possible environmentally sustainable solution from a geotechnical viewpoint is to counteract these phenomena, which may cause significant socio-economic losses, by studying the effects of roots of special plants on the global soil hydro-mechanical behaviour.

To date, most of the earthworks (railway and motorway embankments, canals, flooding protection structures, ...) are mainly covered and penetrated by vegetation. However, there are no specific regulations that guide consulting companies and contractors in the process of construction, maintenance and prediction of the overall response of the work when interacting with atmosphere and vegetation. As a result, the (positive and negative) effects of vegetation are often neglected at the design stage of these works because they are difficult to predict. In this sense, scientific research is required to adopt protocols, advanced methodologies and to produce databases and models that allow characterizing and interpreting the effects of roots on soil geotechnical properties necessary for design, for both ultimate and serviceability limit states.

Many experimental studies on soil-root interactions agree on the fact that plants are enhancing soil mechanical properties (e.g., shear strength). Nevertheless, protocols observed in literature for preparing and testing samples are often deeply different and conflicting with each other. So far, the most commonly used technique to quantify roots reinforcement of soil is the direct shear test (Ghestem, Veylon, Bernard, Vanel, & Stokes, 2014; Gonzalez-Ollauri & Mickovski, 2017; Mickovski et al., 2009; Veylon, Ghestem, Stokes, & Bernard, 2015; Yildiz, Graf, Rickli, & Springman, 2018). Large shear boxes are commonly adopted for laboratory and in-situ investigations, to test representative element volumes of vegetated soils. In most investigations, these tests are carried

out under conditions of total soil saturation and observing the effects of different types of plants and different roots spatial disposition on soil response in terms of shear stress evolution and displacements. These studies have given an insight into the characteristics of the roots that most influenced the response of the soil (roots tensile strength, diameter size, root length and area density). The main limitation of this equipment arises from the small horizontal displacements often allowed: this causes roots partial extension and therefore, partial exploitation of their tensile strength. Moreover, large equipment often needs to be deeply adapted to test vegetated soil under its corresponding low confinement stress level (typical of shallow ground depths). Few investigations focused on the combined effects of suction and roots on soil hydro-mechanical behaviour: partial saturation may affect the mechanical characteristics of roots and soil structure and consequently influence reinforcement's efficiency. Indeed, (Gonzalez-Ollauri & Mickovski, 2017) performed tests at different hydraulic states and observed a very small increase in shear strength for a vegetated soil at high value of suction, compared to bare soil at the same condition. In mechanical tests described in literature, roots effects on volumetric deformations upon shearing and/or loading have been generally neglected, resulting in an important lack of knowledge. Moreover, there is still not a clear insight on how soil hydro-mechanical response observed at the phenomenological scale could be linked to soil micro-structural changes generated by roots growth, even if some recent studies point in that direction (Anselmucci et al., 2019; Fraccica, Romero, & Fourcaud, 2019; Koebernick et al., 2017; Kolb, Hartmann, & Genet, 2012; Scholl et al., 2014a).

Concerning soil hydraulic response, investigations carried out on vegetated soils presented different and counterposed results. Soil water-saturated permeability was enhanced by roots (Scholl et al., 2014a; Smethurst, Clarke, & Powrie, 2012; Vergani & Graf, 2016), whereas plants effects on soil's water retention capacity were found to vary according to the type of soil, its compaction dry density, the type of roots and the chemical interactions between soil and plants (Karup, Moldrup, Tuller, Arthur, & de Jonge, 2017; Ng, Leung, & Woon, 2014; Ni, Leung, & Ng, 2019a; Ohu, Raghavan, Prasher, & Mehuys, 1987; Pagano, Reder, & Rianna, 2019; Read et al., 2003). In this regards, geotechnical and agronomic investigations seem to focus on different phenomena involved in the problem: mechanic aspects (fissuring, void ratio increase, clogging of pores, …) for the former and chemical effects (organic matter/mucilage production) for the latter. Both fields of study bring interesting results to the study of the hydraulic effects of plants on soil: what is missing is a framework that can integrate different points of view and couple all relevant observed phenomena.

All the above aspects must be considered together when simulating the behaviour of a geotechnical earth structure, especially if it is covered by vegetation. Indeed, we know from the principles of geotechnics that the hydraulic state of soil has a great influence on its mechanical behaviour. We also

know that the condition of total saturation is the most critical, all other variables being equal, in most of geotechnical problems. Nevertheless, for a geotechnical work subject to ground-atmosphere interaction, it is important to consider the transition from partially to totally saturated soil.

1.2 Objectives

The aim of the thesis is to achieve an important advance in the state-of-the-art knowledge of the hydro-mechanical behaviour of partially saturated compacted soils with roots within an eminently experimental framework and with analyses at different scales (microstructural and phenomenological). The protocols and the results have been produced, in the thesis, in such a way as to be a useful tool in the assessment of slopes stability with vegetated soil subjected to ground-atmosphere interactions, as well as in projects involving the use of materials in which roots may grow. Specifically, the results have made it possible to identify the main positive and negative aspects of the use of plants in geotechnical engineering problems. The thesis work has been organised in such a way as to achieve the following objectives:

- Execution of a hydro-mechanical testing program on partially saturated soils with roots (large size triaxial, direct shearand oedometers; water retention tests; permeability; direct tensile tests).
- Study of the effect of different roots quantities and plants growing periods on soil response at different scales.
- Experimental characterization of roots main features that should be included in constitutive laws for predicting their reinforcement in partially saturated soils.
- Development of a constitutive model to predict water retention curves of double-porosity vegetated soils.
- Use of the experimental data to compare the hydro-mechanical response of a bare and a vegetated soil slope subject to changes in water content.

1.3 Thesis content

The thesis has been organised in an introduction, four main chapters and conclusions. Main chapters have been prepared in the form of scientific articles.

In the **introduction**, a general state of the art about techniques and results obtained during different investigations on soil-roots interactions and from different scientific fields are presented. From literature review, the objectives of the thesis will be defined, aiming at:

- comparing results obtained, within this thesis, on roots effects on soil hydro-mechanical behaviour at the phenomenological scale, with observations coming from other authors;
- defining the missing or the unclear points in a vegetated soil's geotechnical characterization and to assess them;
- assessing the causes of sometimes-contrasting literature results presented by assessing phenomena occurring at soil micro-scale that were partially or completely unexplored/unquantified;
- understanding which are the most important plant features, from an engineering point of view, to consider when assessing soil hydro-mechanical response after their growth;
- implementing plant characteristics in well-established constitutive laws for bare soil, to predict its response when vegetated;
- bringing a new point of view to the numerical modelling of a possible engineering application, based on the laboratory results obtained.

In **chapter 2,** a multi-scale experimental program and its results are presented on the hydraulic behaviour of a vegetated compacted soil. Standard geotechnical tests were carried out with repetitions, to assess the global hydraulic response. Furthermore, two advanced and complementary techniques were adopted to investigate the causes of the previous observations and to correlate them to the presence of roots. Two main effects of plants on soil structure were observed: fissures generation and pores clogging. Roots geometrical features linked to these effects were carefully characterized and cross-validated through different techniques. The quantification of these two phenomena helped to interpret laboratory results obtained in this chapter and in the following ones, as well as to justify choices made in the building of a numerical model for the simulation of an earth embankment covered with vegetation.

In **chapter 3,** information was gathered from results obtained at soil-microscale presented in the previous chapter. A good correlation was found between some root traits and the volume of fissures generated by plant development. This correlation was used to implement a constitutive model for double-porosity soils to predict changes in soil water retention and permeability due to root penetration in the matrix. The model was then validated by predicting retention and hydraulic conductivity measurements presented in chapter 1. The quantification of several plant traits observed in laboratory samples will aid to extend the model to other types of plants and soils.

In **chapter 4,** different techniques were adopted to assess shear strength and volume change behaviour of a vegetated soil at different hydraulic states. Different plant growing periods were defined to

investigate their effects on soil response. Results were interpreted using constitutive laws for partially saturated soils with strongly coupled hydro-mechanical response. A net increase in soil shear strength was observed as the quantity of roots in soil was rising. However, some aspects of the general mechanical response of the vegetated soil revealed a clear dependence on root-generated changes in soil structure.

In **chapter 5,** results coming from the whole geotechnical characterization presented in the thesis were used to simulate the response of a full-scale embankment covered by plants at different growth stages. After representing the natural condition of the earth structure (partially saturated soil), wetting was imposed. Slope minimum safety factor was then evaluated after different wetting steps and up to complete soil saturation. As expected, vegetated slopes were safe throughout the simulation whereas failure was predicted in the bare slope. Nevertheless, the vegetated soil hydraulic behaviour observed in laboratory has manifested its negative effect on the stability of the vegetated slopes, along the first stages of the simulation.

Finally, **chapter 6** contains the main conclusions of the work carried out, as well as future research proposals.

1.4 Workshops and conference presentations:

The thesis has resulted in several contributions to different international conferences and workshops:

- Fraccica A., Romero E. and Fourcaud T. 2019. Multi-scale effects on the hydraulic behaviour of a root-permeated and compacted soil. IS-GLASGOW 2019, Glasgow 26-28/06/2019. E3S Web of Conferences, 92, 12014.
- Fraccica A., Romero E. and Fourcaud T. 2019. Hydro-mechanical response of bare and root-permeated soil slopes to rainfall: from a multi-scale laboratory research to modelling. MUSLOC, Barcelona 19-20/09/2019.
- Fraccica A., Romero E. and Fourcaud T. 2019. Multi-scale observations on a root-permeated compacted soil at different hydraulic states. ALERT Workshop, Aussois 01/10/2019.
- Fraccica A., Romero E., Fourcaud T. and Gandarillas L. 2019. A new equipment for assessing vegetated and compacted soil tensile strength. Accepted E-UNSAT 2020.

1.5 Publications in ranked scientific journals

- Oorthuis R., Hurlimann M., Fraccica A., Lloret A., Moya J., Puig-Polo C. and Vaunat J. 2018. Monitoring of a full-scale embankment experiment regarding soil-vegetation-atmosphere interactions. Water ,10 (6) 688.
- Fraccica A., Romero E. and Fourcaud T. Effects of plant root growth on soil microstructure and hydro-mechanical behaviour. Acta Geotechnica. In preparation.
- Fraccica A., Romero E. and Fourcaud, T. Hydro-mechanical framework to predict roots effects on a compacted silty soil. Géotechnique Letters. In preparation.
- Fraccica A., Romero E. and Fourcaud, T 2019. Mechanical behaviour of a vegetated soil at different hydraulic states. Acta Geotechnica. In preparation.

References

Anselmucci, F., Andó, E., Sibille, L., Lenoir, N., Peyroux, R., Arson, C., … Bengough, A. G. (2019). Root-reinforced sand : kinematic response of the soil. In A. Tarantino & E. Ibraim (Eds.), *IS-Glasgow* (Vol. 92, p. 12011). https://doi.org/doi.org/10.1051/e3sconf/20199212011

Fraccica, A., Romero, E., & Fourcaud, T. (2019). Multi-scale effects on the hydraulic behaviour of a root-permeated and compacted soil. In A. Tarantino & E. Ibraim (Eds.), *IS-Glasgow* (p. 12014). https://doi.org/doi.org/10.1051/e3sconf/20199212014

Ghestem, M., Veylon, G., Bernard, A., Vanel, Q., & Stokes, A. (2014). Influence of plant root system morphology and architectural traits on soil shear resistance. *Plant and Soil*, *377*(1–2), 43–61. https://doi.org/10.1007/s11104-012-1572-1

Gonzalez-Ollauri, A., & Mickovski, S. (2017). Plant-soil reinforcement response under different soil hydrological regimes. *Geoderma*, *285*, 141–150. https://doi.org/10.1016/j.geoderma.2016.10.002

Karup, D., Moldrup, P., Tuller, M., Arthur, E., & de Jonge, L. W. (2017). Prediction of the soil water retention curve for structured soil from saturation to oven-dryness. *European Journal of Soil Science*, *68*, 57–65. https://doi.org/10.1111/ejss.12401

Koebernick, N., Daly, K. R., Keyes, S. D., George, T. S., Brown, L. K., Raffan, A., … Roose, T. (2017). High-resolution synchrotron imaging shows that root hairs influence rhizosphere soil structure formation. *New Phytologist*, *216*, 124–135. https://doi.org/10.1111/nph.14705

Kolb, E., Hartmann, C., & Genet, P. (2012). Radial force development during root growth measured by photoelasticity. *Plant and Soil*, *360*, 19–35. https://doi.org/10.1007/s11104-012-1316-2

Mickovski, S., Hallett, P. D., Bransby, M. F., Davies, M. C. R., Sonnenberg, R., & Bengough, A. G. (2009). Mechanical Reinforcement of Soil by Willow Roots: Impacts of Root Properties and Root Failure Mechanism. *Soil Science Society of America Journal*, *73*(4), 1276–1285. https://doi.org/10.2136/sssaj2008.0172

Ng, C. W. W., Leung, A. K., & Woon, K. X. (2014). Effects of soil density on grass-induced suction distributions in compacted soil subjected to rainfall. *Canadian Geotechnical Journal*, *51*(3), 311–321. https://doi.org/10.1139/cgj-2013-0221

Ni, J. J., Leung, A. K., & Ng, C. W. W. (2019). Modelling effects of root growth and decay on soil water retention and permeability. *Canadian Geotechnical Journal*, *56*, 1049–1055.

Ohu, J. O., Raghavan, G. S. V., Prasher, S., & Mehuys, G. (1987). Prediction of water retention characteristics from soil compaction data and organic matter content. *Journal of Agricultural Engineering Research*, *38*(1), 27–35. https://doi.org/10.1016/0021-8634(87)90136-3

Pagano, L., Reder, A., & Rianna, G. (2019). The effects of vegetation on the hydrological response of silty volcanic covers. *Canadian Geotechnical Journal*, *56*(9), 1261–1277. https://doi.org/10.1139/cgj-2017-0625

Read, D. B., Bengough, A. G., Gregory, P. J., Crawford, J. W., Robinson, D., Scrimgeour, C. M., … Zhang, X. (2003). Plant roots release phospholipid surfactants that modify the physical and chemical properties of soil. *New Phytologist*, *157*, 315–326. https://doi.org/doi.org/10.1046/j.1469-8137.2003.00665.x

Scholl, P., Leitner, D., Kammerer, G., Loiskandl, W., Kaul, H. P., & Bodner, G. (2014). Root induced changes of effective 1D hydraulic properties in a soil column. *Plant and Soil*, *381*(1–2), 193–213. https://doi.org/10.1007/s11104-014-2121-x

Smethurst, J. A., Clarke, D., & Powrie, W. (2012). Factors controlling the seasonal variation in soil water content and pore water pressures within a lightly vegetated clay slope. *Géotechnique*, *62*(5), 429–446. https://doi.org/10.1680/geot.10.P.097

Vergani, C., & Graf, F. (2016). Soil permeability, aggregate stability and root growth: a pot experiment from a soil bioengineering perspective. *Ecohydrology*, *9*(5), 830–842. https://doi.org/10.1002/eco.1686

Veylon, G., Ghestem, M., Stokes, A., & Bernard, A. (2015). Quantification of mechanical and hydric components of soil reinforcement by plant roots. *Can. Geotech. J.*, *52*, 1839–1849.

Yildiz, A., Graf, F., Rickli, C., & Springman, S. M. (2018). Determination of the shearing behaviour of root-permeated soils with a large-scale direct shear apparatus. *Catena*, *166*, 98–113. https://doi.org/10.1016/j.catena.2018.03.022

2. Effects of plant growth on soil microstructure and hydro-mechanical behaviour

2.1 Abstract

Background. Many studies on soil-root interactions agree on the fact that plants are enhancing soil mechanical properties (e.g., shear strength). Concerning hydraulic aspects, observations performed on different and unrelated phenomena and scales are evidencing counterposed results. Macroscopic features of vegetated soils are rarely linked to soil-root interactions at the microscale which, in addition, have only been described qualitatively.

Scope. The current study is aimed at assessing and correlating the effects induced by roots on soil hydro-mechanical behaviour and microstructure, at different and hydraulic states. Consequences of soil water availability and suction on roots features will be also evaluated. Experiments were carried out on a compacted silty sand seeded with *Cynodon Dactilon* (turfgrass). Net changes were observed comparing bare and vegetated soil's response in terms of water saturated soil permeability, water retention and soil shrinkage upon drying. They were difficult to interpret at the laboratory specimen's scale. X-ray microtomography and mercury intrusion porosimetry were then used to quantify soil fabric changes at the soil-roots interface and at the clay aggregates scale.

Conclusion. The effects of roots on the soil multi-modal pore size distribution were dramatic and caused by multi-physics phenomena: fissures generation and widening, soil and roots shrinkage, voids clogging and soil aggregation. The characterization of these phenomena was used to represent, qualitatively and quantitatively, the vegetated soil behaviour observed at the macro-scale. Measured root geometrical features allowed to correlate the different scales involved in the experiments.

2.2 Introduction

Many investigations have focused on the effect of plants on the hydraulic properties of soils. (Smethurst et al., 2012) found an increase of permeability within clay embankments due to plants; (Ng et al., 2014) showed that clayey soils compacted at different dry densities have contrasting retention behaviours when permeated by roots while (Pagano et al., 2019) did not observe relevant

effects of plants in a high porosity silty soil. (Vergani & Graf, 2016) showed that vegetation could either increase or decrease the saturated permeability depending on the growth stage. (Ng, Ni, Leung, & Wang, 2016) proposed a model dependent on a root geometrical parameter to consider pores clogging and its hydraulic consequences on soil while (Ni, Leung, & Ng, 2019b) analysed the impact of plants growth and decay.

The above-mentioned authors performed observations at the specimen and slope scale. Some of them empirically correlated macroscopic evidences (air-entry value - permeability change) to roots geometrical traits and soil initial compaction state, by means of realistic but undemonstrated theories (void ratio alteration, soil fissuring etc.). In fact, there are few studies on roots effects at the pore-scale: among them, (Scholl et al., 2014b) deduced the effects of roots on the pore size distributions of a fine-grained soil by an inverse estimation while (Koebernick et al., 2017) performed high-resolution X-ray micro-tomography on a loose silty sand, focusing on a single soil-root interface. The latter estimated a general decrease in porosities between 5 and 300 μm due to a compaction process triggered by roots diameter enlargement against the soil interface, and a minor porosity generation due to *root hairs* (root protuberances with a few microns diameter). Nevertheless, the investigated range of porosity was too narrow, and information was missing at the root system scale and at the aggregation level. X-ray micro-tomography was also used by (Soriano et al., 2017) and (Anselmucci et al., 2019). The former built porosity distributions in a soil with fibres, finding an increase of void volume close to them. The latter computed sand grains kinematics due to plant growth, showing important displacements in roots vicinity. Forces exerted due to root growth were measured by (Kolb et al., 2012) as function of the crossed gap between photo-elastic grains.

Agronomic literature is focusing more on chemical interactions between roots and soils fabric, which are indirectly affecting soil macroscopic hydraulic behaviour ((Hinsinger, Bengough, Vetterlein, & Young, 2009; Karup et al., 2017; Moradi et al., 2011; Ohu et al., 1987; Watt, Silk, & Passioura, 2006)). Indeed, polymeric substances produced by roots (mucilage) modify significantly the chemo-physical properties of the soil by reducing the water surface tension, clogging pores, opening fissures and forming and stabilizing aggregates ((Carminati et al., 2010; Read et al., 2003)). Mucilage facilitates water and nutrients uptake from the surfaces of the soil aggregates ((Tinker & Nye, 2000)) and keeps roots strongly bound to solid grains as the soil dries out ((Watt, McCully, & Canny, 1994)). Finally, (Carminati et al., 2013) and (Liu, Zhang, Wang, Cai, & Chang, 2015) observed roots shrinkage upon drying causing gaps opening at the root-soil interface. These microscopic phenomena are often qualitatively described or analysed in a decoupled way with the macro-scale behaviour and soil properties. Considering all this knowledge, the present study aims at investigating jointly the chemical-hydro-mechanical effects that roots have at different scales on soil and the influence that

soil hydro-mechanical states has on microstructure and plants physiology. All these interactions play a role on the resulting soil behaviour: thus, the necessity to consider them in the same framework.

2.3 Soil properties and initial state

The tested silty sand was retrieved in the Llobregat river's delta (Barcelona, Spain). Its grain-size distribution is presented in Figure 1 jointly with the curve obtained for the same material after sieving at 9.5 mm. Further details on soil main physical properties are presented in Table 1.

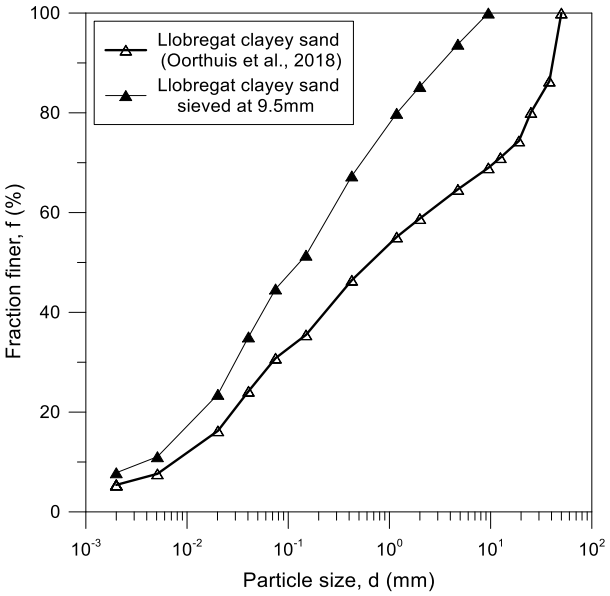

Figure 1 Particle-size distribution for the soil tested in the present study (sieved Llobregat silty sand) and as-retrieved ((Oorthuis et al., 2018)*).*

Table 1 Main soil physical properties and as-compacted state.

Soil properties / as-compacted state	**Value**
Soil fraction < 2 mm (%)	58.8[b]
Soil fraction < 75 μm (%)	30.8[b]
Soil fraction < 2 μm (%)	5.4[b]
Liquid limit (%)	29.5-34.4[a]
Plasticity index (%)	9.6-13.5[a]
Density of solids, ρ_s (Mg/m^3)	2.65-2.70[a]
Gravimetric water content, w (%)	15[+b]
Water ratio, $e_w = \rho_s w/\rho_w$ (-)	0.40[+b]
Void ratio, e (-)	0.67[+b]
Matric suction, s (kPa)	40[+b]
Max compaction vertical load, $\sigma_{v,0}$ (kPa)	100±2[+b]

[a] (Oorthuis et al., 2018) [b] (Fraccica et al., 2019) [+] *As-compacted state*

Soil was statically compacted in PVC cylindrical pots (150 mm in diameter, 70 mm high). To allow fast plant germination, specimens were prepared dry of the optimum of a low-energy dynamic compaction curve (with energy between 120 and 240 kJ/m^3) (point *A* in Figure 2). The initial state and stress variables are summarised in Table 1. After compaction, some pots were seeded with *Cynodon Dactilon* (plant spacing = 50 mm, seeding density = 34 g/m^2), a plant already investigated by several authors for geotechnical purposes (Chen, Zhang, Zhang, & Wang, 2015; Garg, Coo, & Ng, 2015; Leung, Garg, Coo, Ng, & Hau, 2015); (Fraccica et al., 2019). All the pots were watered under unconfined conditions up to a water content of w = 21% to allow plants development (point B in Figure 2). Soil volume change on wetting was not observed and considered as negligible. Roots growth lasted 3 months, until they reached the bottom of the pots (70 mm below the soil surface). After roots establishment, specimens were subjected to air-drying, at zero vertical stress, to be tested when reaching intermediate points between *B* and *C* in Figure 2. Bare soil samples were prepared following the same path.

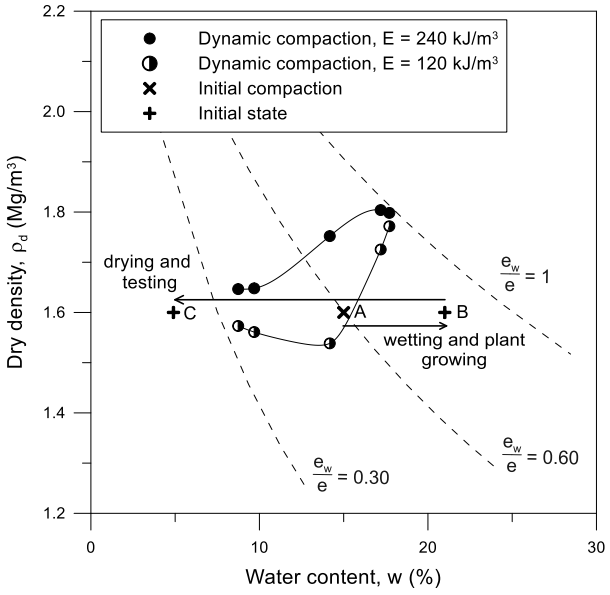

Figure 2 Initial state of compaction for samples tested (point A), and low-energy compaction curves. Hydraulic path followed after compaction: wetting (from A to B), plant growing and drying (from B towards C) prior to test.

2.4 Roots volume and structural features

Roots volume is, for this study, a fundamental parameter to understand the hydro-mechanical behaviour of a granular medium, in which the size and the volume of pores play a major role. Thus, it was necessary to evaluate this structural root trait by destructive and non-destructive techniques, during and after other geotechnical tests. Moreover, roots volume will be used to compute the resulting void ratio within the soil according to the scheme showed in Figure 3a and as $e = V_{voids}/V_{solid}$: this assumption leads to considering roots neither as solid phase nor void phase.

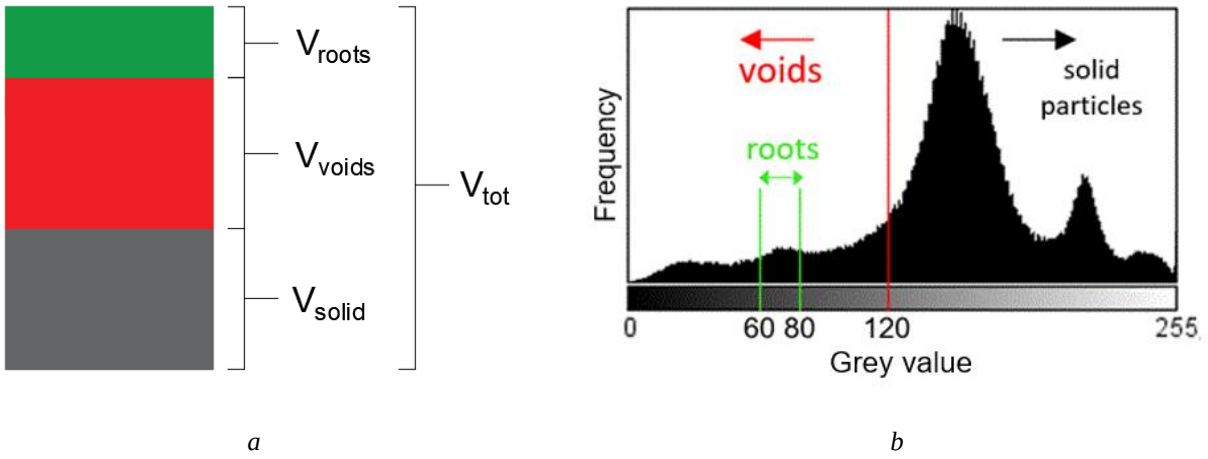

a *b*

Figure 3 a) Scheme of the phases considered in the root-permeated soil (re-adapted from (Wood, Diambra, & Ibraim, 2016)*) b) 8 bit stack histogram of the region of interest, with threshold values considered to distinguish the desired phases.*

2.4.1 X-ray microtomography

X-ray microtomography scans were carried out on two bare and five vegetated soil's samples (Figure 12b), each one containing an individual of *Cynodon Dactilon*. Samples were extracted from pots when the soil was at different states (Table 2). They were scanned by X-ray micro-tomography (MicroCT V|Tome|X s 240, GE Sensing & Inspection Technologies GmbH, Germany). Cone-beam CT scans at 170 kVp / 250 mA were used to reconstruct 2024x2024 pixels, 16 bits image stacks with an isometric voxel size equal to 36 μm. A calibration of bulk density *vs* grey values of air and aluminium allowed determining a density resolution of 0.030 Mg/m^3.

Table 2 Testing state for X-ray micro-CT and Mercury Intrusion Porosimetry samples

Soil initial state	**VEG 1**	**VEG 2**	**VEG 3**	**VEG 4**	**VEG 5**	**BARE 1**	**BARE 2**
Gravimetric water content, w (%)	12	5	13	22	18	12	23.5
Water ratio, $e_w = \rho_s w/\rho_w$ (-)	0.32	0.13	0.36	0.60	0.47	0.33	0.63
Matric suction, s (kPa)	120	1000	40	0.5	3	110	0.3

Image processing was done by *ImageJ* (Fiji) ((Schindelin et al., 2012)). For the treatment, stacks were scaled to an 8 bits format. A region of interest (*ROI*) was defined within the specimen to avoid samples irregularity. From the grey value histogram (Figure 3b) of the original image stack (Figure 4a) it was possible to identify the grey intensity peak mainly corresponding to the roots and to isolate them by a threshold between 60 and 80 (Figure 4b). These values were confirmed by calculating the CT grey value according to the equation:

$$CT_{gray\ val.} = 1000 * \left[1 + \left(\frac{\mu_t - \mu_w}{\mu_w}\right)\right] \quad (1)$$

The equation provided CT gray values for 12-bits images which were then scaled to 8-bit images grayscale. Parameters μ_w and μ_t are, respectively, the linear attenuation coefficients of the water and of the matter of which the roots are composed (water, cellulose and lignin). These coefficients were found on the XCOM database managed by The National Institute of Standards and Technology (NIST) (Berger et al., 2010). The CT values were calculated by the attenuation coefficients also for air and typical soil minerals, for comparison (Table 3).

Table 3 Linear attenuation coefficients for the average energy used in the X-ray tomography, CT gray values calculated for 12-bits and 8-bits scales

Material	**Linear Attenuation Coefficient at 170 kVp (mm^{-1})**	**$CT_{gray\ val.}$ (-) (12-bit scale)**	**$CT_{gray\ val.}$ (-) (8-bit scale)**
Air	$1.63*10^{-3}$ (*)	1.08	0.07
Water	1.51 (*)	1000.00	62.26
Cellulose	2.03 (*)	1324.50	82.46
Lignin	1.80 (*)	1192.05	74.21
Kaolinite	3.03 (*)	2006.62	124.92
Calcite	4.02 (*)	2662.25	165.74
Quartz	3.72 (*)	2463.58	153.37

(*) (Berger et al., 2010)

The binarized stack was treated with the *Local Thickness* plugin (Figure 4c) (B. Dougherty (Optinav, USA)) to remove noise and pores' borders with thickness below 4 pixels (Figure 4d). Finally, roots volume was estimated in *ImageJ* by the plugin *MorphoLibJ* ((Legland, Arganda-Carreras, & Andrey, 2016)).

2.4.2 Pycnometry and WinRHIZO scans

After the laboratory tests later described, soil was washed away to retrieve the plants individuals. Roots were placed in a pycnometer (Figure 5a), already filled with 100 mL of distilled water. The system was vibrated for 30 minutes to let the air bubbles come up and then, the water raised beyond the control line, due to roots immersion, was extracted with a pipette with a capacity of 0.01 mL and was assumed as roots volume.

After pycnometry, the same roots were scanned and analysed with the commercial software WinRHIZO (Regent Instruments Inc., Quebec, Canada). The software can capture and binarize images (Figure 5b) to evaluate root diameters (as projected area per length) and total length.

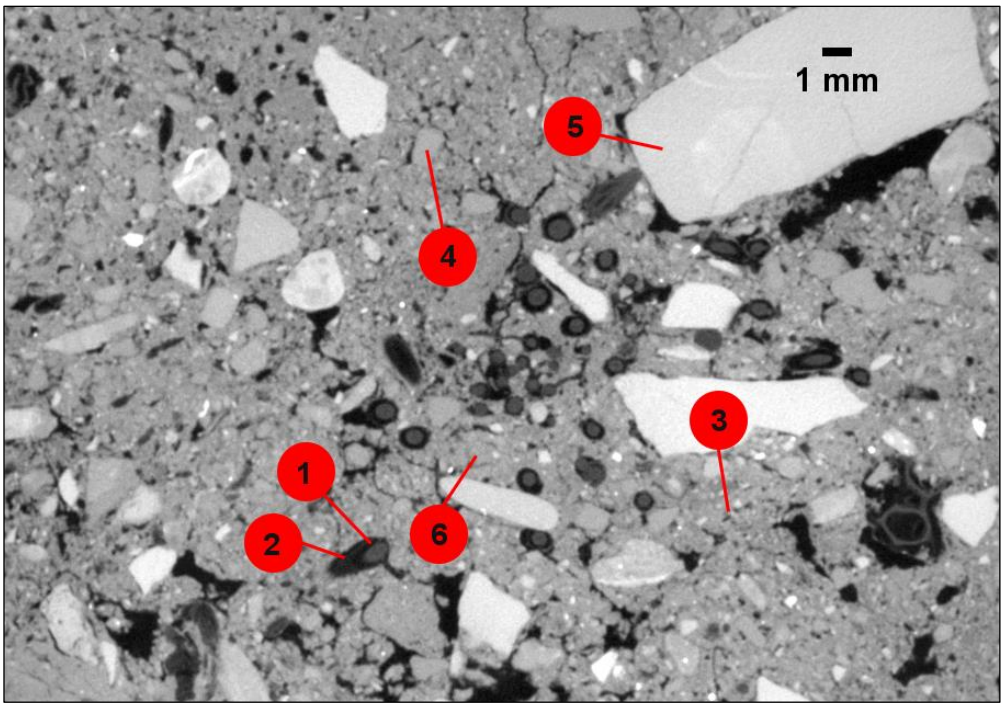

1: root section

2: fissure generated by root growth

3: pre-existing pores

4: sand grain

5: gravel

6: silty and clayey matrix

a

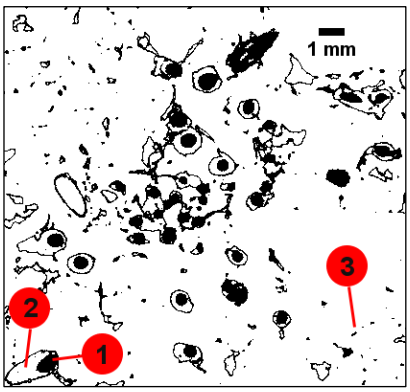

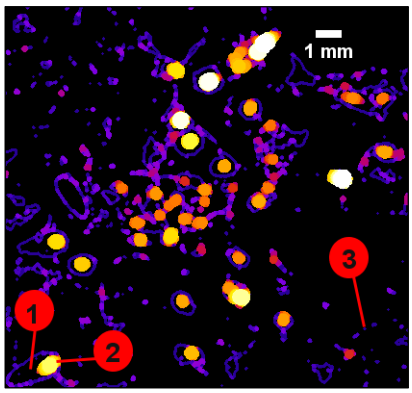

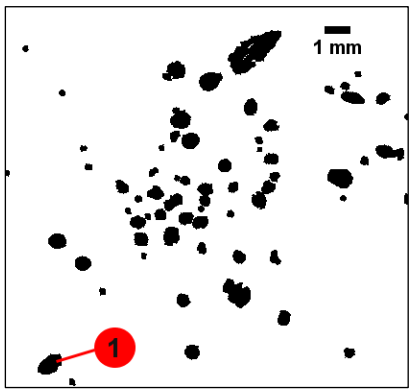

b *c* *d*

Figure 4 a) region of interest (ROI) considered within the image stack to assess roots volume and pore-size distributions b) image threshold between 60 and 80 to isolate roots: fissures and pores boundaries are still visible c) local thickness assessment to filter the roots map d) roots phase completely isolated from other soil elements.

Given the root length (L_i) for each root diameter class (D_i), the total root volume (V) is then estimated by summing up the partial values (V_i), according to the formula:

$$V = \sum_i V_i = \sum_i \pi \frac{D_i^2}{4} L_i \qquad (2)$$

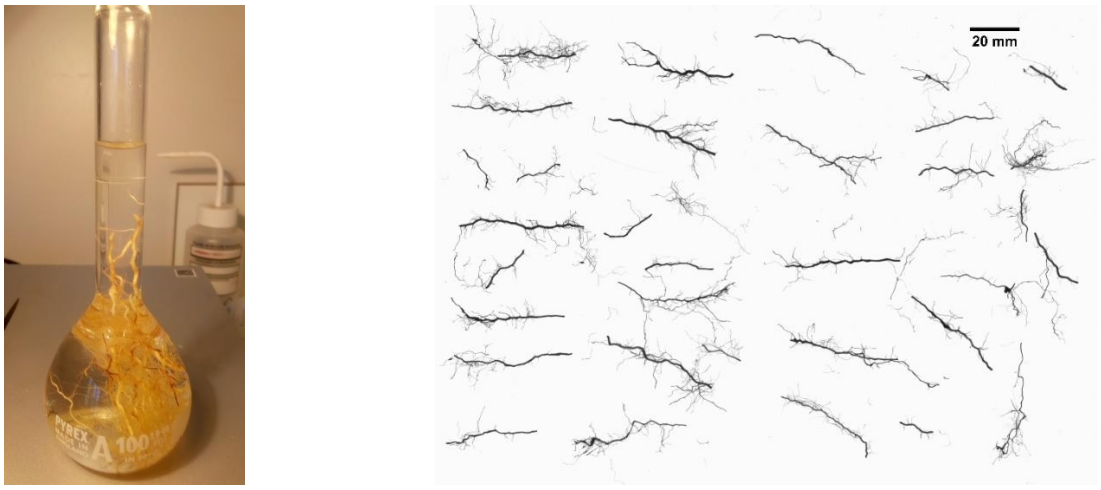

a *b*

Figure 5 a) Roots volume assessment by picnometry b) WinRHIZO acquired image.

2.4.3 Comparison of results

All roots volume estimations for each specimen tested are summarised in Table 4. For large samples used for retention measurements, soil water saturated permeability and oedometer test, X-ray scans were not performed.

For each sample, the root volume ratio ($R_v = V_{roots}/V_{tot}$) was computed (Table 4). This ratio was calculated with the roots volume values given by the different techniques. By subtracting the root volume ratio obtained by pycnometry to the one obtained by X-ray micro-tomography, it was possible to estimate the potential absolute error in porosity made by considering a certain number of *roots* as *pores* while choosing a threshold within tomography images. The potential relative error done in terms of porosity is instead given by the ratio between the absolute error and the initial porosity at which the samples were prepared ($n_o \approx 0.49$). In Figure 6a, the root volume values obtained by the three techniques. In Figure 6b, for the same samples, "potential" relative errors as a function of the water ratio ($e_w = \rho_s w/\rho_w$) at which samples were scanned with X-rays. The relative error is decreasing as the water ratio is increasing: this means that differences observed shall be attributed to roots volume shrinkage, as clearly observed by (Carminati et al., 2013; Liu et al., 2015). The higher and the lower values of root volume ratio found with X-rays were 0.010 and 0.003. Root volume ratio evaluated by pycnometry, for large samples, lies between 0.006 and 0.014.

Root volume ratio profiles with depth were also computed from X-ray images (Figure 7), confirming the average values showed in Table 4.

Discrepancies between root volume values were caused by the different conditions at which measurements were done. For X-ray microtomography, soil and roots were tested under partially

saturation, which induced the phases to shrink. Pycnometry, instead, was done under water, which made the roots swell due to liquid absorption. Finally, WinRHIZO, evaluates the total roots volume assuming a perfectly circular root section and considering the total root length per each root diameter class. Different authors that made comparisons between WinRHIZO and manual measurements observed that the software tends to overestimate root diameters and then, root volumes (Pang et al., 2011; Pornaro, Macolino, Menegon, & Richardson, 2017; Rose, 2017; Wang & Zhang, 2009). WinRHIZO revealed also the root tips density (the number of tips per unit volume of soil), a parameter linked to chemical interactions: its average value for the analysed samples is 0.057 tips/mm^3 (σ^2 = 0.01).

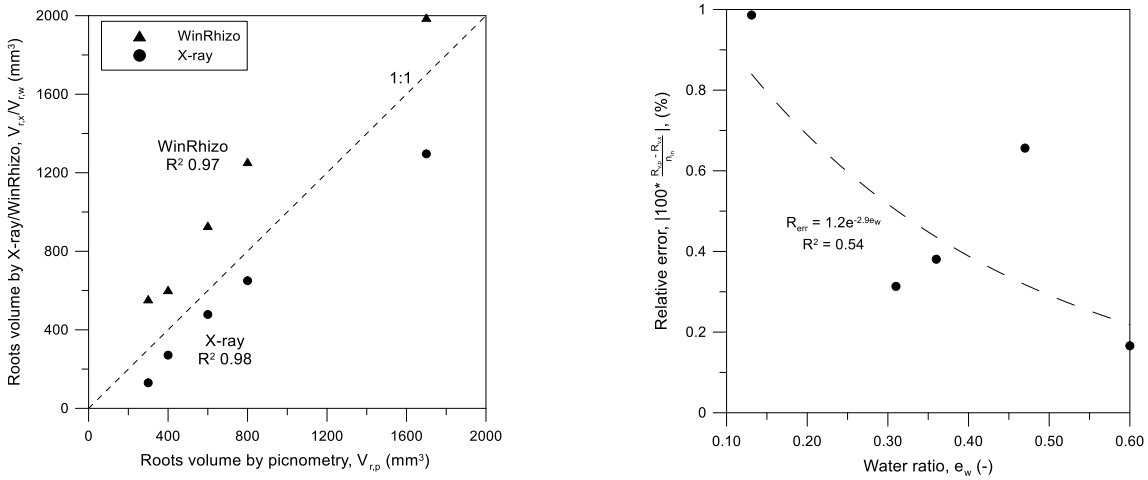

a *b*

Figure 6 a) Comparison of values of roots volume obtained from the different techniques and b) potential relative error in porosity between measurements done with X-ray micro-tomography and picnometry

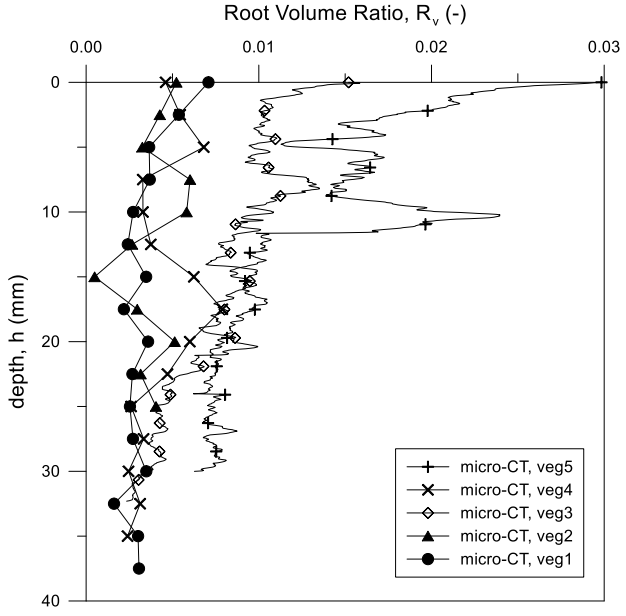

Figure 7 Root volume ratio vs depth, evaluated by X-ray micro-tomography

Table 4 Soil samples' volume, of roots volume comparison for X-ray microtomography, Picnometry and WinRHIZO. Root volume ratio estimated

	Pots for SWRC measurements			**Permeameter**	**Pot for Oedometer test**	**Samples for Pore-size distribution assessment**				
Sample name	17	13	6	Perm1R	Oed1R	Veg1	Veg2	Veg3	Veg4	Veg5
Soil Bulk Vol. (mm^3)	1237002	1237002	1237002	1469122	1237002	83600	35000	80000	149250	125000
Initial porosity, n_{in} (V_v/V_{tot}) (-)	0.49	0.49	0.49	0.49	0.49	0.49	0.49	0.49	0.49	0.49
Roots - X-ray microtomography (mm^3)	n.a.	n.a.	n.a.	n.a.	n.a.	271	130	650	478	1296
Roots - Picnometry (mm^3)	18510	7430	9900	8540	18910	410	340	800	630	1700
Roots - WinRHIZO (mm^3)	19792	8659	12370	10141	20375	603	556	1255	930	1990
Root Volume Ratio (X-ray) (-)	n.a.	n.a.	n.a.	n.a.	n.a.	0.003	0.004	0.008	0.003	0.010
Root Volume Ratio (Pycnometry) (-)	0.014	0.006	0.008	0.006	0.009	0.005	0.009	0.010	0.004	0.014
Root Volume Ratio (WinRHIZO) (-)	0.015	0.008	0.010	0.007	0.010	0.007	0.016	0.016	0.006	0.016
"Potential" absolute error in porosity $\|R_v(\text{X-ray}) - R_v(\text{Picnometry})\|$ (-)	n.a.	n.a.	n.a.	n.a.	n.a.	0.002	0.005	0.002	0.001	0.003
"Potential" relative error in porosity $100*(\|R_v(\text{X-ray}) - R_v(\text{Picnometry})\|)/n_{in}$ (%)	n.a.	n.a.	n.a.	n.a.	n.a.	0.31	0.99	0.38	0.17	0.75

2.5 Plant effects at the macroscale

2.5.1 Water retention properties

Three root-permeated samples and one bare sample were used to determine the soil water retention curves. Matric and total suction were assessed respectively by a ceramic tip laboratory tensiometer (T5x, UMS, München, Germany), up to 0.20 MPa, and a chilled mirror dew point hygrometer (WP4, Decagon Devices, Pullman, WA, USA), from 0.50 MPa upwards. After each drying phase, soil samples were placed for 24 hours in glass desiccators (Figure 8a-b) inside a temperature-controlled room (20±1°C), to allow suction and water content equalisation. After this period, the tensiometer was placed into the specimens up to a depth equal to their half height (35 mm). Specimens with roots were left with the tensiometer in the darkness for at least 2 hours to induce stomatal closure ((Snyder, Richards, & Donovan, 2003)) and to completely stop the plant's transpiration process ((Howard, Van Iersel, Richards, & Donovan, 2009)). Transpiration is in fact inducing hydraulic gradients within the matrix ((Aylmore, 1993)).

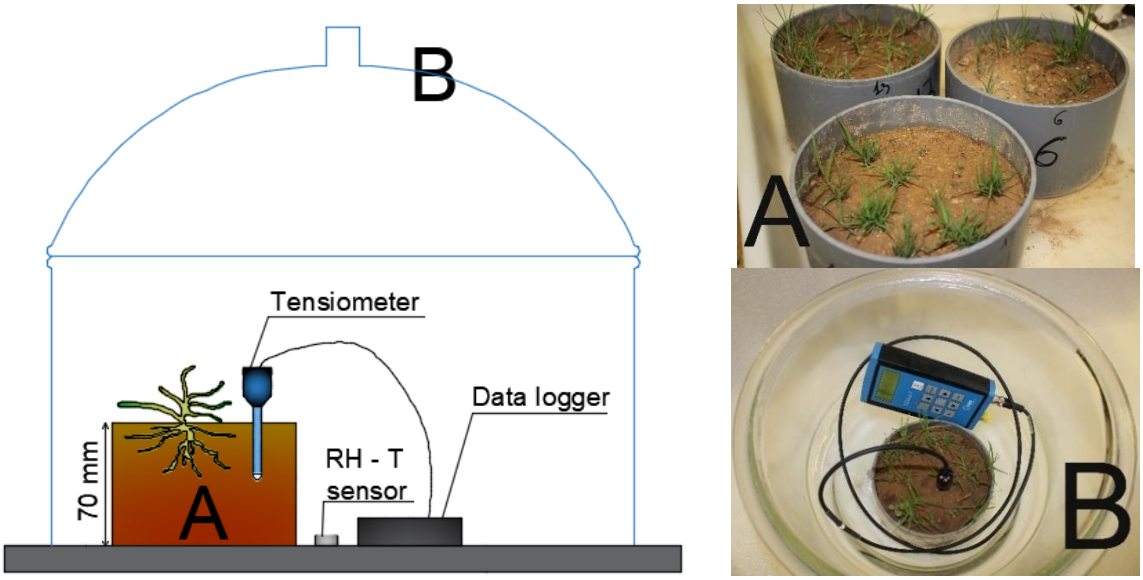

a *b*

Figure 8 a) schematic representation of the glass desiccator used for retention measurements b) replicates used for suction measurements(A) and tensiometer placed within the specimen (B).

Water content during tensiometer measurements was evaluated by oven-drying: roots were not present within the dried samples. When the maximum measurable suction for tensiometer was reached, soil samples were trimmed out from the bottom part of the pots to estimate total suction with the hygrometer. Results are presented in terms of water ratio ($e_w = \rho_s w / \rho_w = S_r e$) because they are

easily comparable with void ratio variations, since the two variables coincide when $S_r = 1$. Matric and total suctions were plotted in the same graph, where osmotic effects are negligible.

Data was fitted using the model of (E. Romero & Vaunat, 2000), based on a modified form of the (van Genuchten, 1980) expression:

$$S_r = C(s)\left(\frac{1}{1+(\alpha s)^n}\right)^m \quad ; \quad C(s) = 1 - \frac{ln\left[1+\frac{s}{a}\right]}{\ln(2)} \tag{3}$$

where S_r is the degree of saturation, C(s) is a function used for adjusting the curve in the higher suction range. Parameter $1/\alpha$ is linked to the air entry value, n to the slope of the curve and m to the residual degree of saturation. Parameter *a* is considered as the maximum suction for $S_r = 0$. Calibrated parameters are summarised in Table 5.

Table 5 Parameters calibrated for soil water retention measurements

	α (MPa^{-1})	**n**	**m**	**a (MPa)**
Bare soil, *e = 0.67*	0.53	0.28	1.77	200
Root-permeated soil, *e = 0.67*	0.15	0.19	2.38	200

A comparison of drying curves obtained by bare and vegetated samples is presented in Figure 9. The range of root volume ratio found within the pots is shown in the plot (see Table 4). It was observed that the air-entry value and the retention capacity of the vegetated soil has decreased.

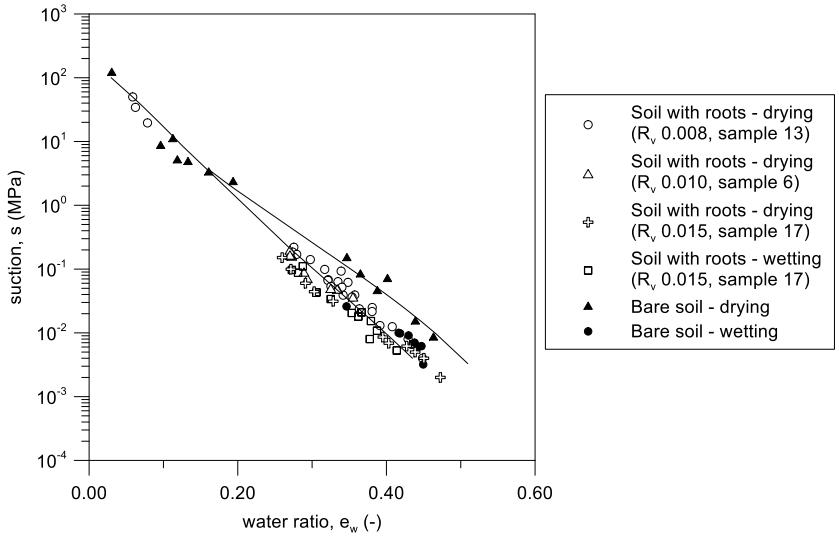

Figure 9 Main drying curves for bare and root permeated soil. Measurements done with T5x tensiometer and WP4 psychrometer.

This phenomenon is accentuated in specimens containing a larger quantity of roots. Finally, all the retention measurements converge at suction close to 3 MPa.

This kind of behaviour was observed by (Ng et al., 2014), for a lightly compacted soil seeded with the same grass of this study. The causes of that response were not assessed.

2.5.2 Volume changes upon drying

The characterization of the entire soil state and stress evolution ($e_w;e;s$) was carried out by paraffin tests on cubes with a size of approximately 30 mm trimmed out of bare and root-permeated pots. In the case of root-permeated pots, cubes were extracted on plants vicinity. Paraffin cubes were furtherly destroyed to measure roots volume, which was excluded by the total volume measured by the technique in order to compute void ratio according to the scheme in Figure 3a and as $e = V_{voids}/V_{solid}$. Root-permeated soil appeared to be stiffer than bare soil upon suction variations, which also means that the soil remained at higher porosities. Results have been interpreted with the laws expressing volumetric deformations during suction elastic virgin states' changes proposed by (Alonso, Gens, & Josa, 1990):

$$d\varepsilon_{vs}{}^{el} = \frac{\kappa_s}{(1+e)}\frac{ds}{(s+p_{at})}\,, s < s_0 \tag{4}$$

$$d\varepsilon_{vs} = \frac{\lambda_s}{(1+e)}\frac{ds_0}{(s_0+p_{at})}\,, s > s_0 \tag{5}$$

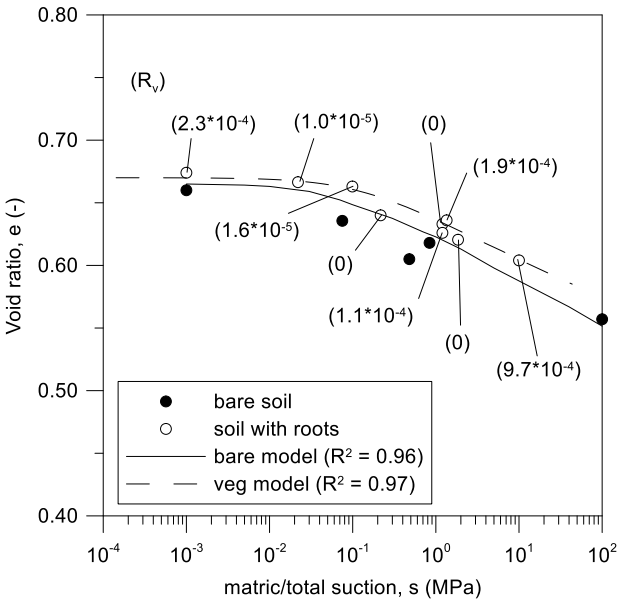

Figure 10 Observed and predicted volumetric deformations, expressed in terms of void ratio along suction increase

It is assumed that only elastic strains occurred for suction below the value at compaction, $s_0 = 40$ kPa. The parameters κ_s and λ_s are the stiffness values with respect to suction changes along elastic and virgin states, e the void ratio and p_{at} the atmospheric pressure.

The parameter κ_s for the two kinds of soils was calibrated and found to be 0.0015 and 0.0010 for bare and rooted soils, respectively. The parameter λ_s was 0.011 and 0.009 for bare and rooted soils, respectively. Results corresponding to volumetric deformations occurred during the drying phase experienced by the samples and modelling due to equations (4) and (5) are shown in Figure 10.

These results are in line with those showed by (Milleret, Le Bayon, Lamy, Gobat, & Boivin, 2009): the authors observed an increase of the specific volume within a vegetated soil, with respect to a bare soil, along a drying process.

2.5.3 Saturated water permeability

Large-cell oedometer tests and variable-head permeameters were used to evaluate the water saturated permeability of the soil before and after root growth.

One bare and one root-permeated soil samples were tested in large oedometer cells whose dimensions allowed their complete insertion (150 mm in diameter, 70 mm in height, Figure 11a).

They were compacted at the state expressed in Table 1 and underwent the same hydraulic path showed in Figure 2 (from A to B). When inside the oedometer, they were soaked and kept under controlled hydraulic gradient conditions throughout all the loading/unloading steps.

A permeameter with a diameter of 92 mm and a height of 221 mm (Figure 11a) was also used. Soil sand was statically compacted within at an initial state and stress expressed in Table 6 and seeded with *Cynodon Dactilon* with the same seeding density as for the abovementioned pots. To allow plants growth, soil was wetted at zero vertical stress up to gravimetric water content of $w = 20$ %. After roots growth, the specimen was completely saturated under a controlled hydraulic gradient close to the one imposed at test beginning.

Table 6 Initial state and stress variables of soil in permeameter

Soil initial state and stress	Value
Gravimetric water content, w (%)	15
Water ratio, $e_w = \rho_s w/\rho_w$ (-)	0.40
Void ratio, e (-)	0.87
Matric suction, s (kPa)	8
Max compaction vertical load, $\sigma_{v,0}$ (kPa)	20

All the values of soil water permeability were plotted together (bare and root-permeated) as function of their void ratio (Figure 11): results obtained by (Oorthuis et al., 2018) for the same bare soil are

included. In the case of root-permeated soil, void ratio is defined as the one at the initial state of compaction (permeameter) or the one calculated according to the volumetric deformations occurred (oedometer test). Close to rooted points, it is expressed the maximum vertical stress imposed on the material and the root volume ratio measured within the samples. The slope of the trend line expressing the water permeability of the rooted soil as function of the void ratio is doubled compared to the bare soil, on a logarithmic axis.

From the plot it is evident that roots growth increased the soil water permeability, at the macro-scale. Anyway, root-permeated soil permeability tends to the bare soil's values as void ratio diminishes and vertical stress experienced by the soil increases. Even if the root volume ratio within the oedometer specimen is higher than the one within the permeameter, the effects of roots on soil water permeability are less pronounced. These results are in good agreement with other authors ((Ng et al., 2014; Vergani & Graf, 2016)) that found that the hydraulic behaviour of a root-permeated soil does not depend only on roots properties and their evolution in time but also on the initial state of the soil. The latter might have an influence on roots ability to displace grains and generate fissures during their growth.

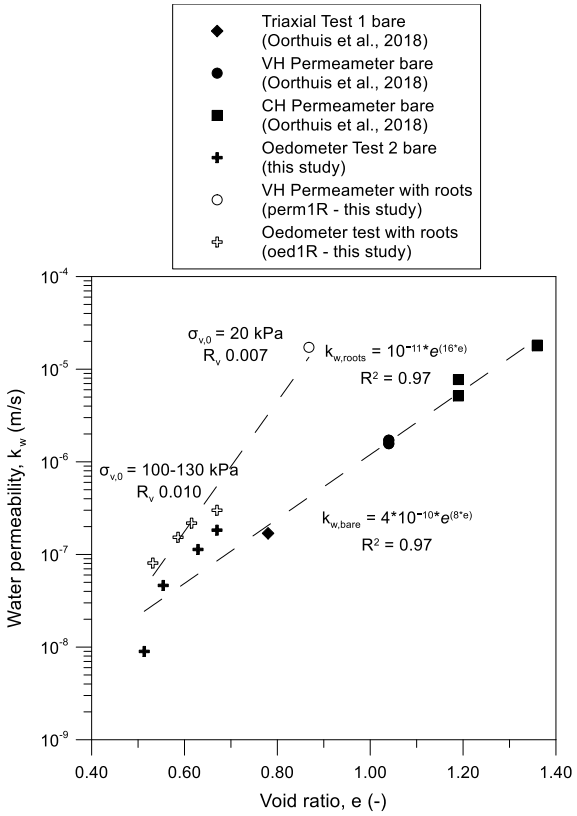

a b

Figure 11 a) Water permeability for bare and vegetated specimens evaluated for different void ratios and with different laboratory tests. Dashed lines indicate the best-fit tendency. B) Specimen with roots installed in an oedometer cell and in a permeameter

2.6 Plant effects at the microscale

We hypothesize that roots affect soil structure due to different processes: pores clogging due to chemical substances produced by roots or by physical pores penetration by roots and root hairs and soil fissuring due to roots growth and development. The domains involved by these phenomena correspond well to the porosity ranges that can be investigated by the two techniques used: Mercury Intrusion Porosimetry and X-ray microtomography.

2.6.1 Distribution of large-pore sizes

The images coming from the seven X-ray microtomography scans (one example is showed in Figure 12), previously analysed to determine the root volumes, have been furtherly processed to assess the effects of plants on the soil structure.

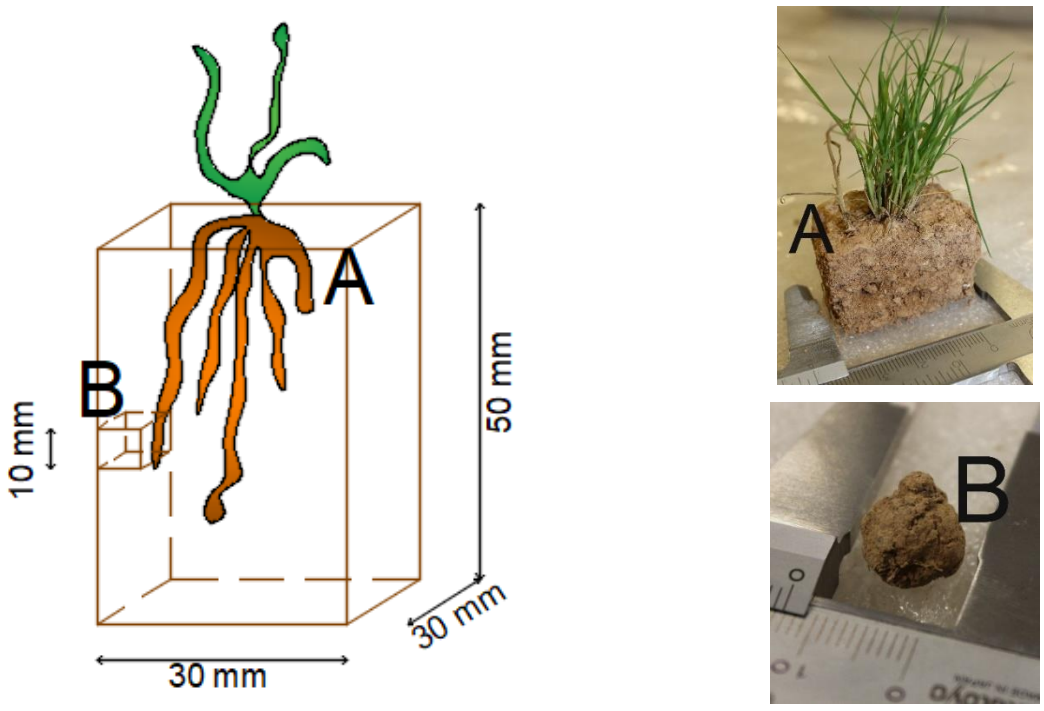

a *b*

Figure 12 a) schematic representation of a sample scanned by micro-tomography and tested by MIP and b) a sample scanned by micro-tomography (A) and a retrieved sample for MIP (B).

Pores and solid particles were identified through an automatic threshold operation, in *ImageJ*, calculated on the histogram of the grey values of the entire image stack and using the *Default* method. The threshold point was always close to 120 (Figure 3b). The image stack containing the roots phase (previously showed in Figure 4d) was then superimposed to the one showing solid and void phases (Figure 13a), in such a way that the roots are again included into the sample (Figure 13b).

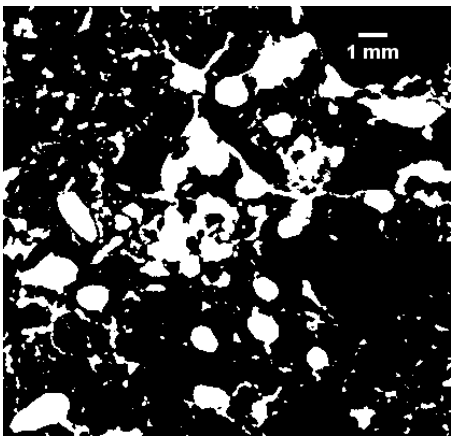

a

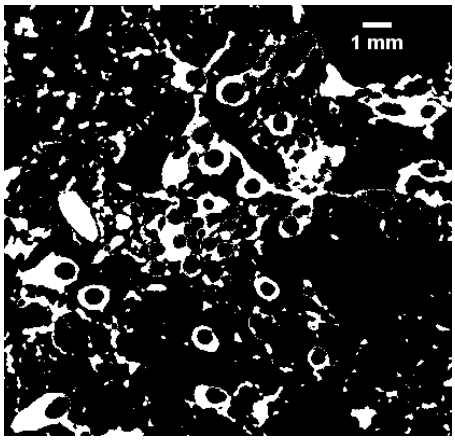

b

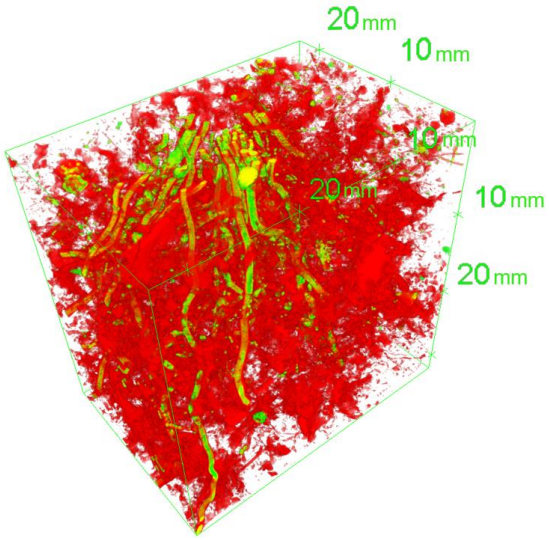

c

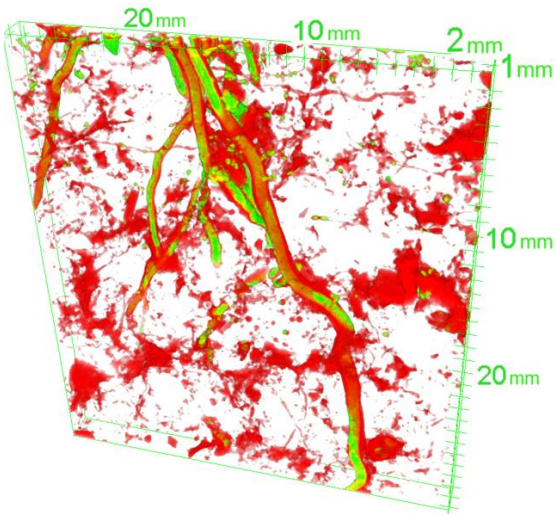

d

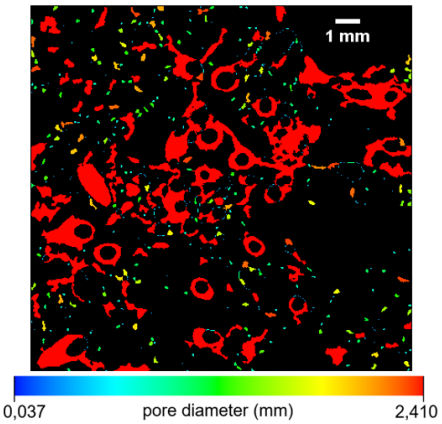

e

Figure 13 a) automatic threshold to separate voids (white pixels) from solid particles b) inclusion of the root phase within the image (voids in white) c-d) 3D rendering of roots (yellow) and pores (red) within the ROI and a slice of it e) individuation of the different pore diameter classes.

This step allowed to build a 3D rendering of roots and voids (Figure 13c-d) that gave a first qualitative insight of the phenomenon occurred: roots are often surrounded by fissures. To better quantify this effect along the hydraulic path studied (Figure 2), a pore-size distribution was assessed for each sample. The analysis was carried out with the *ImageJ* plugin *Pore size distribution* ((Münch & Lorenz, 2008)). The tool can perform a 3D simulation of mercury intrusion within the voxels representing voids and to evaluate the volume occupied for each class of pore diameter (Figure 13e). Resulting images showed a clear distinction between pores generated by root penetration (usually between 1 and 2.41 mm in diameter) and pre-existing ones. The tool described allowed to investigate pores with a minimum diameter of 0.037 mm, which is the voxel size for the microtomography images.

2.6.2 Extension to the micro-pores range

For Mercury Intrusion Porosimetry, soil cubes with a size smaller than 10 mm have been trimmed out from the samples previously scanned by X-ray micro-tomography (Figure 12), thus keeping unvaried their water content and suction (Table 2). Before testing, all the cubes were freeze-dried to remove pore water avoiding soil volumetric deformations ((Enrique Romero, 1999)). Tests were carried out in a porosimeter (AutoPore IV 9500, Micromeritics Instrument Corporation, Norcross, GA, USA) and accordingly to the testing method proposed by ASTM D4404-18. This technique allowed to investigate pore sizes from 7 nm to 400 μm.

2.6.3 Roots effects on soil pore-size distribution

The pore size distribution (PSD) represents the cumulative void ratio occupied up for a given pore diameter, starting from the maximum diameter observed. In the case of X-ray micro-tomography, the cumulative void ratio for a given pore diameter x* was calculated by:

$$e_{cum}^{(x^*)} = \frac{\sum_{x=x_{max}}^{x^*} V_v^{(x)}}{V_s} \quad (6)$$

where $V_v^{(x)}$ is the volume of voids (white pixels in Figure 13b) occupied by a generic pore's diameter x and V_s is the volume of solid particles, calculated as the total volume of the black pixels in Figure 13a. In the case of the results given by MIP, the cumulative void ratio is evaluated directly from mercury intruded volume, as explained in (E Romero, Gens, & Lloret, 1999).

Results have been joined to make the upper end of the microtomography curve coincide with the lower end of the MIP curve (Figure 14). In the plot there is a comparison between PSD curves obtained for bare and root-permeated soil at a water ratio equal to $e_w \approx 0.33$ ($e \approx 0.64$, $S_r \approx 0.52$). The two curves almost approached the same final cumulative void ratio but did not reach the value at

which they were originally compacted. Moreover, root-permeated soil's total cumulative void ratio was always slightly higher than the bare soil's one, for each water ratio tested.

Differences observed, within the PSD curves, in terms of total cumulated void ratios are caused by coupled effect of soil fissuring by roots growth and a different shrinkage behaviour of the two soils (previously shown in Figure 10). Due to these counterposed phenomena it is difficult to state whether the roots are directly increasing the total void ratio within the soil or this is due by the different mechanical response that the root-permeated soil has along drying. Moreover, MIP does not allow to intrude intra-aggregate porosities with diameters below 7 nm. Cumulated void ratio values in the PSD curves comparisons were generally similar, between bare and vegetated samples, whereas their shapes were very different.

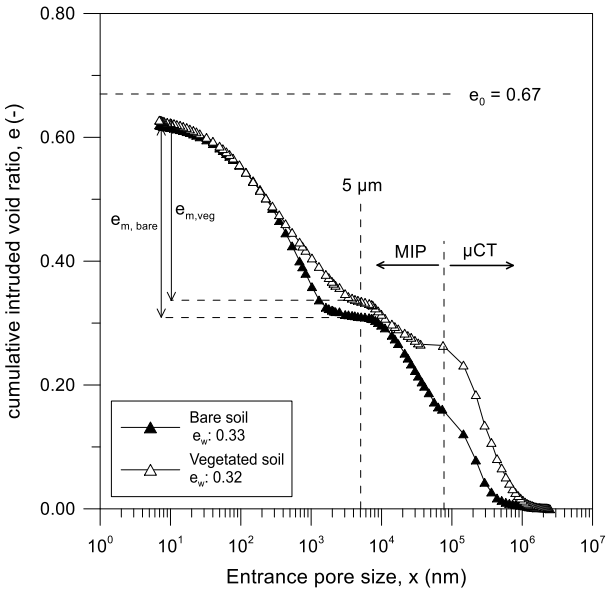

Figure 14 Pore size distribution for a bare and a vegetated sample, both initially compacted at void ratio 0.67.

Results will be furtherly presented as PSD derivatives with respect to the logarithm of pore diameter: this operation allows to represent the volumetric density for each specific pore size (Figure 15). In Figure 15a-b, there is an overview of all the results, detailing the water ratio at which they were tested. The pore sizes below 5 µm are corresponding to the clay aggregation range, which cannot be physically penetrated by roots or root hairs ((Grierson & Schiefelbein, 2002; Lamont, 1983; Wulfsohn & Nyengaard, 1999)). Comparing Figure 15a and b, one can note that, along water ratio e_w decrease, the peak diameter of the clay aggregates in the bare soil undergoes a much larger shifting towards left (from 2.5 to 0.3 µm) than the vegetated one (from 1 to 0.5 µm). This means that aggregates undergo lower shrinkage in the rooted soil. Aggregates mechanical stability generated by roots, is in turn linked to a higher stiffness against volumetric shrinkage previously observed at the macro-scale (Figure 10).

Above the threshold value of 5 μm different and counterposed effects of soil-roots interactions are expected:

- soil fissuring during roots growth;
- channel formation after roots decay;
- increasing gap between roots and soil matrix during the drying phase;
- pores clogging by root hairs;
- pores clogging by mucilage released.

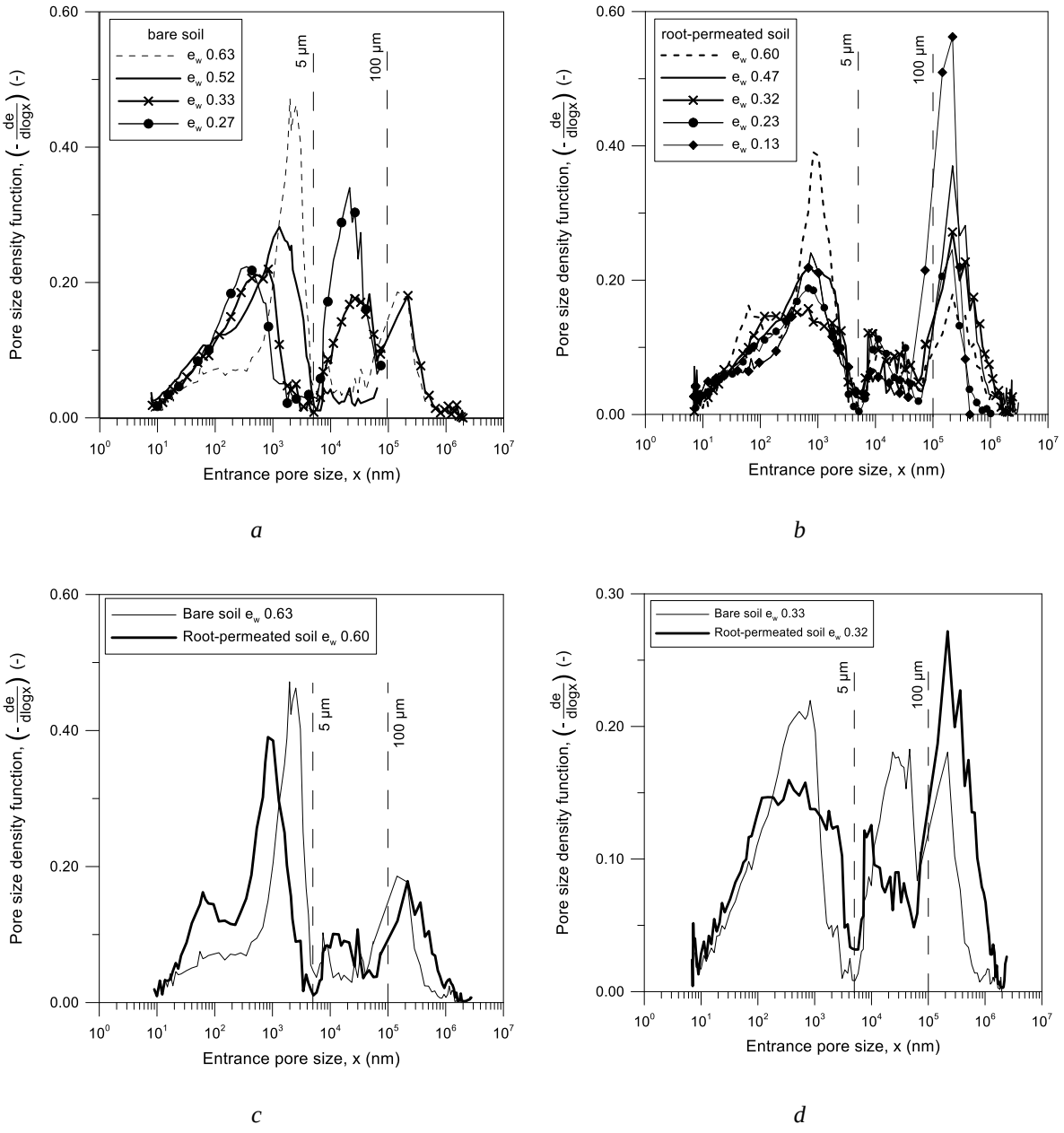

Figure 15 Pore size density functions for: a) all the bare samples, b) all the root-permeated samples, c) bare and root-permeated samples close to saturation (e_w = 0.60) and c) after a drying phase (e_w = 0.33).

Comparing Figure 15a and b, the abovementioned effects are visible. In the pore size range 5 to 100 μm, pores volume density is in average 1.60 (σ = 0.92) times lower in root-permeated soil compared

to bare soil, which can be explained by soil pores being penetrated by fine roots and root hairs. These two root types were characterized by WinRhizo within a unique class of diameter φ ($0< \varphi <0.10$mm). The average root length calculated within the samples, for this diameter class, was 940 mm (σ = 590 mm). Above 100 μm an opposite trend is observed: pores volume density generally increased within rooted soil. These pore sizes are corresponding to the fissures visible around the roots in Figure 13b and computed in Figure 13e. In addition, the volume of this range of porosity is clearly increasing as the soil dries out, jointly with a shifting of the volume density peak towards lower pore diameters. This is explained by considering the concurrent shrinkage of soil and roots ((Carminati et al., 2013; Jones, 2007; Liu et al., 2015)).

Bare and root-permeated pore size density functions calculated for samples at similar water ratios were compared (Figure 15c-d). In correspondence of a water ratio equal to $e_w \approx 0.60$ ($e \approx 0.67$, $S_r \approx 0.90$, Figure 15c), the volume of pores above 100 μm is almost equal between the two soils, even if the peak value corresponds to a higher pore size within the vegetated sample. This is in line with findings showed by (Carminati et al., 2013), who evidenced a quite good capacity of roots to clog the whole fissures generated by their growth, when soil is saturated. In the pore diameter range 5-100 μm, pore size density is increased by roots while for pore diameters below 5 μm some porosities are reduced, and other ones are enhanced. Jointly to a partial pore clogging due to mucilage production, some pores in aggregates might have increased in volume due other chemical activities in soil. Indeed, wetting increases soil nutrient mineralization due to metabolic and enzymatic activities ((Borken & Matzner, 2009; Manzoni, Schimel, & Porporato, 2012)): this is strictly linked to plants nutrition ((Singh & Schulze, 2015)). At a lower water content (Figure 15d, $e_w \approx 0.33$, $e \approx 0.64$, $S_r \approx 0.52$) most of the vegetated soil's intra-aggregate (within aggregates) and inter-aggregate (outside aggregates) pores between 5 and 100 μm appear reduced in volume compared with bare soil. This is caused by a combined effect of chemical and physical clogging, for instance linked to mucilage production that increases upon drying ((Watt et al., 1994)). Porosities above 100 μm are instead evidencing higher pore size densities and pore diameter peaks, due to fissures generated and widened by roots.

2.7 Roots traits and soil microstructure on drying

Soil microstructure evolution is quantitively defined by the intra-aggregate void ratio e_m; this variable is defined on the pore size distribution curve (Figure 14) as the difference between the final cumulative intruded void ratio and the one reached at the pore size of 5 μm. This value is close to the one used by (Enrique Romero, 2013) to identify aggregates porosities in clayey soils. The microstructural variable is linked to the total void ratio by the equation suggested by (E. Romero, Della Vecchia, & Jommi, 2011):

$$e = e_m + e_M \tag{7}$$

where e_M is the void ratio of inter-aggregate space.

Intra-aggregate void ratio is plotted in Figure 16 as a function of the water ratio at which samples were tested. In fact, for the bare soil, the graph is representing the swelling and shrinkage reversible behaviour of clay aggregates along the hydraulic path.

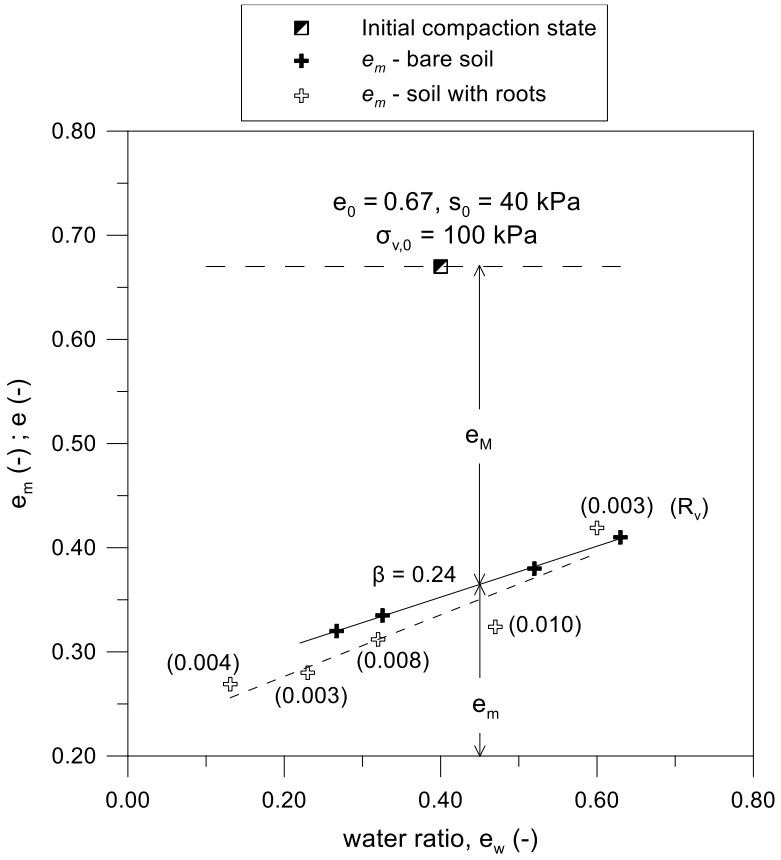

Figure 16 Inter-aggregate void ratio evolution with the water ratio, for bare and root-permeated specimens. Roots volume ratio is indicated for the correspondent vegetated sample

The microstructural parameter β, representing the slope of the fitting line, is in good agreement with results showed by (Enrique Romero, 2013) for similar kind of soils. The interpretation of the points for the root-permeated soil is more complex. Fissures volume is increasing, due to previously commented effects, during drying in the rooted soil: this is expressed by an increase of the macroscopic void ratio, e_M, with a consequent decrease of the intra-aggregate void ratio, e_m. By looking at the root volume ratio values in correspondence of each sample, one can note a good correlation with the macroscopic void ratio generated. WinRHIZO scans revealed that all the roots had very similar diameter distributions and lengths: in this case, the root volume ratio is directly proportional to the number of roots. Hence, the higher is the number of roots, the larger is the volume of fissures generated upon drying.

In addition, the slope of the line fitting microstructural values, for the root-permeated soil, (Figure 16) appears steeper than the bare soil's one: this means that, apart from a natural shrinkage of the clay aggregates (intrinsic for a given material and for clay particles specific surface ((Enrique Romero, 2013))), the vegetated soil has a higher rate of reduction of micro-voids thanks to root mucilage production.

2.8 Micro and macroscale interactions

Pore-size distributions were used to evaluate soil water retention curves. For the part of the PSD obtained by MIP, suction has been calculated from the mercury pressure values achieved for each intrusion step, according to (E Romero et al., 1999), assuming the mercury intrusion process to be similar to air intrusion, during a drying path. For the part of the PSD obtained by X-ray microtomography, suction was deduced by the Young-Laplace's equation, assuming that suction is generated only by capillary effects within this range of large porosities. The degree of saturation of the gas phase was calculated as the ratio between the cumulative void ratio at a given pore diameter and the total one ((E Romero et al., 1999)). The water phase was calculated from the gas phase degree of saturation, and then converted into water ratio. Results were plotted jointly to soil retention measurements (Figure 17): two curves coming from the bare and vegetated samples at a water ratio $e_w \approx 0.33$ ($e \approx 0.64$, $S_r \approx 0.52$, Figure 15d) and the other one from the vegetated sample at a water ratio $e_w \approx 0.60$ ($e \approx 0.67$, $S_r \approx 0.90$, Figure 15c).

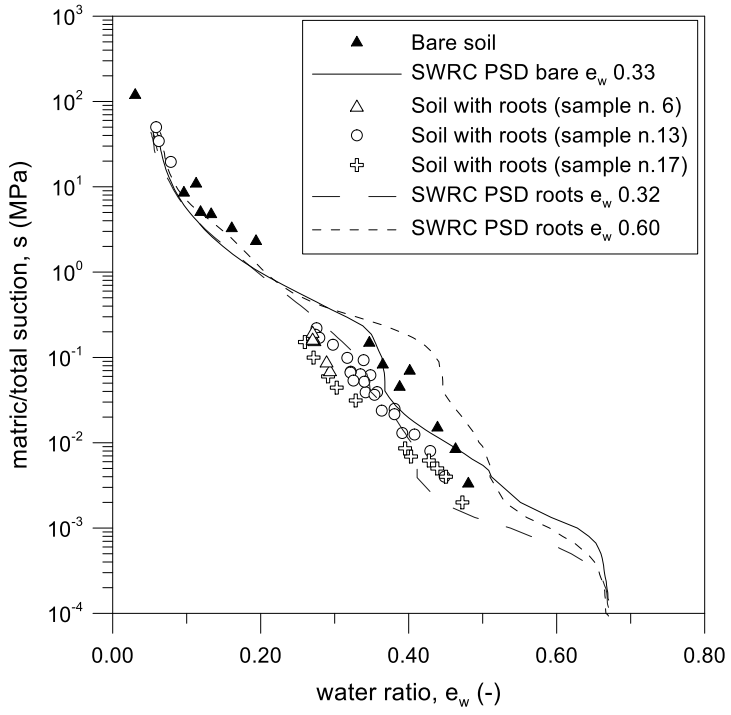

Figure 17 SWRC of bare and root permeated soil measured by tensiometer and psychrometer and calculated from pore-size distributions

From the latter sample, the predicted air-entry value is close to the one calculated for the bare sample, because there are few fissures with size above 100 μm. In the same curve, the desiccation rate after the air-entry value becomes much smaller than the bare soil's one: this is due to a general volume reduction within porosities below 100 μm. As consequence, in a range of suction, the predicted retention behaviour of a root-permeated soil would be above than the bare soil (higher suction for a given water ratio). Indeed, several authors observed similar trends in the retention curves of root-permeated soils (Garg et al., 2015; Ng et al., 2016), for values of suction below 0.1 MPa.

As the soil dries out, its retention properties become affected by the opening of fissures: this is clearly expressed by the retention curve obtained from the PSD evaluated for the soil with roots at a water ratio equal to $e_w \approx 0.33$ ($e \approx 0.64$, $S_r \approx 0.52$, Figure 15d). Fissures are dramatically affecting the air-entry value and the first part of the curve, which is characterised by a high desiccation rate. Subsequently, the decrease in pores volume within the clay aggregates pores is progressively controlling the macroscopic behaviour by reducing the slope of the curve. This response could be linked again to chemo-physical modifications produced by roots exudates on the water contained in the soil. Indeed, it was observed that the surface tension of the liquid present within the rhizosphere is dramatically decreasing and its viscosity was increasing with respect to pure water at 20 °C ((Carminati, Benard, Ahmed, & Zarebanadkouki, 2017; Hinsinger et al., 2009; Read et al., 2003)). Finally, the curves converge in correspondence 1 MPa of suction, which is fairly representing what measured with tensiometers and psychrometers.

2.9 Concluding remarks

The hydro-mechanical behaviour of a root-permeated and compacted soil was investigated considering several variables and scales. Soil was seeded by *Cynodon Dactilon,* at a fixed density of 34 g/m^2 and tested after 3 months of growth. Attention was paid at the initial soil state and stress and at the hydro-mechanical path followed during the tests. Indeed, the dry density, the maximum stresses experienced by the matrix and the water content are imposing constraints on roots diameters, volumes, length and their ability of opening fissures and/or clog pores ((Kolb, Legué, & Bogeat-Triboulot, 2017)). All these roots features, jointly with soil state evolution and physical properties, affected macroscopic soil features: air-entry value, drying rate, saturated soil water permeability and shrinkage behaviour.

Investigations at the micro-scale evidenced pores clogging and fissuring, occurring at different points of the same soil-root system. Roots chemical alterations on soil were also quantified in terms of clogged volumes within pores. The latter had indirect consequences on soil hydro-mechanical behaviour and depend both on roots features (root tips density, roots volume) and soil physical-

chemical properties (clay aggregates specific surface, water content). Root volumetric traits computed were used to link the effects occurring at the different scales of the problem.
Further investigations need to be done, starting from different soil states and stresses, and considering different vegetation characteristics (species, sowing density, …) to build a framework able to predict soil hydro-mechanical behaviour starting from a given bare condition and considering plants features and physiology.

2.10 Acknowledgements

The authors wish to acknowledge the support of the European Commission via the Marie Skłodowska-Curie Innovative Training Networks (ITN-ETN) project TERRE 'Training Engineers and Researchers to Rethink geotechnical Engineering for a low carbon future' (H2020-MSCA-ITN-2015-675762). Micro-tomography scans were performed in the Laboratory of Microscopy and Computed Micro-tomography at CENIEH facilities (Burgos, Spain) with the collaboration of CENIEH staff. Mercury intrusion porosimetry was performed at the UPC Geotechnical Laboratory with the help of Rodrigo Gómez. Roots geometrical characterization was carried out in AMAP (Montpellier, France) with the help of Stephane Fourtier and Dr Philippe Borianne. Alessandro Fraccica also wishes to acknowledge the fruitful discussions with the members of TERRE and SMUCPHY projects, as well as with Dr Vito Tagarelli and Dr Agustín Cuadrado.

References

Alonso, E. E., Gens, A., & Josa, A. (1990). A constitutive model for partially saturated soils. *Géotechnique*, *40*(3), 405–430. https://doi.org/10.1680/geot.1990.40.3.405

Anselmucci, F., Andó, E., Sibille, L., Lenoir, N., Peyroux, R., Arson, C., … Bengough, A. G. (2019). Root-reinforced sand : kinematic response of the soil. In Alessandro Tarantino & E. Ibraim (Eds.), *IS-Glasgow* (Vol. 92, p. 12011). https://doi.org/doi.org/10.1051/e3sconf/20199212011

ASTM D4404-18. (2018). Standard Test Method for Determination of Pore Volume and Pore Volume Distribution of Soil and Rock by Mercury Intrusion Porosimetry.

Aylmore, L. A. G. (1993). Use of Computer-Assisted Tomography in Studying Water Movement Around Plant Roots. *Advances in Agronomy*, *49*, 1–54. https://doi.org/10.1016/S0065-2113(08)60792-0

Berger, M. J., Hubbell, J. H., Seltzer, S. M., Chang, J., Coursey, J. S., Sukumar, R., … Olsen, K. (2010). XCOM: Photon Cross Sections Database. Retrieved from NIST Standard Reference Database 8 (XGAM) website: www.nist.gov/pml/xcom-photon-cross-sections-database

Borken, W., & Matzner, E. (2009). Reappraisal of drying and wetting effects on C and N mineralization and fluxes in soils. *Global Change Biology*, *15*, 808–824.

Carminati, A., Benard, P., Ahmed, M. A., & Zarebanadkouki, M. (2017). Liquid bridges at the root-soil interface. *Plant and Soil*, *417*(1–2), 1–15. https://doi.org/10.1007/s11104-017-3227-8

Carminati, A., Moradi, A. B., Vetterlein, D., Vontobel, P., Lehmann, E., Weller, U., … Oswald, S. E. (2010). Dynamics of soil water content in the rhizosphere. *Plant and Soil*, *332*(1), 163–176. https://doi.org/10.1007/s11104-010-0283-8

Carminati, A., Vetterlein, D., Koebernick, N., Blaser, S., Weller, U., & Vogel, H. J. (2013). Do roots mind the gap ? *Plant and Soil*, *367*, 651–661. https://doi.org/10.1007/s11104-012-1496-9

Chen, F., Zhang, J., Zhang, M., & Wang, J. (2015). Effect of Cynodon dactylon community on the conservation and reinforcement of riparian shallow soil in the Three Gorges Reservoir area. *Ecological Processes*, *4*, 3. https://doi.org/10.1186/s13717-014-0029-2

Dougherty, B. (n.d.). Computing Local Thickness of 3D Structures with ImageJ. Retrieved from http://www.optinav.info/LocalThicknessEd.pdf

Fraccica, A., Romero, E., & Fourcaud, T. (2019). Multi-scale effects on the hydraulic behaviour of a root-permeated and compacted soil. In Alessandro Tarantino & E. Ibraim (Eds.), *IS-Glasgow* (p. 12014). https://doi.org/doi.org/10.1051/e3sconf/20199212014

Garg, A., Coo, J. L., & Ng, C. W. W. (2015). Field study on influence of root characteristics on soil

suction distribution in slopes vegetated with Cynodon dactylon and Schefflera heptaphylla. *Earth Surface Processes and Landforms*, *40*, 1631–1643. https://doi.org/10.1002/esp.3743

Grierson, C., & Schiefelbein, J. (2002). Root Hairs. *The Arabidopsis Book*, *1*, 60. https://doi.org/10.1199/tab.0060

Hinsinger, P., Bengough, A. G., Vetterlein, D., & Young, I. M. (2009). Rhizosphere: biophysics, biogeochemistry and ecological relevance. *Plant and Soil*, *321*, 117–152. https://doi.org/10.1007/s11104-008-9885-9

Howard, A. R., Van Iersel, M. W., Richards, J. H., & Donovan, L. A. (2009). Night-time transpiration can decrease hydraulic redistribution. *Plant, Cell and Environment*, *32*(8), 1060–1070. https://doi.org/10.1111/j.1365-3040.2009.01988.x

Jones, H. G. (2007). Monitoring plant and soil water status: established and novel methods revisited and their relevance to studies of drought tolerance. *Journal of Experimental Botany*, *58*(2), 119–130. https://doi.org/10.1093/jxb/erl118

Karup, D., Moldrup, P., Tuller, M., Arthur, E., & de Jonge, L. W. (2017). Prediction of the soil water retention curve for structured soil from saturation to oven-dryness. *European Journal of Soil Science*, *68*, 57–65. https://doi.org/10.1111/ejss.12401

Koebernick, N., Daly, K. R., Keyes, S. D., George, T. S., Brown, L. K., Raffan, A., … Roose, T. (2017). High-resolution synchrotron imaging shows that root hairs influence rhizosphere soil structure formation. *New Phytologist*, *216*, 124–135. https://doi.org/10.1111/nph.14705

Kolb, E., Hartmann, C., & Genet, P. (2012). Radial force development during root growth measured by photoelasticity. *Plant and Soil*, *360*, 19–35. https://doi.org/10.1007/s11104-012-1316-2

Kolb, E., Legué, V., & Bogeat-Triboulot, M. B. (2017). Physical Root-Soil Interactions. *Physical Biology*, *14*(6), 1–40. https://doi.org/10.1088/1478-3975/aa90dd

Lamont, B. (1983). Root hair dimensions and surface/volume/weight ratios of roots with the aid of scanning electron microscopy. *Plant and Soil*, *74*(1), 149–152. https://doi.org/10.1007/BF02178753

Legland, D., Arganda-Carreras, I., & Andrey, P. (2016). MorphoLibJ: integrated library and plugins for mathematical morphology with ImageJ. *Bioinformatics*, *32*(22), 3532–3534. https://doi.org/10.1093/bioinformatics/btw413

Leung, A. K., Garg, A., Coo, J. L., Ng, C. W. W., & Hau, B. C. H. (2015). Effects of the roots of Cynodon dactylon and Schefflera heptaphylla on water infiltration rate and soil hydraulic conductivity. *Hydrological Processes*, *29*, 3342–3354. https://doi.org/10.1002/hyp.10452

Liu, X. P., Zhang, W. J., Wang, X. Y., Cai, Y. J., & Chang, J. G. (2015). Root – soil air gap and resistance to water flow at the soil – root interface of Robinia pseudoacacia. *Tree Physiology*,

35, 1343–1355. https://doi.org/10.1093/treephys/tpv075

Manzoni, S., Schimel, J. P., & Porporato, A. (2012). Responses of soil microbial communities to water stress: results from a meta-analysis. *Ecology*, *93*(4), 930–938. https://doi.org/10.1890/11-0026.1

Milleret, R., Le Bayon, R. C., Lamy, F., Gobat, J. M., & Boivin, P. (2009). Impact of roots, mycorrhizas and earthworms on soil physical properties as assessed by shrinkage analysis. *Journal of Hydrology*, *373*(3–4), 499–507. https://doi.org/10.1016/j.jhydrol.2009.05.013

Moradi, A. B., Carminati, A., Vetterlein, D., Vontobel, P., Lehmann, E., Oswald, S. E., … Hopmans, J. W. (2011). Three-dimensional visualization and quantification of water content in the rhizosphere. *New Phytologist*, *192*, 653–663. https://doi.org/10.1111/j.1469-8137.2011.03826.x Key

Münch, B., & Lorenz, H. (2008). Contradicting Geometrical Concepts in Pore Size Analysis Attained with Electron Microscopy and Mercury Intrusion. *Journal of American Ceramic Society*, *91*(12), 4059–4067. https://doi.org/10.1111/j.1551-2916.2008.02736.x

Ng, C. W. W., Leung, A. K., & Woon, K. X. (2014). Effects of soil density on grass-induced suction distributions in compacted soil subjected to rainfall. *Canadian Geotechnical Journal*, *51*(3), 311–321. https://doi.org/10.1139/cgj-2013-0221

Ng, C. W. W., Ni, J. J., Leung, A. K., & Wang, Z. J. (2016). A new and simple water retention model for root-permeated soils. *Géotechnique Letters*, *6*(1), 106–111. https://doi.org/10.1680/jgele.15.00187

Ni, J. J., Leung, A. K., & Ng, C. W. W. (2019). Modelling effects of root growth and decay on soil water retention and permeability. *Canadian Geotechnical Journal*, *56*, 1049–1055. https://doi.org/dx.doi.org/10.1139/cgj-2018-0402

Ohu, J. O., Raghavan, G. S. V., Prasher, S., & Mehuys, G. (1987). Prediction of water retention characteristics from soil compaction data and organic matter content. *Journal of Agricultural Engineering Research*, *38*(1), 27–35. https://doi.org/10.1016/0021-8634(87)90136-3

Oorthuis, R., Hürlimann, M., Fraccica, A., Lloret, A., Moya, J., Puig-Polo, C., & Vaunat, J. (2018). Monitoring of a full-scale embankment experiment regarding soil-vegetation-atmosphere interactions. *Water (Switzerland)*, *10*, 688. https://doi.org/10.3390/w10060688

Pagano, L., Reder, A., & Rianna, G. (2019). The effects of vegetation on the hydrological response of silty volcanic covers. *Canadian Geotechnical Journal*, *56*(9), 1261–1277. https://doi.org/10.1139/cgj-2017-0625

Pang, W., Crow, W. T., Luc, J. E., McSorley, R., Giblin-Davis, R. M., Kenworthy, K. E., & Kruse, J. (2011). Comparison of Water Displacement and WinRHIZO Software for Plant Root

Parameter Assessment. *Plant Disease*, *95*(10), 1308–1310.

Pornaro, C., Macolino, S., Menegon, A., & Richardson, M. (2017). WinRHIZO Technology for Measuring Morphological Traits of Bermudagrass Stolons. *Agronomy Journal*, *109*(6), 3007–3010. https://doi.org/10.2134/agronj2017.03.0187

Read, D. B., Bengough, A. G., Gregory, P. J., Crawford, J. W., Robinson, D., Scrimgeour, C. M., … Zhang, X. (2003). Plant roots release phospholipid surfactants that modify the physical and chemical properties of soil. *New Phytologist*, *157*, 315–326. https://doi.org/doi.org/10.1046/j.1469-8137.2003.00665.x

Romero, E., Della Vecchia, G., & Jommi, C. (2011). An insight into the water retention properties of compacted clayey soils. *Géotechnique*, *61*(4), 313–328. https://doi.org/10.1680/geot.2011.61.4.313

Romero, E., & Vaunat, J. (2000). Retention curves of deformable clays. In A. Tarantino & C. Mancuso (Eds.), *International Workshop on Unsaturated Soils: Experimental Evidence and Theoretical Approaches in Unsaturated Soils* (pp. 91–106). A.A. Balkema, Rotterdam, Netherlands.

Romero, E, Gens, A., & Lloret, A. (1999). Water permeability , water retention and microstructure of unsaturated compacted Boom clay. *Engineering Geology*, *54*(1–2), 117–127. https://doi.org/10.1016/S0013-7952(99)00067-8

Romero, Enrique. (1999). *Characterisation and thermo-hydro-mechanical behaviour of unsaturated boom clay: an experimental study*. Universitat Politècnica de Catalunya.

Romero, Enrique. (2013). A microstructural insight into compacted clayey soils and their hydraulic properties. *Engineering Geology*, *165*, 3–19. https://doi.org/10.1016/j.enggeo.2013.05.024

Rose, L. (2017). Pitfalls in Root Trait Calculations : How Ignoring Diameter Heterogeneity Can Lead to Overestimation of Functional Traits. *Frontiers in Plant Science*, *8*, 898. https://doi.org/10.3389/fpls.2017.00898

Schindelin, J., Arganda-Carreras, I., Frise, E., Kaynig, V., Longair, M., Pietzsch, T., … Cardona, A. (2012). Fiji: an open-source platform for biological-image analysis. *Nature Methods*, *9*, 676. Retrieved from https://doi.org/10.1038/nmeth.2019

Scholl, P., Leitner, D., Kammerer, G., Loiskandl, W., Kaul, H. P., & Bodner, G. (2014). Root induced changes of effective 1D hydraulic properties in a soil column. *Plant and Soil*, *381*(1–2), 193–213. https://doi.org/10.1007/s11104-014-2121-x

Singh, B., & Schulze, D. G. (2015). Soil Minerals and Plant Nutrition. *Nature Education Knowledge*, *6*(1), 1.

Smethurst, J. A., Clarke, D., & Powrie, W. (2012). Factors controlling the seasonal variation in soil

water content and pore water pressures within a lightly vegetated clay slope. *Géotechnique*, *62*(5), 429–446. https://doi.org/10.1680/geot.10.P.097

Snyder, K., Richards, J. H., & Donovan, L. A. (2003). Night-time conductance in C3 and C4 species: do plants lose water at night ? *Journal of Experimental Botany*, *54*(383), 861–865. https://doi.org/10.1093/jxb/erg082

Soriano, I., Ibraim, E., Andò, E., Diambra, A., Laurencin, T., Moro, P., & Viggiani, G. (2017). 3D fibre architecture of fibre-reinforced sand. *Granular Matter*, *19*, 75. https://doi.org/10.1007/s10035-017-0760-3

Tinker, P. B., & Nye, P. H. (2000). *Solute movement in the rhizosphere* (2nd ed.). New York, NY, USA: Oxford University Press.

van Genuchten, M. T. (1980). A Closed-form Equation for Predicting the Hydraulic Conductivity of Unsaturated Soils. *Soil Science Society of America Journal*, *44*(5), 892. https://doi.org/10.2136/sssaj1980.03615995004400050002x

Vergani, C., & Graf, F. (2016). Soil permeability, aggregate stability and root growth: a pot experiment from a soil bioengineering perspective. *Ecohydrology*, *9*(5), 830–842. https://doi.org/10.1002/eco.1686

Wang, M. B., & Zhang, Q. (2009). Issues in using the WinRHIZO system to determine physical characteristics of plant fine roots. *Acta Ecologica Sinica*, *29*(2), 136–138. https://doi.org/10.1016/j.chnaes.2009.05.007

Watt, M., McCully, M. E., & Canny, M. J. (1994). Formation and stabilization of rhizosheaths of Zea mays L. *Plant Physiology*, *106*, 179–186.

Watt, M., Silk, W. K., & Passioura, J. B. (2006). Rates of Root and Organism Growth, Soil Conditions, and Temporal and Spatial Development of the Rhizosphere. *Annals of Botany*, *97*, 839–855. https://doi.org/10.1093/aob/mcl028

Wood, D. M., Diambra, A., & Ibraim, E. (2016). Fibres and soils: a route towards modelling of root-soil systems. *Soils and Foundations*, *56*(5), 765–778.

Wulfsohn, D., & Nyengaard, J. R. (1999). Simple stereological procedure to estimate the number and dimensions of root hairs. *Plant and Soil*, *209*, 129–136. https://doi.org/10.1023/A:100450083

3. Hydro-mechanical framework to predic roots effects on a compacted silty soil

3.1 Abstract

In this study, a hydro-mechanical multi-scale framework was built to predict the behaviour of a compacted silty soil penetrated by roots. The framework includes a model proposed to predict the soil micro-structure evolution along hydraulic paths and depending on roots geometrical features. The latter has been calibrated according to pore size distribution curves obtained from bare and vegetated samples, at different hydraulic states. Total volume change behaviour under hydro-mechanical trajectories was introduced to the framework and calibrated through shrinkage and oedometer tests. Finally, a soil water retention law for double-porosity soils was calibrated on bare soil data and used in conjunction with the rest of the framework to predict the vegetated soil hydro-mechanical response. Hence, the framework has been validated thanks to the prediction of several water retention curves and saturated permeability values obtained from vegetated soil samples. A statistical analysis quantified the good quality of the modelled results.

3.2 Introduction

So far, engineering models predicting roots effects on soil hydro-mechanical behaviour were often based on empirical correlations between macroscopic observations (air-entry value - retention capacity – saturated permeability change), roots geometrical features and soil initial compaction state. These relationships are built by means of realistic and unassessed theories that formulate roots effects on soil micro-structure: void ratio changes, soil fissuring, pores clogging, roots decay ((Ng et al., 2016; Ni et al., 2019b)). Anyway, there are few studies on roots direct effects on soil fabric: among them, (Scholl et al., 2014b) deduced the effects of roots on the pore size distributions of a fine-grained soil by an inverse estimation while (Koebernick et al., 2017) performed high-resolution X-ray micro-tomography on a loose silty sand, focusing on a single soil-root interface.

Models coming from agronomy, instead, are more focused on linking vegetated soil's hydraulic behaviour to chemical alterations induced by roots on soil structure (organic matter increase, water surface tension decrease) but neglecting the mechanical implications of roots growth (fissures/interfaces generations, soil grains displacements, …) ((Karup et al., 2017; Ohu et al., 1987; Read et al., 2003)).

To unify the different fields of knowledge and the multi-physics processes involved in the problem, plants effects on the hydro-mechanical behaviour of a silty soil have been observed at different scales and hydraulic states in the chapter 2. Important alterations in terms of water retention properties, permeability and shrinkage upon drying have been evidenced. The causes of these changes were clear after evaluating the soil multi-modal pore-size distribution, before and after roots growth. The use of complementary techniques (X-ray CT and MIP) allowed to have an overview of the main phenomena occurred within different porosity ranges: fissures generation due to roots growth and opening upon drying, micro-pores clogging by fine roots and released fluids (roots mucilage). For each sample, roots geometrical features have been identified.

Given these observations, a hydro-mechanical framework is proposed to predict the water retention curve and the soil water permeability of a vegetated silty soil, by considering microstructural changes induced by roots on soil. In the framework, a model proposed by (E. Romero et al., 2011) is readapted to predict the evolution of the micro- and macro-porosity along water content changes and to include dependence on the characteristics of the roots. The readapted model was then included within a constitutive law for double-porosity soils ((Dieudonné, Levasseur, Charlier, Della Vecchia, & Jommi, 2013)). Observed soil volumetric strains due to mechanical stresses and suction variations are also considered through the laws proposed by (Alonso et al., 1990). The model is calibrated with bare soil retention measurements and validated by predicting the retention measurements carried out on three vegetated samples and the soil water permeability measurements done on vegetated and bare soil.

3.3 Micro-scale model formulation and calibration

The microstructural model is based on the soil pore-size distribution (PSD, example in Figure 18) obtained in the chapter 2 for bare and vegetated compacted soil. For each curve, the final cumulated void ratio was assumed as the actual total void ratio of the sample. For the PSD curves evaluated under unsaturated conditions, this value was always below the void ratio at compaction (e0 in Figure 18) , due to the shrinkage occurred upon drying. The intra-aggregates (or microstructural) void ratio em was calculated on the PSD curves as the cumulated void ratio below the pore size of 5 μm. A similar value for characterizing the clay aggregates was used by (Enrique Romero, 2013). The evolution of this variable along water ratio changes ($e_w = \rho_{sw}/\rho_w$) is presented in Figure 19. In the

same plot is showed the evolution of the total void ratio, measured with paraffin tests in the chapter 2. The total and the intra-aggregates void ratio are linked by the equation:

$$e = e_m + e_M \qquad 8$$

where e_M is the inter-aggregates (or macrostructural) void ratio. Close to each vegetated e_m point, it is indicated the value of root length density, R_{ld} (ratio between the total root length and the bulk soil volume) evaluated for the correspondent sample.

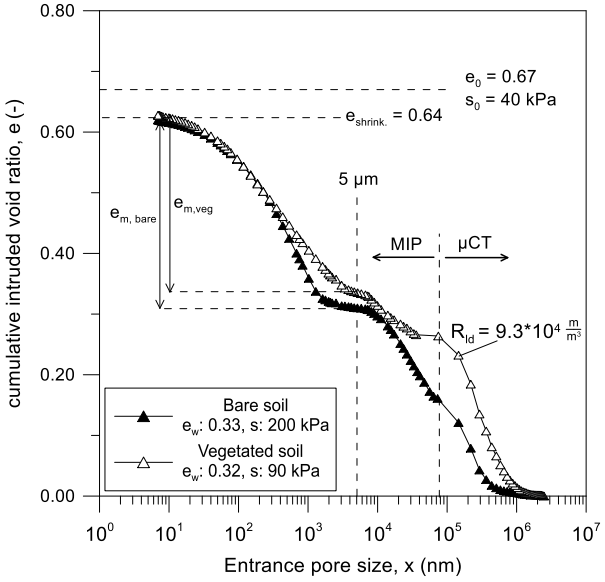

Figure 18 PSD comparison of bare and root-penetrated soil at a given water ratio. Root length density within the vegetated soil is indicated in the graph. Data from the chapter 2.

This parameter was evaluated by scanning the washed roots with the software WinRHIZO (see chapter 2 for further details). Its value within the different samples is summarised in Table 7, jointly with other root features (samples: *veg1* to *veg5*). For the vegetated soil points (Figure 19), an increase of the macrostructural void ratio and a decrease in the intra-aggregate values was observed along drying. To formalize this reduction, the law proposed by (E. Romero et al., 2011) was adapted as follows:

$$e_m = e_m^* + (\beta + \gamma)e_w - \alpha R_{ld} \qquad 9$$

In which γ and αR_{ld} are the model additions. The product αR_{ld} is indicating the quantity of macropores generated by a given root quantity. The parameter γ controls the coupled effects of roots presence and water ratio variations (i.e. soil fissures opening due to soil and roots shrinkage and clogging due to roots swelling on wetting (phenomenon observed by (Carminati et al., 2013)), evolution of micropores along drying and due to chemical activities. The parameter γ is summed to β, which is the slope of the microstructural evolution along the water ratio. According to (Enrique Romero, 2013), β depends on the total specific surface of the different clay particles. The parameters α and γ were calibrated by minimizing the mean squared error between measurements and values of e_m predicted

by the equation 9 (R^2 = 0.96): their values are $7*10^{-7}$ and 0.030, respectively. A good correlation (R^2 = 0.96) was also found expressing the model as function of the root volume ratio, R_v, which is the ratio between roots total volume and bulk soil volume:

$$e_m = e_m^* + (\beta + \gamma)e_w - \alpha R_v \qquad 10$$

For which, calibrated values for α and γ were 2.2 and 0.028 respectively. The reason of this double formulation is the fact that R_{ld} could make it easier to extend the model to other types of plants whereas the R_v is more easily measurable in field applications involving plants with similar characteristics to those studied.

Table 7 Root parameters found with WinRhizo scans (mean, variance and peak root diameters were evaluated as parameters of a gamma distribution of probability).

sample name	**testing soil water ratio (-)**	**R_{ld} root length density (m/m^3)**	**R_v root volume ratio (m^3/m^3)**	**mean root diameter (mm)**	**peak root diameter (mm)**	**soil bulk volume (mm^3)**	**tips density (n.tips/ mm^3)**
veg1	0.23	$5.0*10^4$	0.003	0.41 (σ^2 = 0.04)	0.31	83600	0.04
veg2	0.13	$4.6*10^4$	0.004	0.38 (σ^2 = 0.03)	0.30	35000	0.04
veg3	0.32	$9.3*10^4$	0.008	0.44 (σ^2 = 0.05)	0.32	80000	0.07
veg4	0.60	$4.0*10^4$	0.003	0.42 (σ^2 = 0.01)	0.40	149250	0.02
veg5	0.47	$8.1*10^4$	0.010	0.47 (σ^2 = 0.07)	0.32	125000	0.08
oed1R	0.60	$4.7*10^4$	0.010	0.44 (σ^2 = 0.04)	0.35	1237002	0.02
oed2R	0.32	$1.1*10^5$	0.014	0.31 (σ^2 = 0.02)	0.25	1237002	0.04
perm1R	0.60	$3.5*10^4$	0.007	0.39 (σ^2 = 0.05)	0.25	1469122	0.04
sample6	0.28-0.60	$7.6*10^4$	0.010	0.41 (σ^2 = 0.06)	0.25	1237002	0.04
sample13	0.08-0.60	$5.0*10^4$	0.008	0.34 (σ^2 = 0.03)	0.24	1237002	0.01
sample 17	0.28-0.60	$1.7*10^5$	0.015	0.30 (σ^2 = 0.002)	0.29	1237002	0.03

The former theory comes from the assumption that soil fissuring is occurring mainly at the soil-root interface and that fissures volume is depending mainly on the length of the interface rather than on

other roots properties (such as diameter). For reasons of brevity, the rest of the study will be presented in terms of R_{ld}, however the same results have been obtained in terms of R_v.

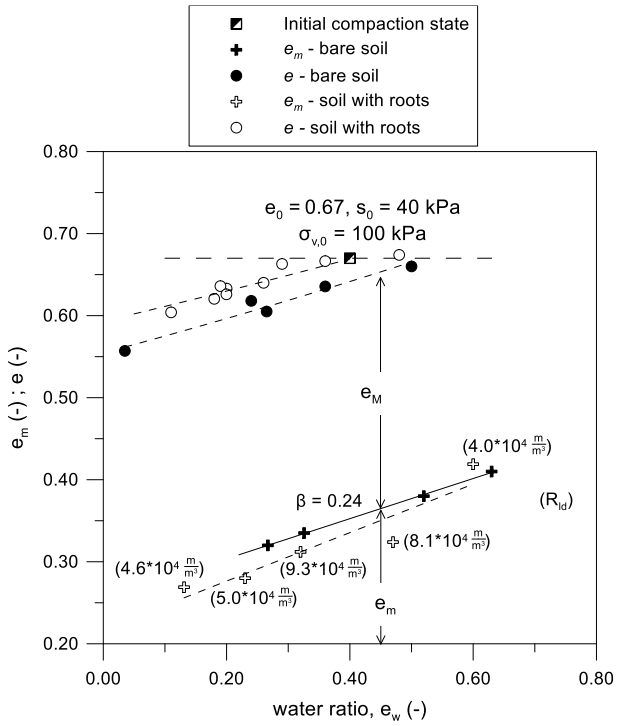

Figure 19 Microscopic and total void ratio evolution along water ratio, during a drying phase. Root length density values are plotted jointly to their relative points. Data from chapter 2.

3.4 Macroscopic hydro-mechanical framework

Once the microstructural void ratio law is formalised, it is necessary to introduce the equations describing macroscopic volumetric deformations, to fully characterize the state and stress (e, e_m, s, e_w) evolution along hydro-mechanical trajectories. In this regard, shrinkage and oedometer tests were carried out on the bare and root-permeated soil.

Paraffin tests results are showed in Figure 20a: specimens were retrieved from soil pots compacted at initial suction $s_0 \approx 40$ kPa, then wetted under unconfined conditions and tested along drying (chapter 2). For the case of vegetated pots, 30-millimetres soil cubes were extracted between the different plant individuals and their amount of roots is expressed as R_{ld} in Figure 20. In the case of vegetated soil, void ratio was calculated as $e = V_v/V_s$ and according to the scheme in Figure 20b (see chapter 1 for more information). Soil coming from root-permeated pots remained at higher void ratios than bare soil, with respect to suction changes. Volume deformations upon drying were formalised according to the law proposed by (Alonso et al., 1990):

$$d\varepsilon_{vs}{}^{el} = \frac{\kappa_s}{(1+e)} \frac{ds}{(s+p_{at})} \, , s < s_0 \qquad 11$$

$$d\varepsilon_{vs} = \frac{\lambda_s}{(1+e)} \frac{ds_0}{(s_0 + p_{at})}, s > s_0 \quad (12)$$

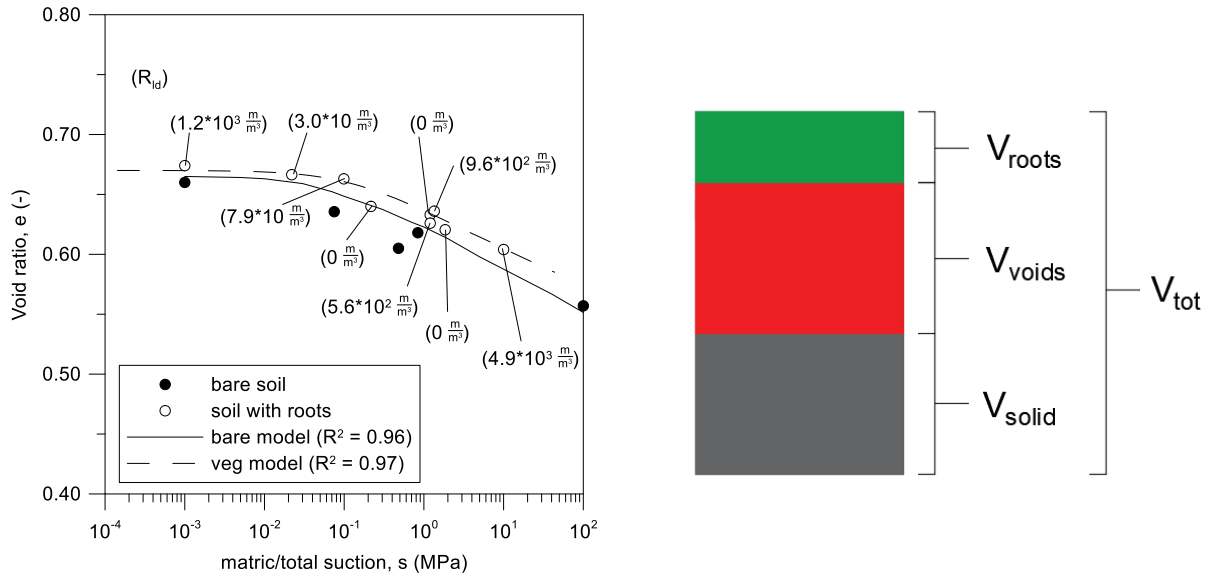

a *b*

Figure 20a Void ratio evolution along suction. Root length density values are plotted jointly to their relative points. Data from the chapter 2. B) scheme of volumetric phases in soil to calculate the void ratio as Vvoids/Vsolid

It is assumed that only elastic strains occurred for suction below the compaction value, s_0. The parameters κ_s and λ_s are the stiffness values with respect to suction changes along elastic and virgin states, e the void ratio and p_{at} the atmospheric pressure. Stiffness calibrated parameters are summarised in Table 8.

Table 8 Soil stiffness parameters calibrated for the laws formalized by (Alonso et al., 1990)

	Bare soil	**Soil with roots**
κ	0.0063	0.005
λ	0.065	0.026
κ_s	0.0015	0.001
λ_s	0.011	0.009

Results from large oedometer tests (diameter 150 mm, height 70 mm) with and without roots are presented in Figure 21. Samples were compacted at a void ratio e ≈ 0.73, water ratio ew ≈ 0.40, suction s0 ≈ 40 kPa and at a net mean stress p0 ≈ 25 kPa. Roots were let to grow inside the soil after compaction and under saturated conditions. The tests were carried out then at a constant water ratio $e_w \approx 0.32$ ($S_r \approx 0.44$). Initial suction was 190 kPa and 150 kPa in the bare and root-permeated sample, respectively. Root length density within the tested sample is showed in the Figure 21 (other roots

features are expressed in Table 7 - sample *oed2R*). The yielding stress in the vegetated sample appeared lower than that of bare soil, probably due to fissures generated by roots and collapsed in the first stages of loading. Nevertheless, the vegetated soil exhibited a higher stiffness than the bare one, especially in the virgin part of the curve.

Elastic and total volume strains upon loading were interpreted according to (Alonso et al., 1990):

$$d\varepsilon_{vp}{}^{el} = \frac{\kappa}{(1+e)}\frac{dp}{p}, p < p_0 \quad 13$$

$$d\varepsilon_{vp} = \frac{\lambda(s)}{(1+e)}\frac{dp_0}{p_0}, p > p_0 \quad 14$$

Where κ and $\lambda(s)$ are the soil stiffness against changes in net mean stress along elastic and virgin states. Calibrated values are summarised in Table 8.

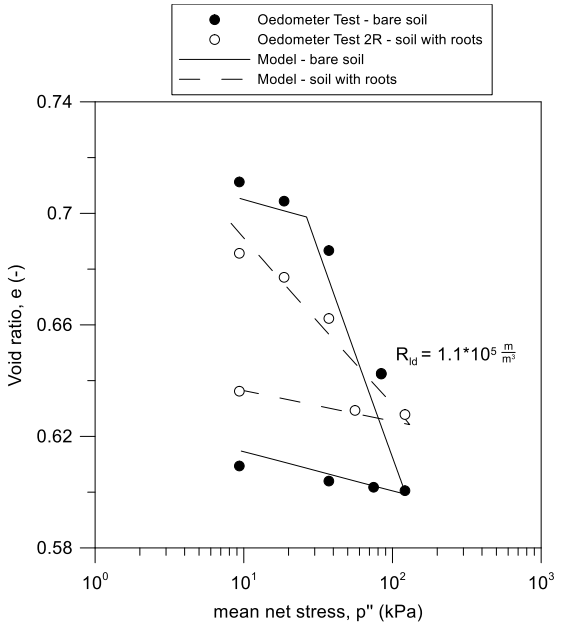

Figure 21 Oedometer tests, carried out at constant water content, with and without roots. Measurements and hydro-mechanical modelling.

As it's possible to observe in Figure 20 and Figure 21, the equations are well representing the observations. The oedometer tests results were predicted considering suction variations within the samples due to volumetric deformations at constant water ratio. Macroscopic volumetric strains, expressed by equations 11 to 14, are not depending directly from the PSD of the material. The evolution of microstructural and macrostructural void ratio is evaluated at each hydraulic state and loading step assuming that intra-aggregates void ratio depends only on the water content and is not affected by total void ratio changes ((Enrique Romero, 2013)).

Last component of the framework is a law to predict the water retention behaviour in double porosity soils ((Dieudonné et al., 2013)). The macrostructural and microstructural parameters of the curve have been calibrated as showed by the algorithm in Figure 22.

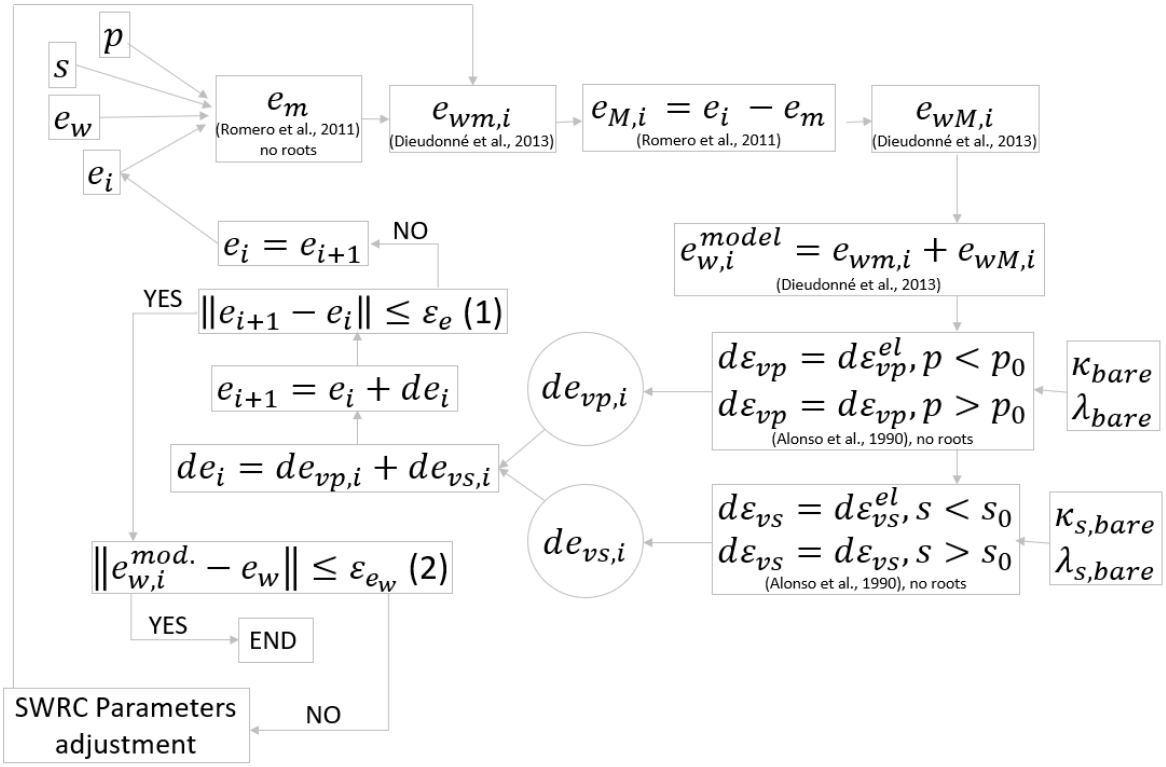

Figure 22 Algorithm used for the calibration of the SWRC parameters through the hydro-mechanical framework and using the bare soil measurements

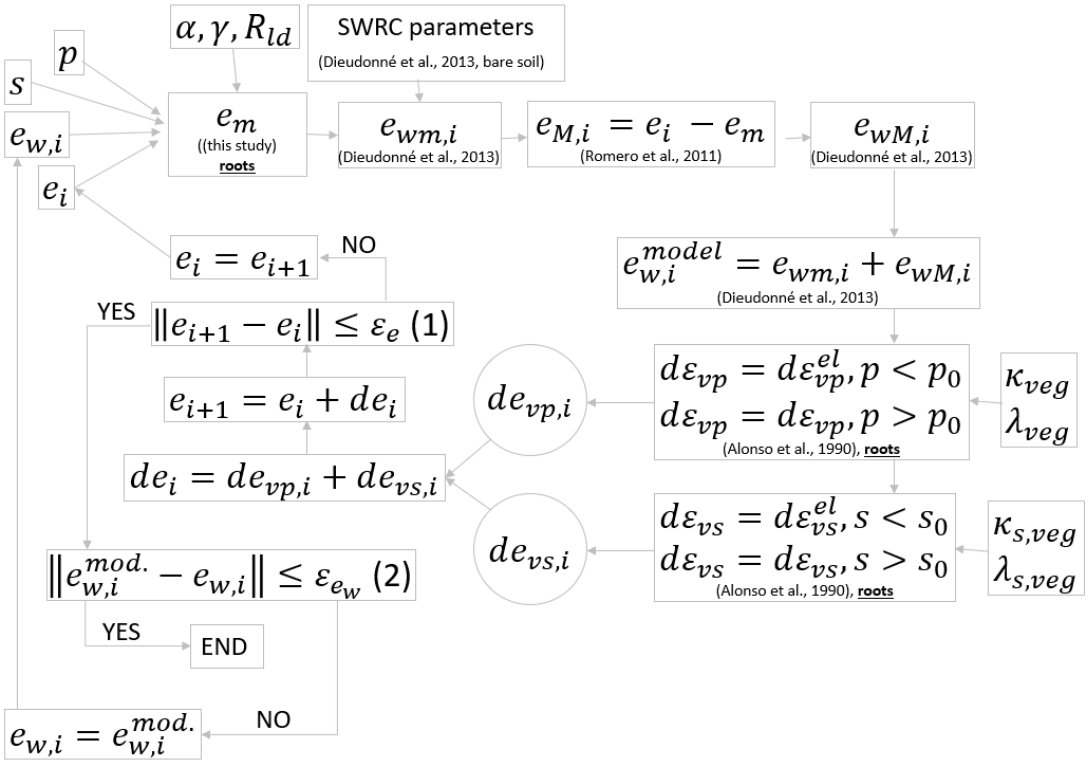

Figure 23 Algorithm for predicting the SWRC curve for the vegetated soil, through the hydro-mechanical framework

Void ratio at saturation was assumed as e = 0.67 ($p \approx 90$ kPa). For each suction value (s), inputs of the i-steps iterative process are the mean net stress (p), the water ratio (e_w) measured for the bare soil in the chapter 2, and a tentative void ratio (e_i). The variables $e_{w,m}$ and $e_{w,M}$ are the water ratios within the micro- and the macro-voids, respectively. Variations of mean stress were not included during the calibration. Suction changes along drying were considered to compute volumetric strains according to equations 11 and 12. Iterations continued until void/water ratios predicted were in good agreement with the tentative/measured ones. The convergence parameters ε_e and ε_{ew} were equal to 0.001. The calibrated parameters of the retention curve ((Dieudonné et al., 2013)) are summarised in Table 9.

Table 9 Parameters calibrated for the double-porosity SWRC law formalized by (Dieudonné et al., 2013). *Calibration from bare soil retention measurements*

$\alpha_1^{(m)}$	$\alpha_2^{(m)}$	$n^{(m)}$	$m^{(m)}$	$\alpha_1^{(M)}$	$\alpha_2^{(M)}$	$n^{(m)}$	$m^{(M)}$
10^{-1}	10^{-10}	5.92*10	$4.23*10^{-3}$	$7.38*10^{-4}$	$7.88*10^{-3}$	3.23*10	$1.36*10^{-1}$

3.5 Model validation and performance

Once the retention curve parameters have been calibrated, they were used to predict the behaviour of a soil presenting a given root length density (*samples 6-13-17* in Table 7). Equation 9 was used in the framework (algorithm in Figure 23) to predict the micro-structural void ratio (e_m) evolution. The parameters calibrated by shrinkage and oedometer tests for the vegetated soil were used within equations 11 to 14 to predict volumetric strains due to loads and drying. Iterations lasted until water and void ratios predicted were in good agreement with the tentative initial values, for a given suction s (Figure 23). The curves predicted by the H-M framework, for the bare and for a vegetated sample, are showed in Figure 24, jointly with the points measured in the chapter 2 and other points measured on wetting after the drying phase.

The drying behaviour was reproduced by assuming elastic volumetric deformations below suctions of 40 kPa and elasto-plastic strains above. The wetting phase was reproduced by the framework, assuming a purely elastic strain behaviour (s_0 moved to 100 MPa consequently to drying, as formalized by the suction increase yielding surface in (Alonso et al., 1990)). On wetting, the vegetated soil recovers higher water ratios than the bare soil, due to its higher stiffness to shrinkage. This behaviour was less evident by just observing the measurements.

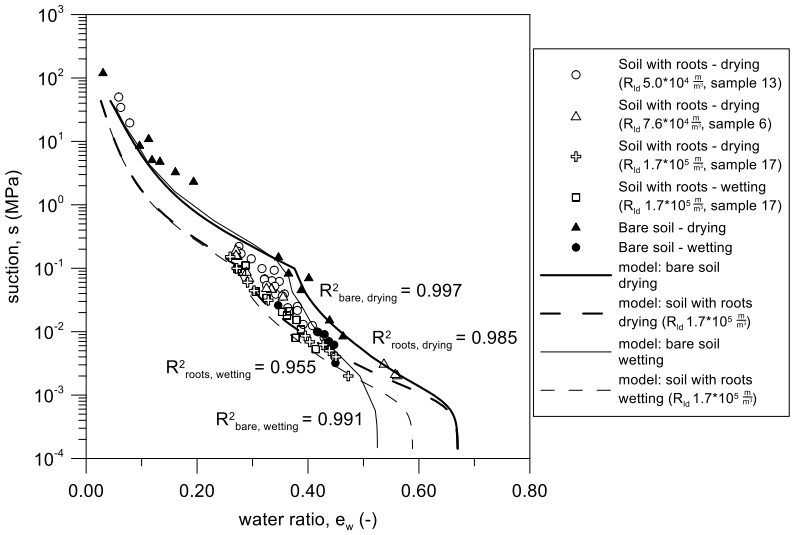

Figure 24 Modelled Soil water retention curves on drying and wetting. Measurements from the chapter 2.

A good agreement between retention model and measurements is evident in the figure. For the remaining samples, their correspondent retention curve was also modelled by changing the input R_{ld} in the algorithm. The coefficients of determination (R^2) were calculated considering the different measurements obtained for the three vegetated samples and the bare soil tested (Table 10). The coefficient of determination slightly decreases as the R_{ld} increases. This may be due to several variables that need further investigation. The model might have overestimated the fissures volume when dealing with high values of root length density, since it is not considering possible "group effects" of roots, depending on their different architecture. Indeed, the same length density can produce different volumes of fissures, if roots are more sorted or spaced. Also, the model is not considering the root diameters distribution, which may have a role in the generation of fissures. Nevertheless, the model is capable to well predict the behaviour of a vegetated soil within a very large range of root length density values. Further investigations are needed to find a dependency of α and γ on the other abovementioned root features.

The framework predicts also changes in the retention properties due to confinement stress changes, according to the algorithm in Figure 23. As example, bare and vegetated soil retention curves are compared when loading from $\sigma_{v,0} \approx 100$ kPa (which is the stress at which samples for retention measurements were compacted) to $\sigma_{v,0} \approx 730$ kPa. The lower compressibility showed by the vegetated soil allows it to keep a higher porosity and then, to develop higher water ratios at saturation (Figure 25).

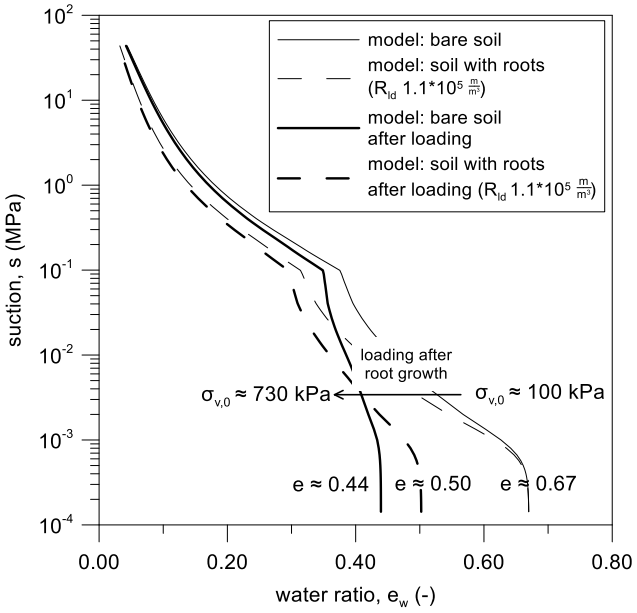

Figure 25 Prediction of bare and vegetated swrc before and after loading

The micro-scale model (equation 9) was used also to predict measurements of permeability carried out in the chapter 2 and by (Oorthuis et al., 2018) (Figure 26a).

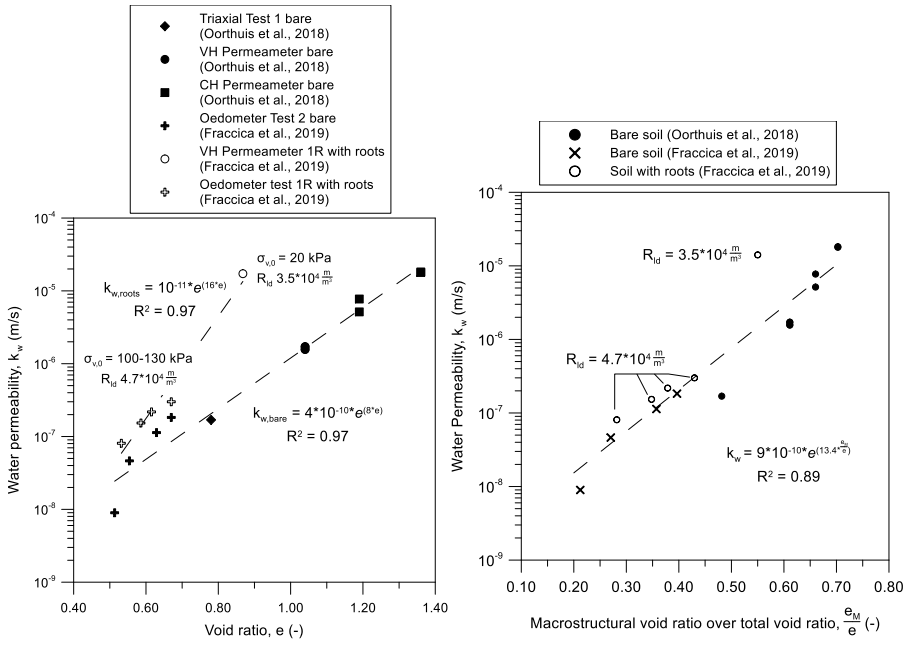

Figure 26 Soil water permeability of bare and root-permeated soil as function of a) the void ratio and b) the degree of macro-pores. For the vegetated soil, the degree of macro-pores was calculated considering the measured root length density and the void ratio at compaction.

The quantity of macropores was evaluated for the samples in which permeability was measured, knowing their roots length density (samples *oed1R* and *perm1R* in Table 7). Soil water permeability was plotted as function of the ratio between the macrostructural and the total void ratio. The quantity of macropores as a fraction of the total volume of voids has a direct influence on soil permeability:

as it can be seen in Figure 26b, the results obtained by an oedometer test with roots done under saturated conditions (*oed1R*) are well aligned with the bare measurements. The point representing the permeability measured by the permeameter (*perm1R*) is the most far from the tendency, presenting higher values with respect to those predicted. This case is evidencing another limitation of the model: the equation developed, in fact, is not considering the number of different roots within the samples. This last feature is expressed as *tips density*, which is given by the ratio between the number of root tips and the soil bulk volume (see Table 7). Given the same root length density, the different number of roots developed may affect the total volume of fissures generated within the soil. Indeed, considering Table 7 and Figure 26a, one can note that, even if permeameter test 1R and oedometer test 1R have a similar root length density and volume ratio, the *tips density* in the permeameter test 1R is two times higher than the other test. Finally, the model does not even include the effect of the initial void ratio (higher in the permeameter) on plants development and growth. The lower confinement imposed by soil grains to plant roots may have amplified the phenomenon of fissuring with respect to what is happening within soils more compacted.

Table 10 Root length density, coefficients of determinations and number of measurements of each modelled SWRC

swrc	**R_{ld} (m/m^3)**	**R^2 (model/measurements)**	**n. of measurements**
bare drying	-	0.996	13
bare wetting	-	0.991	7
sample 13 (roots) drying	$5.0*10^4$	0.996	18
sample 6 (roots) drying	$7.6*10^4$	0.989	11
sample 17 (roots) drying	$1.7*10^5$	0.985	15
sample 17 (roots) wetting	$1.7*10^5$	0.955	12

3.6 Conclusions

Information about soil microstructure and root properties have been used to develop a model able to predict the macro- and micro-pores volume generated by a certain root quantity. The parameters calibrated are controlling soil-root chemo-hydro-mechanical interactions and they are dependent on the type and on the architecture of roots and on the soil nature. Observations at the specimen scale (shrinkage and mono-dimensional loading) made possible to develop a hydro-mechanical framework to predict soil volumetric strains. A double-porosity model for soil water retention curve was coupled

to the microstructural vegetated model proposed in the study and to the macroscopic framework. The parameters for the retention curve were calibrated on the bare soil measurements and used to predict the behaviour of the soil with roots. The introduction of laws defining soil yielding upon suction and loading changes allowed to predict both drying and wetting retention curves. Soil behaviour was also simulated after a certain loading stage, evidencing contrasting tendencies with respect to what observed at lower confinement. Macropores increase predicted by the new model allowed to explain the increase of permeability observed within the vegetated samples. The model predicts well the behaviour of a silty soil penetrated by roots and it can be easily extended to other type of soils and plants.

3.7 Acknowledgments

The authors wish to acknowledge the support of the European Commission via the Marie Skłodowska-Curie Innovative Training Networks (ITN-ETN) project TERRE ‘Training Engineers and Researchers to Rethink geotechnical Engineering for a low carbon future’ (H2020-MSCA-ITN-2015-675762). Micro-tomography scans were performed in the Laboratory of Microscopy and Computed Micro-tomography at CENIEH facilities (Burgos, Spain) with the collaboration of CENIEH staff. Mercury intrusion porosimetry was performed at the UPC Geotechnical Laboratory with the help of Rodrigo Gómez. Alessandro Fraccica also wishes to acknowledge the fruitful discussions with the members of TERRE and SMUCPHY projects.

References

Alonso, EE; Gens, A and Josa, A. 1990. “A constitutive model for partially saturated soils.” *Géotechnique* no. 340: 405–30.

Carminati, Andrea et al. 2013. “Do roots mind the gap ?” *Plant and Soil*367: 651–61.

Dieudonné, Anne-Catherine et al. 2013. “A water retention model for compacted clayey soils.” *3rd International Symposium on Computational Geomechanics (ComGeo III)*: 23–31.

Karup, D et al. 2017. “Prediction of the soil water retention curve for structured soil from saturation to oven-dryness.” *European Journal of Soil Science*68: 57–65.

Koebernick, Nicolai et al. 2017. “High-resolution synchrotron imaging shows that root hairs influence rhizosphere soil structure formation.” *New Phytologist*216: 124–35.

Ng, CWW et al. 2016. “A new and simple water retention model for root-permeated soils.” *Géotechnique Letters* no. 16: 106–11.

Ni, JJ; Leung, AK and Ng, CWW. 2019. “Modelling effects of root growth and decay on soil water retention and permeability.” *Canadian Geotechnical Journal*56: 1049–55.

Ohu, JO et al. 1987. “Prediction of water retention characteristics from soil compaction data and organic matter content.” *Journal of Agricultural Engineering Research* no. 138: 27–35.

Oorthuis, Raül et al. 2018. “Monitoring of a full-scale embankment experiment regarding soil-vegetation-atmosphere interactions.” *Water (Switzerland)*10: 688.

Read, DB et al. 2003. “Plant roots release phospholipid surfactants that modify the physical and chemical properties of soil.” *New Phytologist*157: 315–26.

Romero, E; Della Vecchia, G and Jommi, C. 2011. “An insight into the water retention properties of compacted clayey soils.” *Géotechnique* no. 461: 313–28.

Romero, Enrique. 2013. “A microstructural insight into compacted clayey soils and their hydraulic properties.” *Engineering Geology*165: 3–19.

Scholl, P et al. 2014. “Root induced changes of effective 1D hydraulic properties in a soil column.” *Plant and Soil* nos. 1–2381: 193–213.

4. Mechanical behaviour of a vegetated soil at different hydraulic states

4.1 Abstract

The objective of this study is to assess the effects of *Cynodon Dactilon* roots on the shear and tensile strength of a compacted silty soil, under different hydraulic states and after different plants growing periods. Triaxial compressions were carried out within large cell equipment to evaluate the shear strength increase and the volumetric deformations induced by roots. A new equipment was developed to evaluate soil tensile resistance by pulling at constant water content.

Soil shear and tensile resistance increased with suction jointly with an accentuation of its fragile behaviour. Vegetated soil presented a greater resistance than that without roots and two different stress-displacement responses, depending on whether it was dry or moist. Moreover, roots growing periods had an impact on the results.

Roots slightly affected soil friction angle: results have been interpreted as an increase of cohesion and according to different constitutive laws, considering soil suction, degree of saturation and roots geometrical and mechanical features. A good agreement was found with the cohesion tendency obtained through triaxial tests carried out on the same soil and plant. Finally, a correlation was found between the increase in apparent cohesion, the roots properties and the soil hydraulic state. Roots provided a mechanical reinforcement to the soil even if they produced changes on the soil structure, which affected the macroscopic mechanical behaviour at high values of suction.

4.2 Introduction

Global warming has led to longer periods of drought and more frequent heavy rains in the recent decades. These events are particularly damaging in fine-grained soils: very frequent and extensive drying and wetting cycles generate fissures and alter their hydro-mechanical and structural properties (Albrecht & Benson, 2001; Cordero, Useche, Prat, Ledesma, & Santamarina, 2017). This affects the behaviour of slopes and embankments made with these kind of soils, causing a faster response to rainfall, affecting their behaviour at the service state and producing phenomena of superficial or deep instability (Sánchez, Wang, Briaud, & Douglas, 2014; Vardon, 2014).

In the framework of sustainable engineering it is important to understand which is the role of vegetation in affecting the hydro-mechanical behaviour of geotechnical structures (Oorthuis et al., 2018). Plant roots contribute to enhance soil shear resistance thanks to their tensile strength (Mickovski et al., 2009; Wu, McKinnell III, & Swanston, 1979). So far, the most commonly used laboratory test to quantify this reinforcement is the direct shear one (Ghestem, Veylon, Bernard, Vanel, & Stokes, 2014; Gonzalez-Ollauri & Mickovski, 2017; Mickovski et al., 2009; Veylon, Ghestem, Stokes, & Bernard, 2015; Yildiz, Graf, Rickli, & Springman, 2018). (Gonzalez-Ollauri & Mickovski, 2017) carried out tests at different hydraulic states, finding out that suction might have a negative effect on roots mechanical reinforcement.

During mechanical tests present in literature, volumetric deformations upon shearing observed within vegetated soils were generally neglected. Moreover, there was no insight on how soil micro-structural changes generated by roots growth (Fraccica, Romero, & Fourcaud, 2019) could have affected the overall mechanical behaviour.

The increase in shear resistance generated by plants was often interpreted as an increase in its apparent cohesion, as minimal effects of the roots on the friction angle have been observed. Apparent cohesion represents soil shear resistance at null confinement: due to difficulties to reach this stress condition, it is often estimated by linearizing the soil failure envelope. This procedure implies neglecting the non-linearities and the risk of overestimating soil strength. Moreover, it is important to quantify soil shear strength increase at low confinement, since vegetation occupies the most superficial part of the ground. This is the reason for separately assess soil shear and tensile strength with laboratory equipment.

Few example of bare soil tensile strength assessment were provided in literature (Lakshmikantha, Prat, & Ledesma, 2012). The authors observed a peak and a subsequent decrease of tensile strength in the material, below a certain value of degree of saturation: this was due to a decrease of the number of capillary bridges inside the soil despite an increase in suction. (Divya, Viswanadham, & Gourc, 2014) performed tensile tests on soil reinforced by natural fibres manually distributed within the matrix. To our knowledge, there is no literature on tensile tests at different hydraulic states on vegetated soils.

The study of roots reinforcement models gives an insight on the plant features that could play a major role in increasing soil shear and tensile strength. The first analytical model to correlate the increase in soil cohesion to typical plant parameters is the model given by (Wu et al., 1979): it was calibrated from in situ large direct shear tests, root diameter measurements in escarpment areas of landslides, tensile tests on singular roots and back-analysis. In this model it is assumed that all roots fail at the same time: this prediction is unlikely, since it is known that not all soil roots are equal and that their

resistance varies according to their diameter and the rupture mechanism due to their spatial arrangement in the soil. Nevertheless, the use of the plant traits included in this model (roots tensile strength and area), was proved to give good predictions of the results, in more recent investigations (Mickovski et al., 2009). Roots reinforcement also depends on soil hydraulic conditions: (Pollen, 2007) observed that in a humid soil the roots have a greater tendency to be extracted by sliding (pull-out) while in a drier soil they fail by breakage.

In this regard, an investigation, at different hydraulic states, has been carried out to characterize shear and tensile strength of a silty sand lightly compacted and penetrated by a turf-grass (*Cynodon Dactilon*). Direct tensile, shrinkage and triaxial tests have been performed on bare and vegetated soil. Roots geometrical and mechanical properties were characterized. A constitutive law was proposed to predict the increase in cohesion knowing the properties of roots, soil suction and saturation degree of the soil.

4.3 Soil properties and compaction

The laboratory characterization of the material retrieved in situ and sieved for this study shown in Figure 27 and By means of the granulometric curve it has also been possible to estimate the average diameter of pores in the soil as:

$$d_{pores,aver.} = 0.3 * d_{50,solids} \quad (15)$$

where $d_{50,solids}$ is the solid particle size corresponding to 50% of soil passing fraction. According to this formula, the average pore size is 0.10 mm. This implies that roots larger than this diameter will have to create fissures in the material during their growth.

Table 11 (Fraccica et al., 2019; Oorthuis et al., 2018).

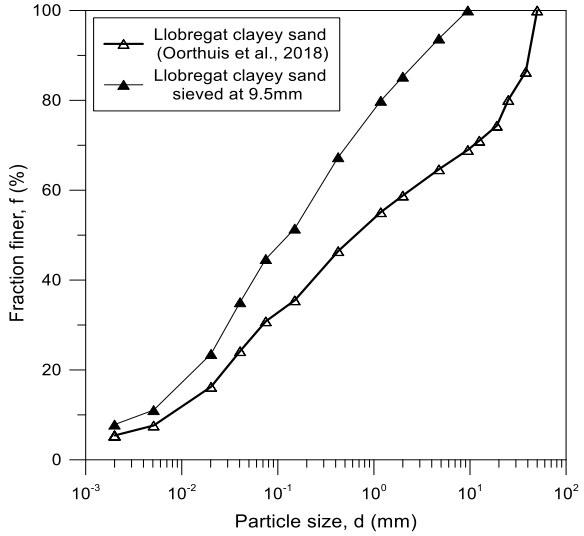

Figure 27 Particle size distribution of non-sieved soil (Oorthuis et al., 2018) and sieved soil for the laboratory study (in Fraccica et al. (2019)).

By means of the granulometric curve it has also been possible to estimate the average diameter of pores in the soil as:

$$d_{pores,aver.} = 0.3 * d_{50,solids} \quad (15)$$

where $d_{50,solids}$ is the solid particle size corresponding to 50% of soil passing fraction. According to this formula, the average pore size is 0.10 mm. This implies that roots larger than this diameter will have to create fissures in the material during their growth.

Table 11 Soil properties - material used in the embankment a(Oorthuis et al., 2018) b(Fraccica et al., 2019).

Soil property	*Value*
Soil fraction < 2 mm (%)	58.8[b]
Soil fraction < 75 μm (%)	30.8[b]
Soil fraction < 2 μm (%)	5.4[b]
Liquid limit (%)	29.5-34.4[a]
Plasticity index (%)	9.6-13.5[a]
Density of solids, ρ_s (Mg/m^3)	2.65-2.70[a]
Hydraulic conductivity (m/s)	$7.7*10^{-8} – 1.8*10^{-7}$ [a]

Samples for triaxial tests were prepared by statically compacting the soil on the dry side of the optimum, as indicated by the point A in Figure 28, obtaining a void ratio, e ≈ 0.67 at a water content w ≈ 15%. Samples for direct tensile tests were prepared in order to have an initial void ratio e ≈ 0.60 (and water content w ≈ 15%) which is close to average values obtained in triaxial tests during the shearing phase. After compaction, the soil was wetted under unconfined conditions up to a water content w ≈ 21% to allow plants growth. In fact, the process of germination and growth of the plants was carried out entirely in correspondence with the state characterized by the letter B in the Figure 28. Samples were then left to dry to be tested under triaxial compression and pulling at different water contents (points between B and C, Figure 28). Bare samples were subjected to the same compaction and hydraulic trajectory.

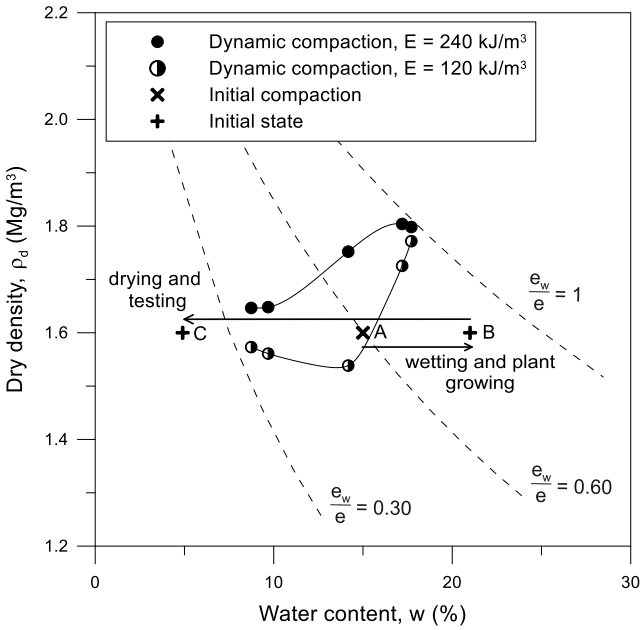

Figure 28 Dry density – water content table. Compaction and hydraulic path followed in this study.

Samples for triaxial compression tests were compacted in PVC moulds (represented in Figure 30) (Φ 200 mm and h 400 mm) whereas samples for direct tensile tests were prepared in ABS 3D-printed moulds (Φ 100 mm and h 40 mm) indicated in Figure 29.

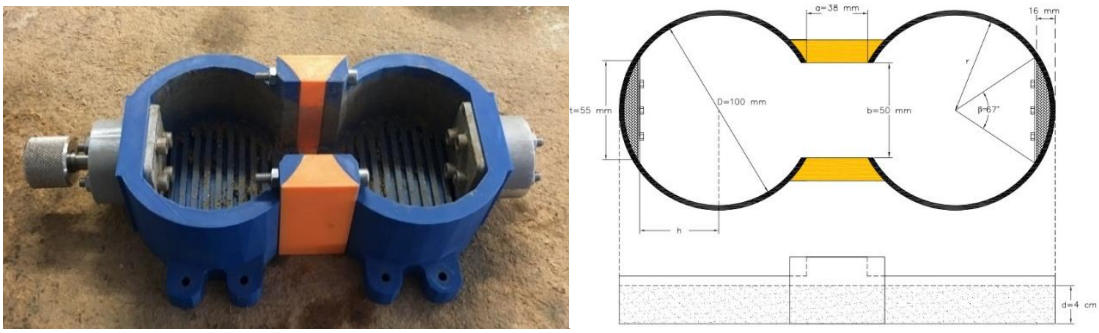

Figure 29 Moulds for direct tensile and shrinkage tests

4.4 Roots growth and characterization

The growth of plants took place inside the moulds (Figure 29 and Figure 30), after soil compaction. The seeds of the plants are inserted into the soil through holes spaced 40 mm apart and with a seeding density of 34 g/m^2. Throughout growth, the soil was maintained at a constant water content (w = 21%) through an irrigation system and suction was controlled by a tensiometer, to facilitate root development and not induce hydraulic trajectories different to those followed for the bare soil.

Figure 30 Plants seeding in 40 mm spaced holes and after growth in moulds

Plants in triaxial tests samples were left to grow for 8 months while, in direct tensile moulds, growth period varied from 1 to 3 months. This choice aimed at finding out the effect of roots growth on the tensile strength of the soil.

After triaxial and tensile tests, soil samples were washed to retrieve the roots (Figure 31a) and characterize them. For triaxial tests, roots volume was characterized by pycnometry (Figure 31b) whereas roots diameter, tips number and length were evaluated by image acquisition and treatment through WinRhizo software (Figure 31c).

a

b

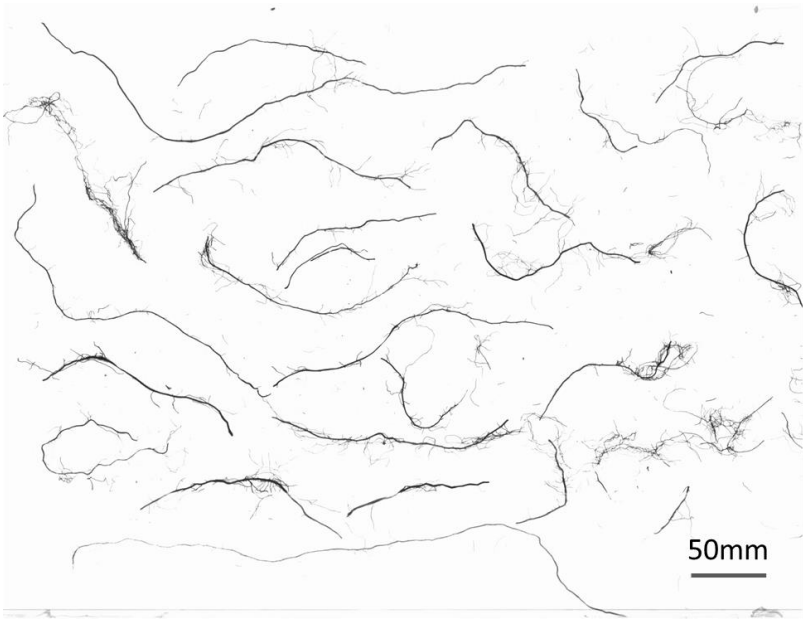

c

Figure 31 a) roots retrieved from soil sample, b) pycnometer test to calculate roots volume, c) WinRhizo scan to evaluate roots geometrical properties (diameter, length).

After tensile tests, the roots crossing the fissure produced by the tests were counted. The respective diameters were measured by a calibre with an accuracy of 0.02 mm. The material was washed to retrieve all the roots. For each root, length and diameter have been estimated with an accuracy of 0.02 mm (calibre). Finally, the volume of each root was obtained by multiplying the area of its cross section by its length.

From data obtained by roots characterization, it was possible to build the average root length distribution as function of root diameters. Distributions were built for plants at different growing periods (Figure 32).

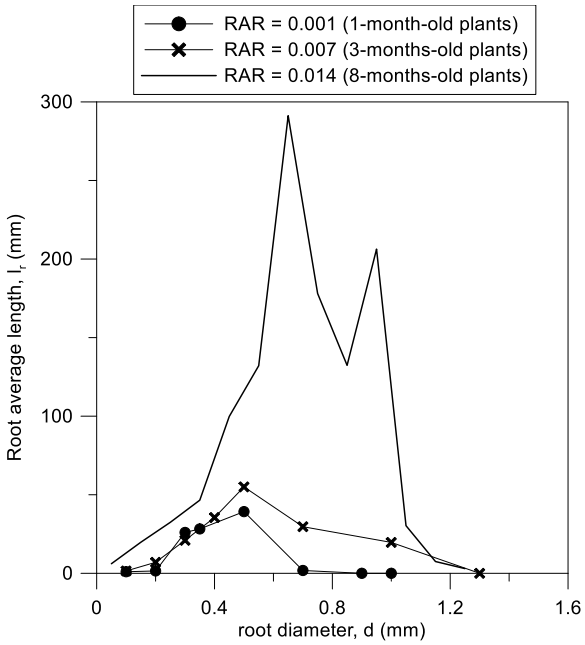

Figure 32 Distribution of average root length for each class of root diameter and for different plants growing periods.

Some of the retrieved unbroken roots have been furtherly tested in traction. The tensile strength of fresh roots was plotted as a function of its diameter. The tests have been carried out with special equipment (Figure 33a) with a load cell with a maximum capacity of 5 N and results are shown in Figure 33b.

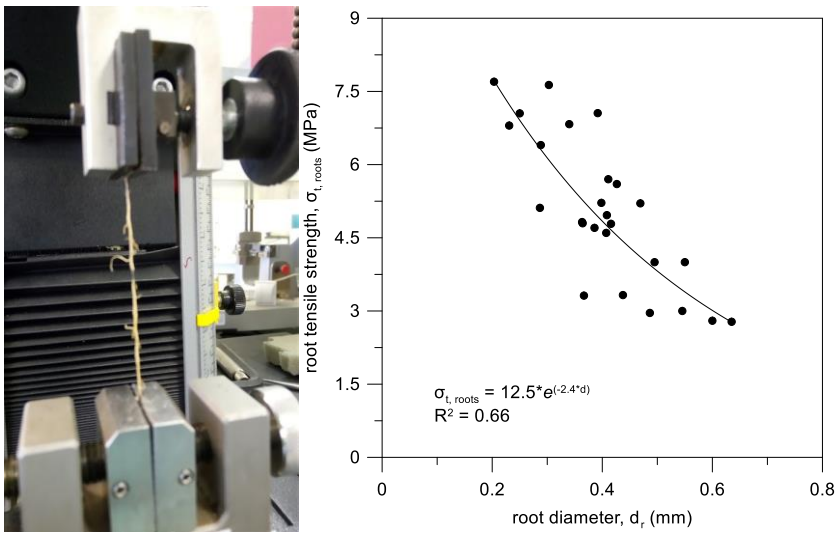

Figure 33 a) root installed in the traction equipment b) tensile strength of Cynodon Dactilon roots as function of their diameter

4.5 Methodology

4.5.1 Triaxial Compression Tests

Triaxial compression tests were carried out on the soil with and without roots, using equipment that allows the testing of large samples (Φ 200 mm and h 400 mm). Soil samples were firstly let to dry, then sealed for 24 hours to allow suction and water content equalization. Before testing, water content was evaluated by oven-drying soil retrieved in four point of the cylinders (two on the upper surface and two on the lower). An average value out of the four measurements was considered. In the same way, suction was evaluated in four points of the specimen. When possible, a ceramic tip tensiometer with a 100 mm shaft was used (T5x, UMS, München, Germany, measurements up to 0.2 MPa). The tensiometer was completely inserted within the sample, to have matric suction measurements 100 mm below the upper surface and above the lower surface of the sample. When water content was too low, a chilled mirror dew point hygrometer (WP4, Decagon Devices, Pullman, WA, USA, measurements from 0.50 MPa upwards) was used. In this case, soil for total suction measurements were retrieved in four points of the two sample surfaces.

Before triaxial compression, samples were subjected to isotropic consolidation. Confinement was imposed by air pressure, checked by a pressure transducer. Consolidation step was considered concluded when volumetric strain rate observed in the sample was lower than 0.1%/day. Triaxial compression was carried out with displacement control (displacement rate = 0.016 mm/min) and at constant soil water content. Axial and horizontal displacements in the soil were measured by one vertical and eight horizontal LVDTs. Horizontal transducers were placed to be in contact with the sample's membrane at different heights and orientations, as showed in Figure 34. After tests, soil water content and suction were measured in the same way as at the beginning.

4.5.1 Direct tensile test

A new prototype was designed in order to determine soil tensile strength on pulling. This mould consists of 2 independent cylinders joined by a bridge (orange pieces in Figure 35), which is removed, after compaction, to start the experiment. Cylinders are fixed on sliding rails with minimized and calibrated friction. One of them is connected to a motor and the other one, to a load cell (Figure 35). A ceramic-tip tensiometer with a 5 mm long shaft (matric suction measurements up to 0.2 MPa) was used to measure suction, recording the value of suction throughout the test period. Matric suction measured in correspondence to the peak of resistance of each test was finally considered. The water content was measured by an oven drying test at 110 °C at the beginning and at the end of each test: to analyse the results, an average of the measurements was taken.

Pulling was carried out with controlled displacement rate equal to 0.013 mm/min. Displacement control was adopted to study the post-peak tensile behaviour, especially in the case of vegetated soil. In fact, it was intended to observe the mechanical response of the roots in the soil subjected to pulling and after soil cracking.

Figure 34 triaxial cell and horizontal LVDT supports used in the investigation.

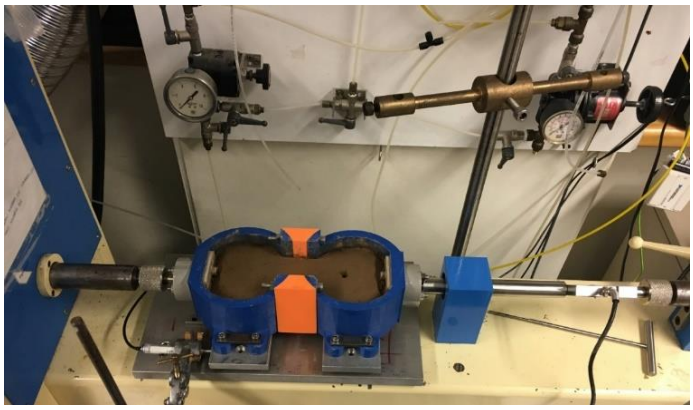

Figure 35 Tensile test equipment in its final configuration, before testing. On the left side: the motor for controlled displacement, the horizontal LVDT. On the right side: the load cell.

4.5.2 Void ratio measurements in vegetated soil

After triaxial and tensile tests, soil blocks were trimmed out the sample, to check their final void ratio. Vegetated cubes were extracted including roots. Before covering soil with paraffin, the aerial part of plants was cut out of the sample (Figure 36).

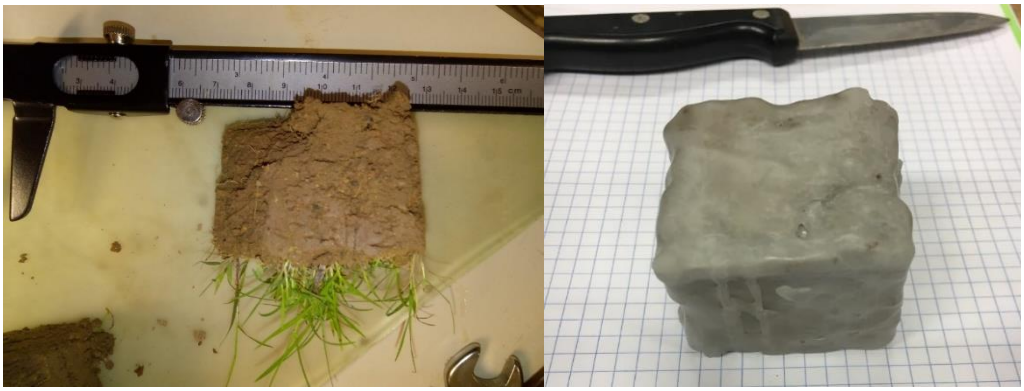

Figure 36 Paraffin tests on vegetated soil: before and after soil covering

In the case of vegetated soil, paraffin tests allowed to evaluate the total volume of the cube, in which the volume of roots was also included (Figure 37). Hence, after submerged weighing, paraffin samples were destroyed to weight and to measure roots volume contained and to estimate the soil dry weight. Knowing soil dry weight and solid particles density it was possible to calculate the volume of solids (V_{solid}). Then it was possible to evaluate the voids volume (V_{voids}) subtracting solids and roots volume to the total volume calculated by paraffin test. This procedure allowed to properly calculate the void ratio (as $e = V_{voids}/V_{solid}$) and according to the scheme proposed in Figure 37. Indeed, roots "phase" was considered, in this study, neither as a solid phase nor as voids.

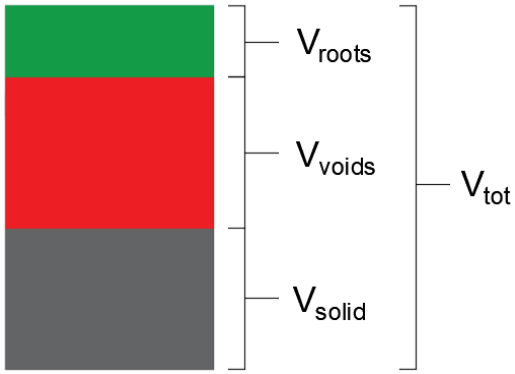

Figure 37 Volumetric scheme of the different phases in a vegetated soil

4.5.3 Constitutive laws used

Results coming from triaxial compression and direct tensile tests will be interpreted according to two different failure criterions for partially saturated soils. The first one, proposed by (Cárdenas, 2018) is formulated as:

$$\tau = c'_0 + (\sigma - u_a)tan\varphi' + \frac{s}{a + bs} \tag{16}$$

Where apparent cohesion as function of suction is defined as:

$$c'(s) = c'_0 + \frac{s}{a + bs} \quad (17)$$

Where $(\sigma - u_a)$ is the net stress, s is suction, c'$_0$ is the soil cohesion at null suction, a and b are material parameters.

The second failure criterion used is the one proposed by (Alonso, Pereira, Vaunat, & Olivella, 2010):

$$\tau = c'_0 + (\sigma - u_a) tan\varphi' + S_r^e s\ tan\varphi' \quad (18)$$

Where apparent cohesion as function of suction becomes:

$$c'(s) = c'_0 + S_r^e s\ tan\varphi' \quad (19)$$

In which the effective saturation degree is $S_r^e = (S_r)^\alpha$, with α a material parameter.

An adaptation to the model proposed by (Wu et al., 1979) was adopted to interpret and model vegetated soil behaviour:

$$c'_{0,roots} \approx \gamma * \sigma_{t,roots,aver.} * RAR \quad (20)$$

Where γ is a parameter depending on the type of plant, $\sigma_{t,roots,aver.}$ is the average roots tensile strength and RAR is the root area ratio (A_{roots}/A_{soil}): this parameter is used in the literature to quantify the amount of roots within the soil matrix. The average roots tensile strength used was assigned according to Figure 33 and in correspondence to the average diameter calculated from distributions in Figure 32.

4.6 Results

4.6.1 Hydraulic state and stress evolution during tests

Figure 38a shows some retention measurements (water content (w), suction (s)) and Figure 38b void ratio changes with suction along drying, for direct tensile tests. In the case of vegetated soils, a decrease in air entry value and retention capacity is observed compared to bare soil. The same trend has been observed by (Fraccica et al., 2019). Thanks to paraffin tests, it was possible to follow the evolution of the void ratio with suction in the soil. For vegetated soil, void ratio values are shown after correction for root volume. Figure 38b presents void ratio evolution obtained by paraffin tests. Although this value is slightly higher in rooted soil than in bare soil, it was decided to interpret all the results with a single trendline.

From this characterization of the stress and state (e, w, s) variables, it was possible to evaluate the degree of saturation S_r for each tested sample and to follow the evolution of this variable along suction changes.

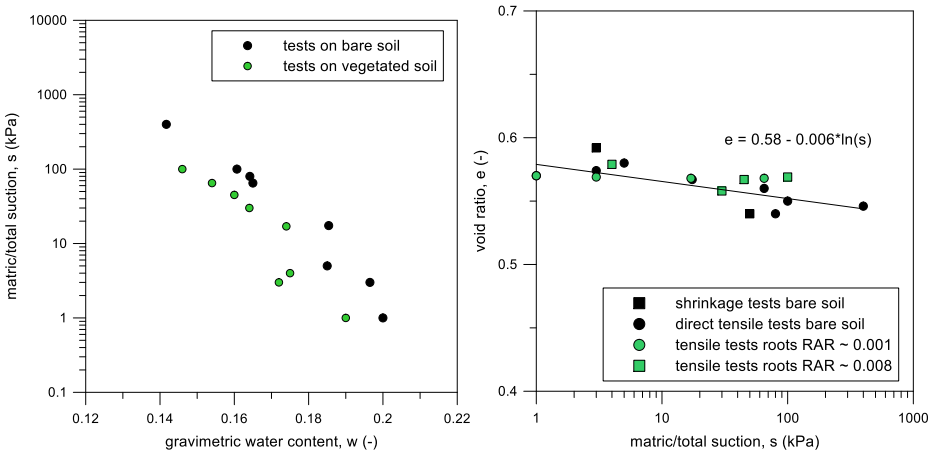

Figure 38 a) Average water content and suction at peak resistance for direct tensile tests and b) evolution of void ratio with suction along drying

4.6.2 Triaxial Compressions

Several triaxial compression tests were carried out on bare and root-permeated samples, at different confinement stresses and at different water contents. Some of the obtained curves, in terms of deviator stress and axial strains are shown in Figure 39a-b. More information about all the tests is presented in Table 12. Void ratio after shearing was calculated by paraffin tests, while void ratio before shearing (after consolidation) was back-calculated by knowing volumetric strains during triaxial compressions. Close to each stress-strain curve for vegetated samples is indicated the average R_v (root volume ratio) contained by the soil sample. Since it was impossible to evaluate the RAR in the shear bands produced by the compression, this ratio was considered as the 2D equivalent of the root volume ratio R_v (V_{roots}/V_{soil}), which was finally calculated. Therefore, on average, root area ratio and root volume ratio have been given the same value.

Figure 40 presents a comparison in the mechanical behaviour of bare and vegetated curves done at similar suction and confinement stress. As it's possible to observe in Figure 40a, no deviator stress plateau is reached in vegetated soil at low suction. This is due to the general root failure mechanism expected at low suction: pull-out with large displacements. In Figure 40b, a deviator stress plateau is almost reached: this is due to the general root failure mechanism expected at high suction: breakage with small displacements. The volumetric behaviour on shearing is showed in Figure 40c-d. Larger compression deformations were observed in the vegetated soil due to fissures generated by roots, already showed and quantified in the first chapter of the thesis.

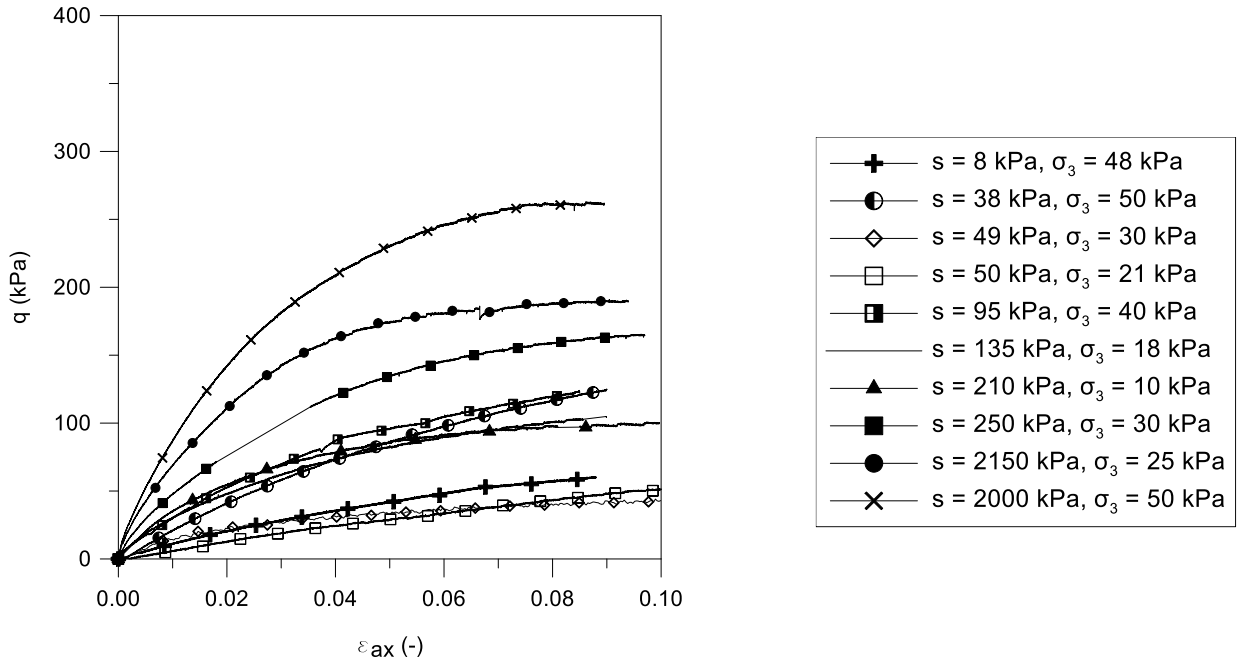

a

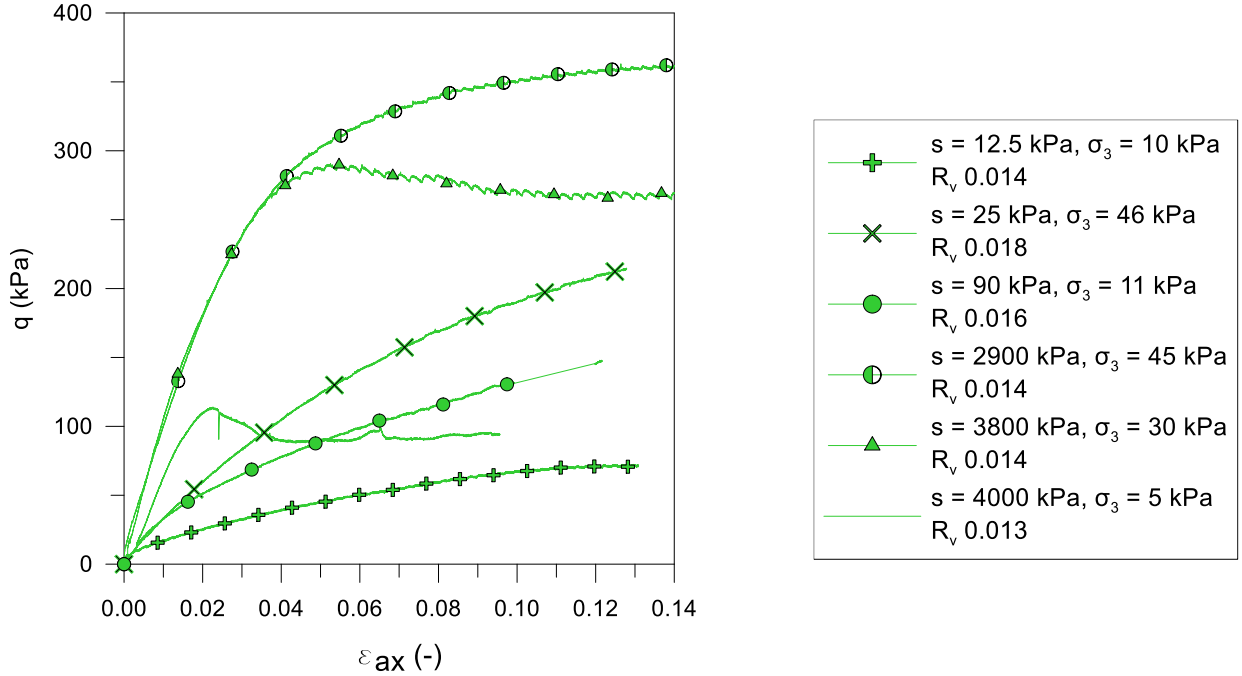

b

Figure 39 Deviator stress vs axial strain curves obtained during triaxial compression tests of: a) bare soil b) vegetated soil

Table 12 Triaxial compression tests. B=Bare soil, V=Vegetated soil. w_{in} , w_{fin} = initial and final measured water content, $e_{average}$ = average void ratio (between values after consolidation and after shearing). $S_{r,average}$ = average saturation degree, s_{in} , s_{fin} = initial and final measured/estimated suction.

test #	w_{in} (-)	w_{fin} (-)	e after consolidation (-)	e after shearing (-)	e average (-)	S_r average (-)	S_{in} (kPa)	S_{fin} (kPa)
TRX B2	0.075	0.062	0.624	0.567	0.595	0.301	1800	2200
TRX B3	0.152	0.150	0.631	0.533	0.582	0.693	11	5
TRX B4	0.126	0.122	0.667	0.589	0.628	0.527	90	100
TRX B6	0.136	0.130	0.672	0.590	0.631	0.546	39	59
TRX B8	0.145	0.138	0.649	0.571	0.610	0.619	30	45
TRX B9	0.127	0.122	0.644	0.578	0.611	0.544	130	140
TRX B10	0.146	0.140	0.682	0.606	0.644	0.593	30	70
TRX B12	0.113	0.114	0.699	0.614	0.657	0.462	200	220
TRX B13	0.114	0.104	0.674	0.600	0.637	0.457	200	300
TRX B15	0.091	0.083	0.654	0.588	0.621	0.375	1280	2230
TRX V1	0.127	0.124	0.680	0.570	0.625	0.536	77.5	100
TRX V2	0.062	0.057	0.658	0.658	0.658	0.242	3400	4210
TRX V3	0.060	0.054	0.664	0.764	0.714	0.213	3420	4495
TRX V4	0.178	0.175	0.699	0.512	0.605	0.779	10	15
TRX V5	0.075	0.068	0.684	0.549	0.616	0.311	2800	3000
TRX V6	0.154	0.149	0.653	0.505	0.579	0.697	20	30
TRX V7	0.202	0.200	0.664	0.481	0.573	0.938	1	1
TRX V8	0.191	0.183	0.662	0.462	0.562	0.887	5	6

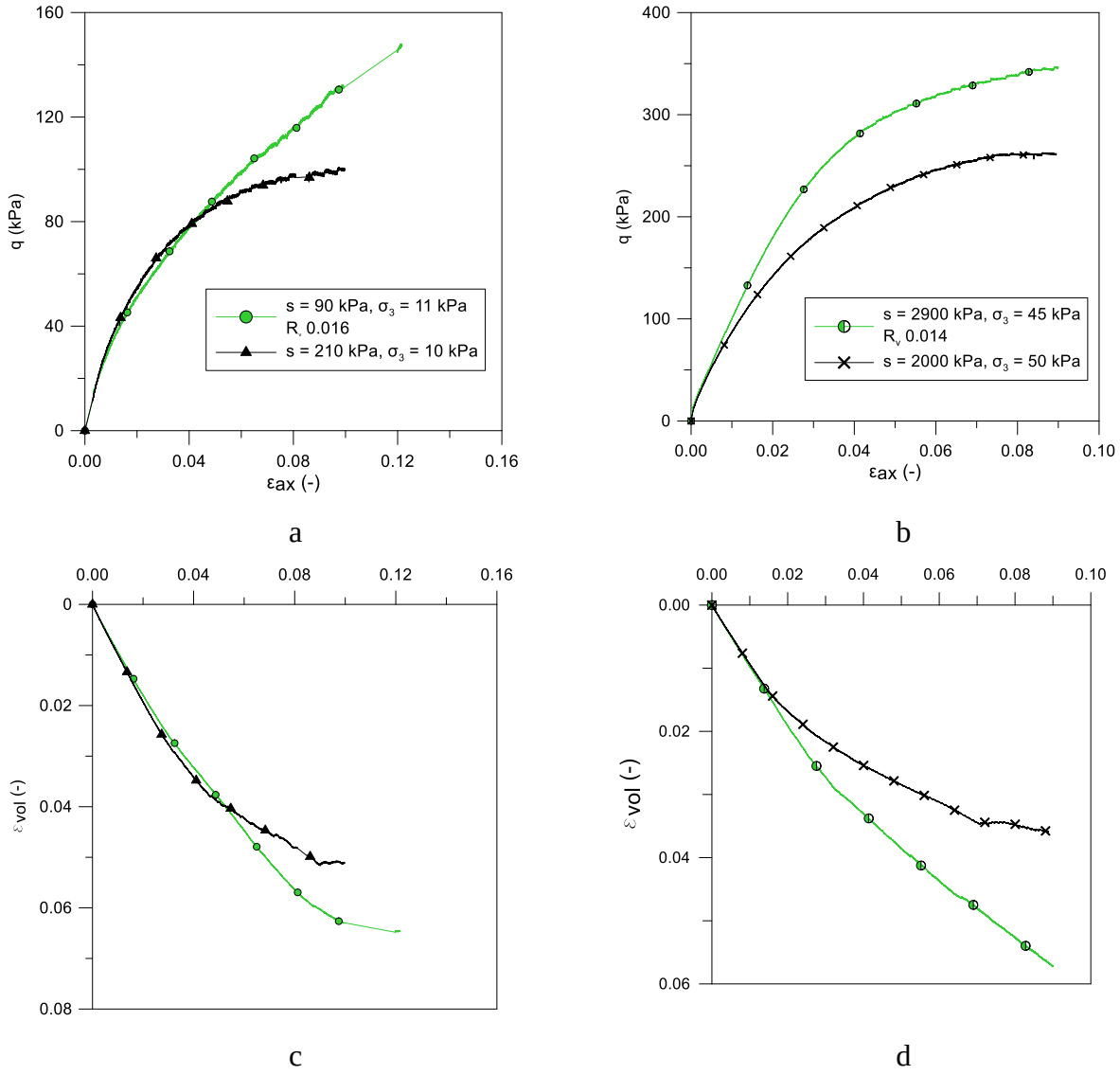

Figure 40 Stress strain behaviour under triaxial compression of bare and vegetated soils at a) low suction, low confinement b) high suction, high confinement stress. The respective volumetric deformations are in c and d.

Figure 41 a and b show the failure envelopes obtained by analysing the results. It has been assumed that the friction angle was constant with respect to the suction changes, while the increase in shear strength was due to apparent cohesion increase. The validity of this assumption was demonstrated by calibrating, at the minimum squared error, the friction angle, the cohesion at null suction $c'_{(0)}$ and the parameters required by the two laws expressed in equations (16) and (18) . Results obtained have been plotted as deviator stress vs normalized mean stress axis.

The evolution of apparent cohesion calculated with the two laws is shown in Figure 42. Calibrated cohesion at null suction was $c'_{(0)}$ = 0 kPa, in bare soil whereas higher values of cohesion ($c'_{(0)}$ = 9-10 kPa) have been calibrated for vegetated soil (Table 13).

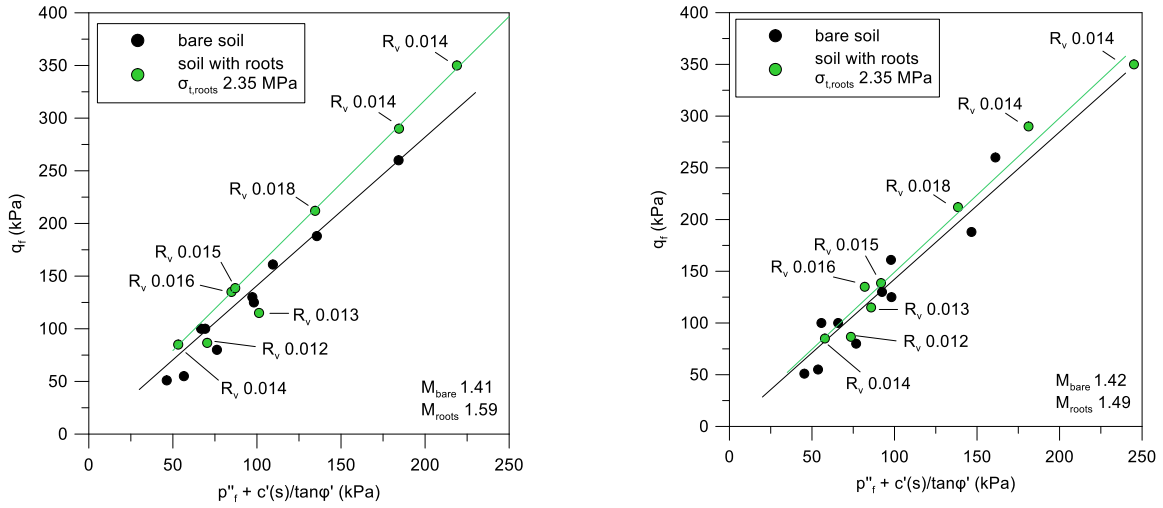

Figure 41 Calculated failure envelopes for soil with and without roots with two different cohesion evolution laws: a) Cárdenas hyperbolic model (2018) and b) (Alonso et al., 2010).

Table 13 Mechanical parameters calibrated with triaxial tests and according to two different failure criterion for partially saturated soils

	Model from (Cárdenas, 2018):	Model from (Alonso et al., 2010):
Bare soil	c'(0) = 0 kPa ; φ' = 34.8°	c'(0) = 0 kPa ; φ' = 35.1°
Vegetated soil	c'(0) = 9 kPa ; φ' = 38.8°	c'(0) = 10 kPa ; φ' = 36.6°

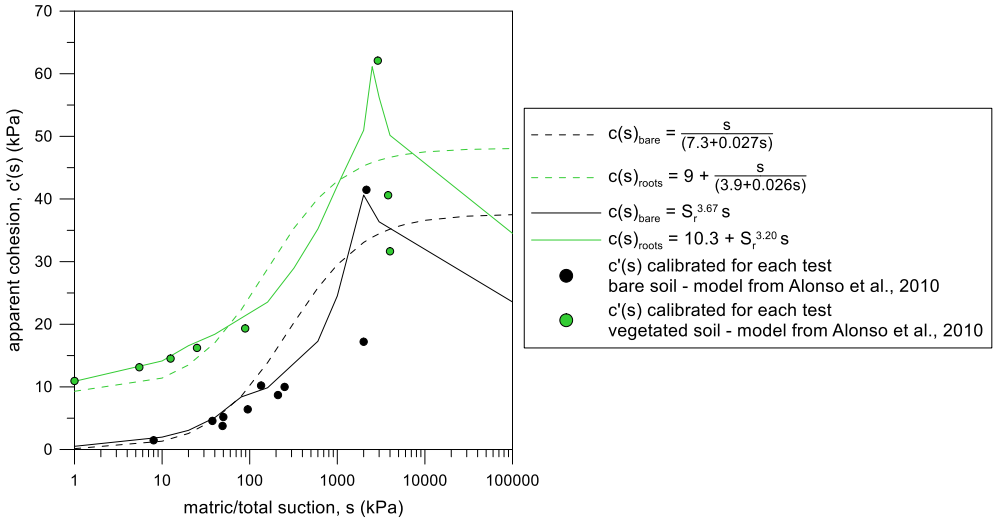

Figure 42 Evolution of apparent cohesion calculated through triaxial compression tests in soil with and without roots and with two laws of evolution of cohesion as a function of suction and degree of saturation.

4.7 Direct Tensile Tests

Figure 43 shows the results of the tensile tests performed on bare and vegetated soil. The legend shows the values of the estimated suction at the time of the stress peak. It was impossible dry the soil above the value of suction of 400 kPa, to perform tests. The geometrical constraints of the equipment have indeed caused the material to reach the maximum tensile stress it can withstand during shrinkage. More information about the stress and state variables in each test can be found in Table 14.

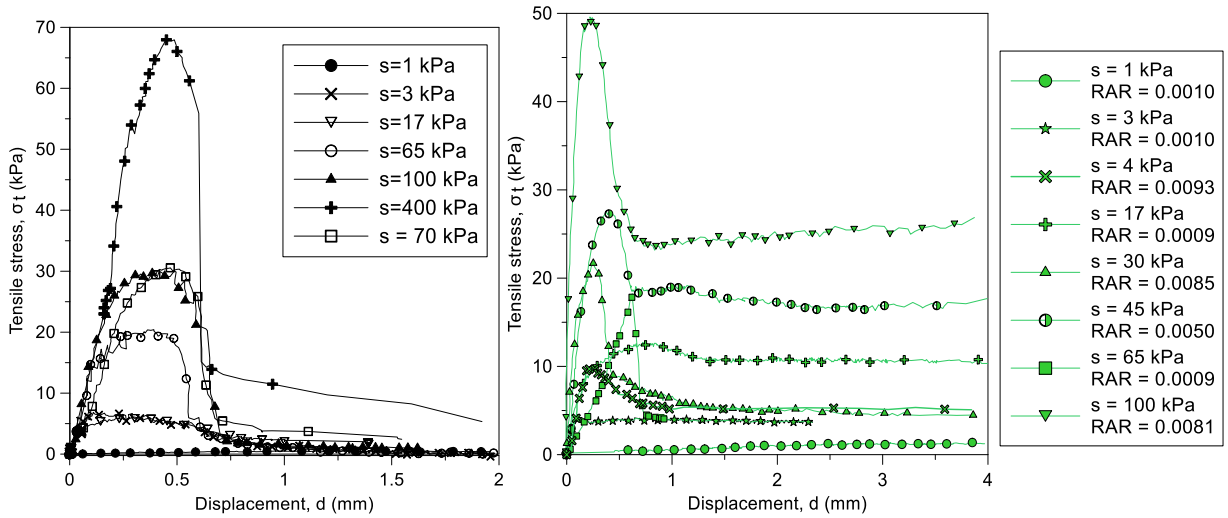

Figure 43 Curves from direct tensile tests on bare and vegetated soil at different water contents

Table 14 Direct Tensile Tests. B = bare soil, V = vegetated soil. w_{in} and w_{fin} = gravimetric water content before and after the test. s_{in} and s_{peak} = suction at the beginning and at the maximum stress observed during tensile test. $S_{r,\,average}$ = average saturation degree during the test.

Results are in line with the expected behaviour: the material reaches tensile stress values that are gradually higher as the suction increases. The stress-displacement behaviour is more ductile at low suction values and more fragile at high suction values. In fact, at low suction values, it was observed that the crack initially opened on the surface and propagated due to induced displacement. For higher suction values, on the other hand, the crack opening extended almost instantaneously over the entire height of the bridge.

For vegetated soil curves, the legend indicates the RAR values measured within the crack induced by the test (Figure 44) and the suctions measured during the peak resistance. It is important to note that, after the peak, the tensile strength does not suddenly drop to zero, but that the roots continue to withstand the induced stresses, even if the soil is partially or totally cracked.

Analysing the results of tensile tests on a sample of bare soil and on two samples with plants grown at 1 and 3 months, under the same suction, we obtain as a result that the tensile stress peak is clearly influenced by the density of roots that are in the area of failure. Figure 45 shows that the sample with

a lower RAR has a strength of approximately 4 kPa, just slightly above the tensile strength of unrooted soil. The sample with the highest RAR reaches almost 10 kPa of resistance.

Table 15 state and stress variables for direct tensile tests. B=Bare soil, V=Vegetated soil

test #	w_{in} (-)	w_{fin} (-)	e_{fin} (-)	s_{in} (kPa)	s_{peak} (kPa)	$S_{r,\ average}$ (-)
DT B2	0.202	0.198	0.571	1.0	1.0	0.937
DT B3	0.168	0.165	0.560	63.5	65.0	0.787
DT B5	0.163	0.161	0.553	100.3	100.5	0.780
DT B7	0.195	0.192	0.574	2.0	3.0	0.914
DT B9	0.189	0.185	0.580	3.5	5.0	0.852
DT B11	0.185	0.180	0.567	17.0	17.4	0.873
DT B12	0.168	0.164	0.545	78.5	80.0	0.812
DT B14	0.146	0.142	0.546	n.m.	400.0 (estim. by SWRC)	0.693
DT V19	0.192	0.190	0.570	0.7	1.0	0.875
DT V20	0.177	0.174	0.568	16.5	17.7	0.825
DT V21	0.175	0.172	0.569	2.2	3.0	0.801
DT V22	0.156	0.154	0.568	63.5	65.3	0.741
DT V24	0.168	0.160	0.567	42.8	45.0	0.767
DT V25	0.140	0.146	0.569	98.0	101.2	0.706
DT V26	0.162	0.164	0.558	31.0	30.0	0.783
DT V27	0.178	0.175	0.579	3.5	4.0	0.817
DT V28	0.195	0.191	0.583	1.5	1.0	0.875
DT V29	0.115	0.112	0.548	188.7	190.5	0.547

Figure 44 Unbroken roots after test, within the fissure generated by the tensile test

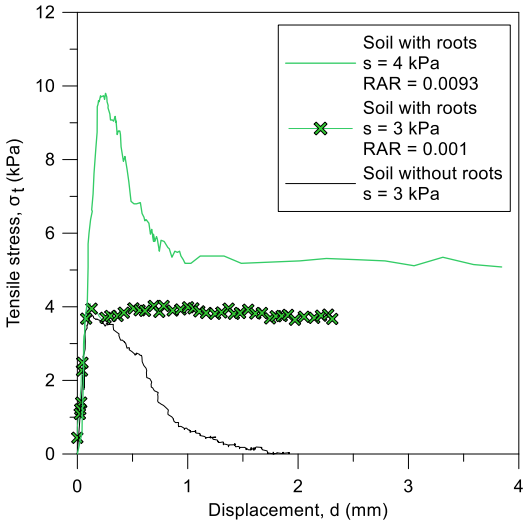

Figure 45 Bare soil and vegetated soil with different roots quantities, for the same suction value.

Bare and root permeated tensile tests were compared at the same suction in Figure 46. At a low suction value (Figure 46a), vegetated soil presents a higher strength, reached after a larger displacement. This was caused by roots pull-out phenomenon, which occurs after large displacements. At high suction (Figure 46b), roots breakage phenomenon is prevailing, making the soil response more fragile.

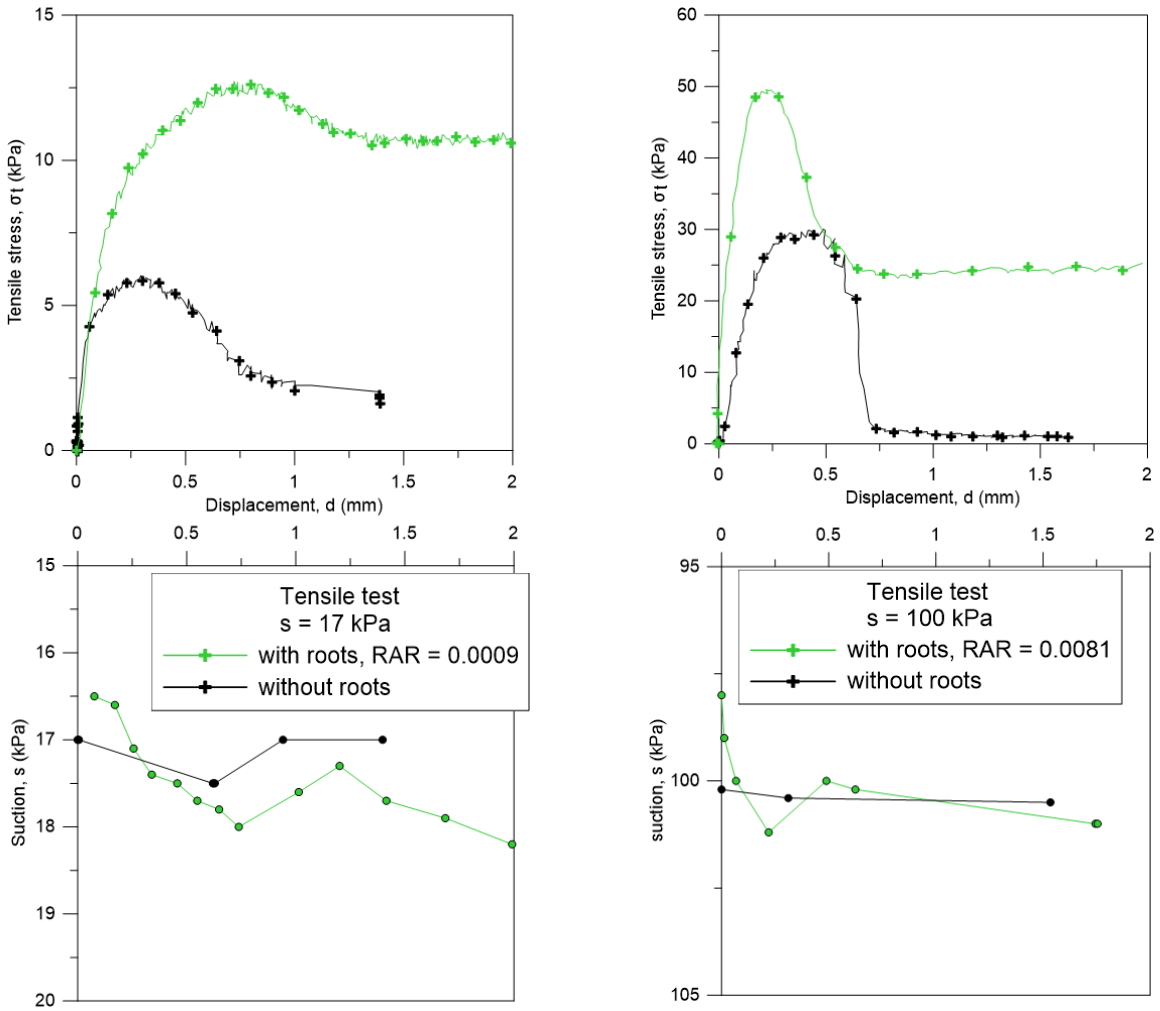

a b

Figure 46 Comparison of direct tensile tests carried out at different suction, for bare and root-permeated soil. A) test carried out at suction equal to 17 kPa, B) test run at 100 kPa

4.8 Joint interpretation of the results

Tensile strength values observed with direct tensile tests have been plotted as a function of suction. (Figure 47). Vegetated results were differentiated by growth periods (1 and 3 months). Samples with 1 month-grown plants showed an average RAR of 0.001 whereas 3 months-grown plants were characterized by an average RAR of 0.007. Roots traits characterized within this study are synthetized in Table 16.

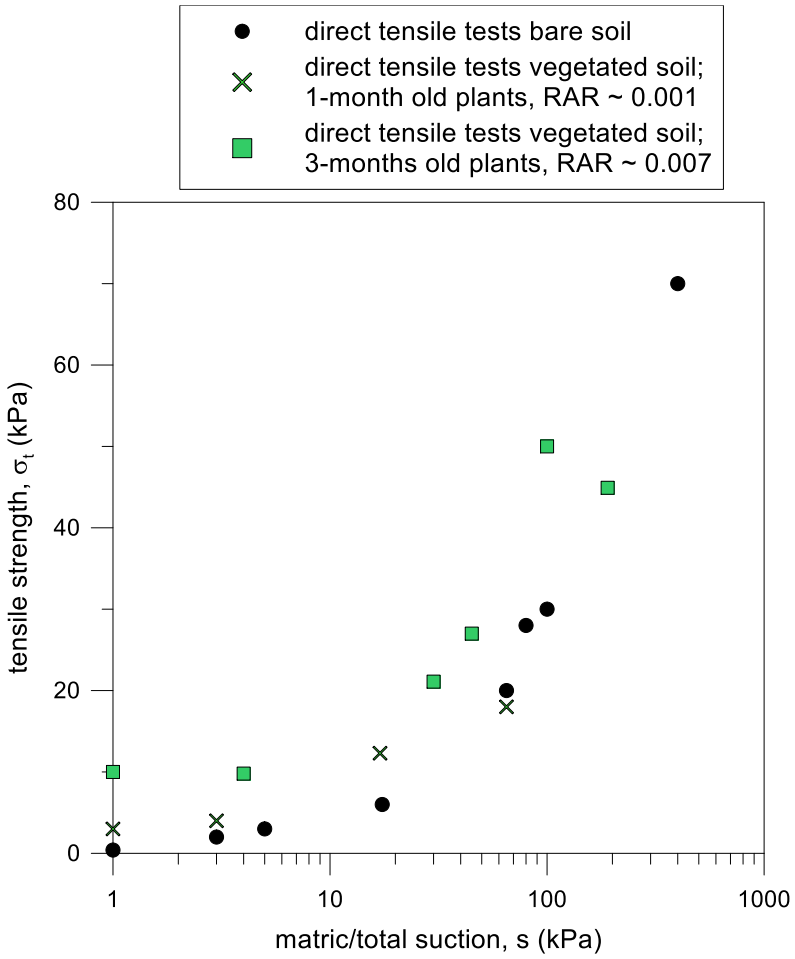

Figure 47 Tensile strength with suction

Tensile strength clearly tends to increase with suction, reaching values close to 70 kPa, for suction values of approximately 400 kPa.

In order to compare these results with those obtained in the triaxial compression tests, the apparent cohesion was calculated, from tensile strength values, using the formula:

$$c'(s) = \sigma_t(s) tan\varphi' \qquad (21)$$

which was derived from the Mohr-Coulomb failure criterion. The friction angle used was calibrated by the triaxial compression tests. Results have been interpreted through the two laws describing the evolution of apparent cohesion with suction indicated in the equations (17) and (19). In order to calibrate the parameters of the respective laws of evolution of cohesion, all the tests carried out on vegetated soil were analysed together. In order to jointly analyse the results with different root quantities, it was assumed, for each test, that cohesion at null suction is given by the model proposed in equation (20). The two laws were adapted in this way:

$$c'(s) = \gamma * \sigma_{t,roots,aver.} * RAR + S_r^{\alpha} s \, tan\varphi' \qquad (22)$$

$$c'(s) = \gamma * \sigma_{t,roots,aver.} * RAR + \frac{s}{a + bs} \qquad (23)$$

Knowing the average values of water content and void ratio in the various tests, it was possible to calculate the degree of saturation of each sample. For each test with vegetated soil, root area ratio (RAR) and the average roots tensile strength were also known ($\sigma_{t,roots,aver.}$ = 4.8MPa for samples with RAR = 0.001 and $\sigma_{t,roots,aver.}$ = 3.5MPa for samples with RAR = 0.007). Thus, only the values α, γ and the values of a and b were calibrated for vegetated soil through an estimation at the minimum squared error. For the bare soil, the value of c_0 was additionally calibrated, resulting, anyway, close to zero. All the calibrated parameters are indicated in Table 17.

Table 16 Root properties estimated and/or measured within the different samples tested

Roots growing period	Test	Root Volume Ratio – R_v	Root area ratio – RAR	Average root diameter (mm)	Root length density – R_{ld} (m/m^3)
8 months	TRX V1	0.016	-	0.700	$2.10*10^5$
	TRX V2	0.014	-	0.685	$1.89*10^5$
	TRX V3	0.013	-	0.688	$1.79*10^5$
	TRX V4	0.014	-	0.705	$1.91*10^5$
	TRX V5	0.014	-	0.710	$1.47*10^5$
	TRX V6	0.018	-	0.679	$1.11*10^5$
	TRX V7	0.012	-	0.652	$6.30*10^4$
	TRX V8	0.015	-	0.704	$1.89*10^5$
1 month	DT V19	0.0015	0.001	0.384	$8.17*10^3$
	DT V20	0.0034	0.0009	0.400	$1.10*10^4$
	DT V21	0.001	0.001	0.398	$6.75*10^3$
	DT V22	0.002	0.0009	0.405	$9.78*10^3$
3 months	DT V24	0.011	0.0054	0.532	$1.04*10^4$
	DT V25	0.012	0.0081	0.526	$1.42*10^4$
	DT V26	0.015	0.0085	0.531	$7.47*10^3$
	DT V27	0.013	0.0093	0.557	$1.23*10^4$
	DT V28	0.009	0.0075	0.499	$1.18*10^4$
	DT V29	0.010	0.0078	0.509	$1.20*10^4$

Table 17 Parameters calibrated through direct tensile tests to predict apparent cohesion evolution with suction

	Model from (Cárdenas, 2018): equation (17) for bare soil, equation (23) for vegetated soil	Model from (Alonso et al., 2010): equation (19) for bare soil, equation (22) for vegetated soil(23
Bare soil	$c'_{(0)} = 0$ kPa; a = 3.5; b = 0.011 kPa^{-1}	$c'_{(0)} = 0$ kPa; $\alpha = 4.01$
Vegetated soil	$\gamma = 0.31$; a = 2.3; b = 0.019 kPa^{-1}	$\gamma = 0.23$; $\alpha = 3.3$;

For the law proposed by (Alonso et al., 2010), the values of α calibrated were between 3.3 and 4.01: these values are in line with those observed in the literature for soils with characteristics similar to those of the studied soil.

The points estimated through direct tensile are presented in Figure 48 and Figure 49 along with the trends given by the two laws used to predict results from direct tensile tests.

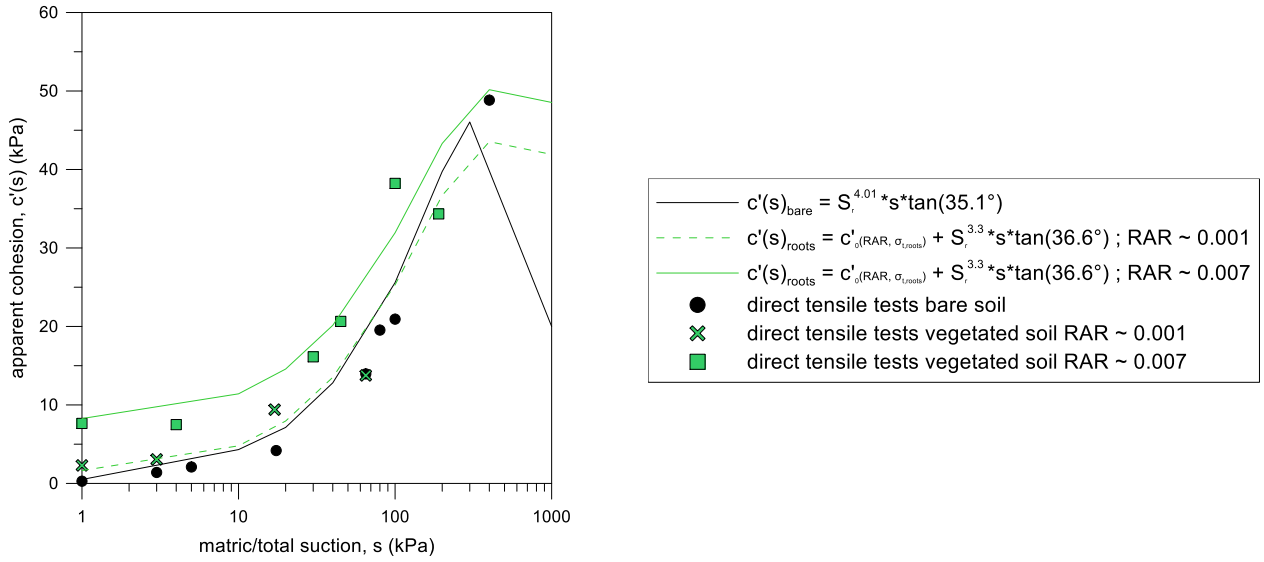

Figure 48 Cohesion evolution with suction, evaluated according to Alonso et al., 2010

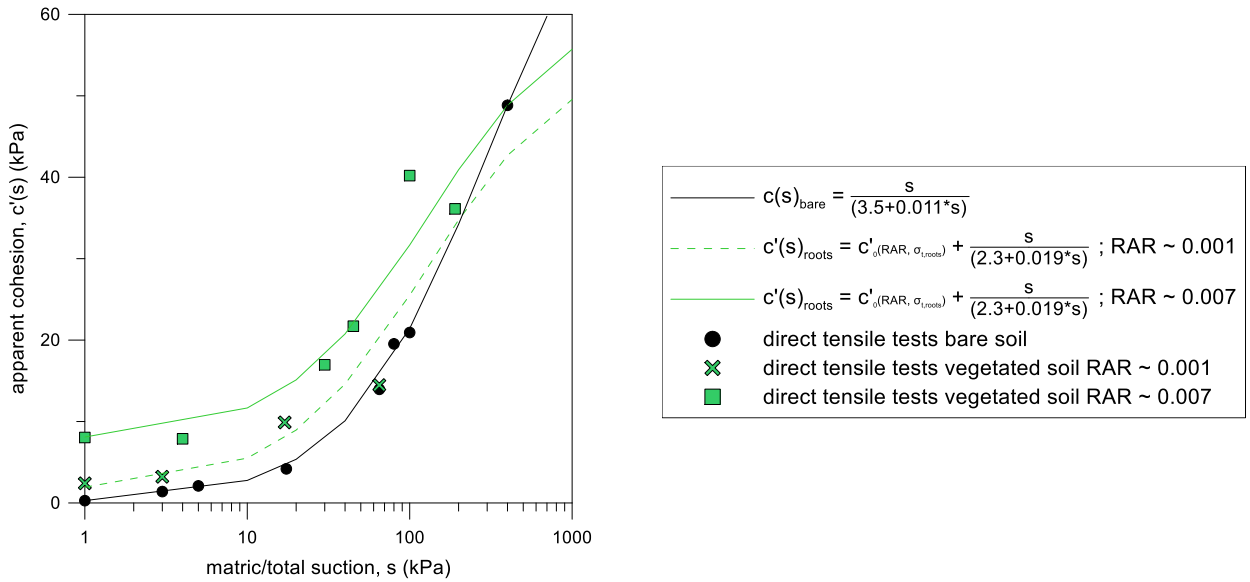

Figure 49 Cohesion evolution with suction, evaluated according to Cárdenas, 2018

Results and predictions show that the apparent cohesion in a soil with roots increases, compared to a bare soil, thanks to the roots tensile strength and quantity (generated by different growing periods). This result is important in the context of slope stability because it indicates that in saturated conditions (the worst for a slope) a soil with plants has greater shear strength than a bare soil. However, the cohesion increase tendency with suction, predicted by the two constitutive laws, in vegetated soil is lower than the one observed for bare soil. As consequence, for certain values of suction, apparent cohesion observed and predicted for a vegetated soil is lower than that for bare soil. This kind of behaviour was already lightly evident in the apparent cohesion evolution obtained from the analysis of triaxial compressions. It is supposed that this behaviour is due to the fissures generated by the growth of roots in the soil, which are furtherly opening during soil drying, thanks to a concurrent soil and roots shrinkage, as demonstrated in the first chapter of the thesis. These alterations at the soil structural level are weakening the matrix and decompensating the positive effects generated by roots tensile strength.

4.9 Conclusions

In the current study, an investigation on the effects of roots on the mechanical behaviour of soil was carried out with triaxial compression and direct tensile tests. Tests were carried out after different growing periods (1 and 3 months) and at different hydraulic states. In addition, the characteristics of plants that can affect soil mechanical behaviour were assessed, such as root tensile strength, diameter, root area ratio. These parameters were used in an adapted equation for soil reinforcement with roots. The equation was then included in constitutive laws for partially saturated soils to predict the

evolution of soil shear strength and apparent cohesion with suction already observed within the laboratory tests.

From the results interpreted in terms of apparent cohesion with suction it was possible to observe that soil with plants had a higher tensile strength and therefore greater cohesion than tests without roots. However, the fissures generated by the growth of the roots, during soil drying, influenced sometimes negatively the macroscopic soil mechanical behaviour. Moreover, it was possible to demonstrate the validity of adapting constitutive laws for partially saturated soils with equations representing roots reinforcement: in this way, vegetated soil behaviour can be predicted over a good range of suction values. A good agreement between cohesion evolution evaluated by triaxial compression tests and by direct tensile tests was also observed.

References

Albrecht, B., & Benson, C. H. (2001). Effect of Desiccation on Compacted Natural Clays. *Journal of Geotechnical & Geoenvironmental Engineering*, *127*(1), 67–75. https://doi.org/10.1061/(ASCE)1090-0241(2001)127

Alonso, E. E., Pereira, J. M., Vaunat, J., & Olivella, S. (2010). A microstructurally based effective stress for unsaturated soils. *Géotechnique*, *60*(12), 913–925. https://doi.org/10.1680/geot.8.P.002

Cárdenas, O. E. (2018). *Estudio del comportamiento de colapso en arenas arcillosas bajo un estado generalizado de tensiones*. Universitat Politècnica de Catalunya, PhD thesis.

Cordero, J. A., Useche, G., Prat, P. C., Ledesma, A., & Santamarina, J. C. (2017). Soil desiccation cracks as a suction – contraction process, 272–278.

Divya, P. V, Viswanadham, B. V. S., & Gourc, J. P. (2014). Evaluation of Tensile Strength-Strain Characteristics of Fiber-Reinforced Soil through Laboratory Tests. *Journal Of Materials In Civil Engineering*, *26*(1), 14–23. https://doi.org/10.1061/(ASCE)MT.1943-5533.0000772.

Fraccica, A., Romero, E., & Fourcaud, T. (2019). Multi-scale effects on the hydraulic behaviour of a root-permeated and compacted soil. In A. Tarantino & E. Ibraim (Eds.), *IS-Glasgow* (p. 12014). Glasgow: EDP Sciences. https://doi.org/doi.org/10.1051/e3sconf/20199212014

Ghestem, M., Veylon, G., Bernard, A., Vanel, Q., & Stokes, A. (2014). Influence of plant root system morphology and architectural traits on soil shear resistance. *Plant and Soil*, *377*(1–2), 43–61. https://doi.org/10.1007/s11104-012-1572-1

Gonzalez-Ollauri, A., & Mickovski, S. (2017). Plant-soil reinforcement response under different soil hydrological regimes. *Geoderma*, *285*, 141–150. https://doi.org/10.1016/j.geoderma.2016.10.002

Lakshmikantha, M. R., Prat, P. C., & Ledesma, A. (2012). Experimental evidence of size effect in soil cracking, *284*, 264–284. https://doi.org/10.1139/T11-102

Mickovski, S., Hallett, P. D., Bransby, M. F., Davies, M. C. R., Sonnenberg, R., & Bengough, A. G. (2009). Mechanical Reinforcement of Soil by Willow Roots: Impacts of Root Properties and Root Failure Mechanism. *Soil Science Society of America Journal*, *73*(4), 1276–1285. https://doi.org/10.2136/sssaj2008.0172

Oorthuis, R., Hürlimann, M., Fraccica, A., Lloret, A., Moya, J., Puig-Polo, C., & Vaunat, J. (2018). Monitoring of a full-scale embankment experiment regarding soil-vegetation-atmosphere interactions. *Water (Switzerland)*, *10*, 688. https://doi.org/10.3390/w10060688

Pollen, N. (2007). Temporal and spatial variability in root reinforcement of streambanks: Accounting for soil shear strength and moisture. *Catena*, *69*(3), 197–205. https://doi.org/10.1016/j.catena.2006.05.004

Sánchez, M., Wang, D., Briaud, J. L., & Douglas, C. (2014). Typical geomechanical problems associated with railroads on shrink-swell soils. *Transportation Geotechnics*, *1*(4), 257–274. https://doi.org/10.1016/j.trgeo.2014.07.002

Vardon, P. J. (2014). Climatic influence on geotechnical infrastructure : a review. https://doi.org/10.1680/envgeo.13.00055

Veylon, G., Ghestem, M., Stokes, A., & Bernard, A. (2015). Quantification of mechanical and hydric components of soil reinforcement by plant roots. *Can. Geotech. J.*, *52*, 1839–1849.

Wu, T. H., McKinnell III, W. P., & Swanston, D. N. (1979). Strength of tree roots and landslides on Prince of Wales Island, Alaska. *Canadian Geotechnical Journal*, *16*(1), 19–33. https://doi.org/10.1139/t79-003

Yildiz, A., Graf, F., Rickli, C., & Springman, S. M. (2018). Determination of the shearing behaviour of root-permeated soils with a large-scale direct shear apparatus. *Catena*, *166*, 98–113. https://doi.org/10.1016/j.catena.2018.03.022

5. Numerical analysis of a bare and a vegetated embankment

The results on the hydro-mechanical behaviour of bare and vegetated soil obtained within the thesis were used to assess the effects of different root quantities (RAR ≈ R_v ≈ 0.007 and 0.014) on the stability of a monitored embankment built with the same soil and seeded with the same plant investigated.

Triaxial compression and direct tensile tests have been performed under saturated and partially saturated conditions to quantify the effect of roots on the stress-strain behaviour of soil. Results showed that roots provided a noticeable increase of soil strength, even if larger volumetric compressive deformations were traced as shear displacements progressed. Results have been analysed within the context of the shear strength criterion for unsaturated soils proposed by (Fredlund & Rahardjo, 1993) (Figure 50), which is needed by GeoStudio to assess slope stability adopting a limit equilibrium approach. Roots didn't affect so much the friction angle, thus results have been interpreted as an increase of apparent cohesion, which is evident even under saturated conditions and is evolving as function of the suction at which the tests were carried out. Roots geometrical and mechanical traits were assessed in order to be used within a soil-root reinforcement well-established model, which provided results in good agreement with observations.

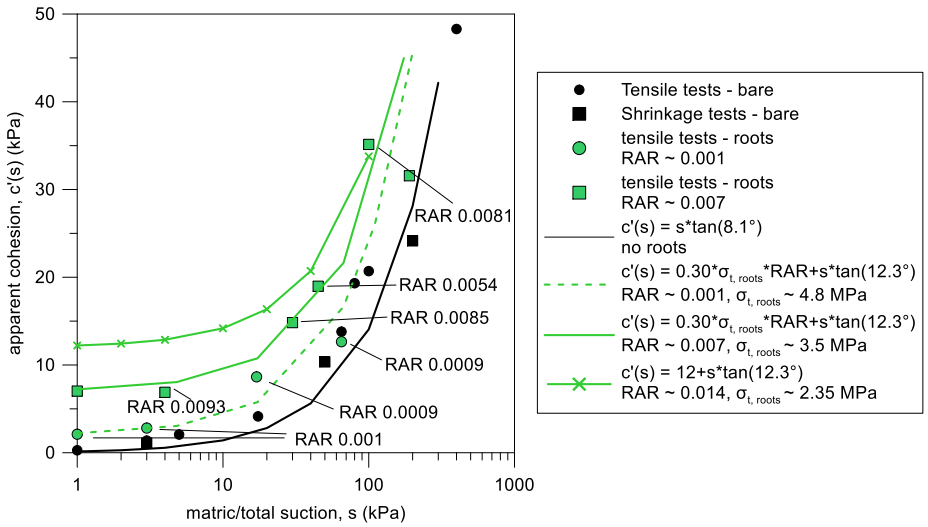

Figure 50 Cohesion evolution with suction according to (Fredlund & Rahardjo, 1993) *calibrated with triaxial compression and direct tensile tests and for different plant growing periods.*

The hydraulic properties of the silty soil were evaluated as well, for the same range of porosity as the mechanical tests. Results coming from the analysis of oedometer and permeameter tests evidenced that roots caused an increase of the water saturated permeability, in the order of three times that obtained for bare soil (Fraccica, Romero, & Fourcaud, 2019). Retention properties were affected by roots as well: in particular, the air-entry value and the suction correspondent to each water content decreased.

The hydro-mechanical model built in chapter 2 of this thesis was used to obtain the retention curve and the water saturated permeability of the soil before and after roots growth, as indicated in Figure 51.

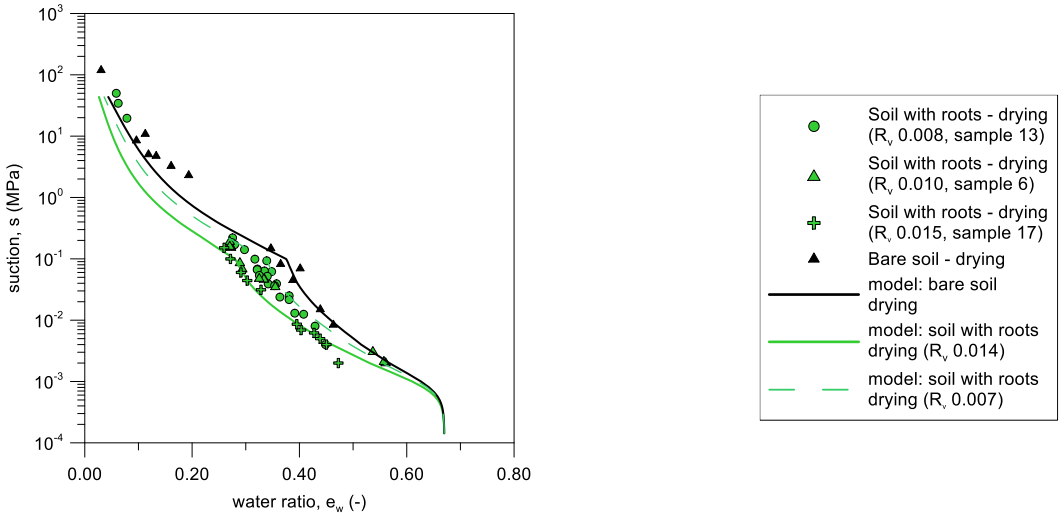

a

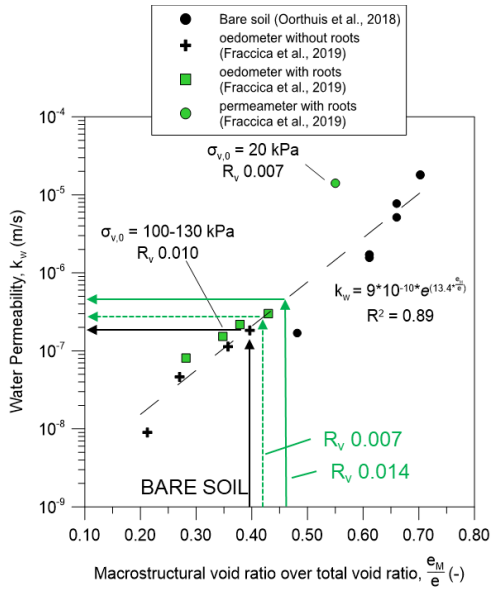

b

Figure 51 Retention curves and water saturated permeability evaluated by the hydro-mechanical framework developed in chapter 2

The intrinsic unsaturated permeability was evaluated in GeoStudio according to the law proposed by (Fredlund & Xing, 1994).

These laws were used to simulate the behaviour of an embankment initially under partially saturated conditions and subject to rain. The geometry of the embankment is showed in Figure 52. A geomembrane with high roughness was used to produce soil breakage in the first 700 mm from the soil surface. The inclination angle of the slope is of 34°.

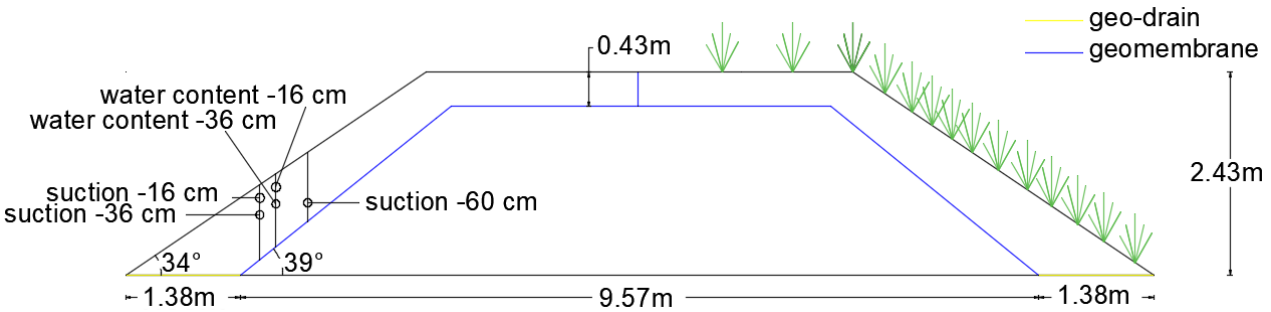

Figure 52 Monitored embankment geometry

The properties of vegetated soil were attributed to the first 400 mm of soil, below the soil surface, as indicated in Figure 53

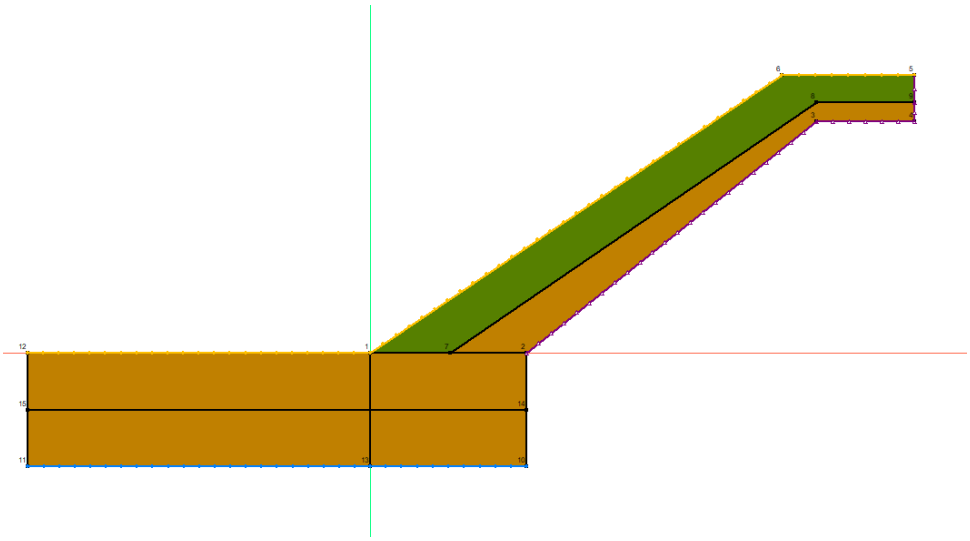

Figure 53 Geometrical model of the vegetated slope of the embankment

The initial boundary conditions given to all the slopes (one bare and two vegetated by different roots quantities) are showed in Figure 54.

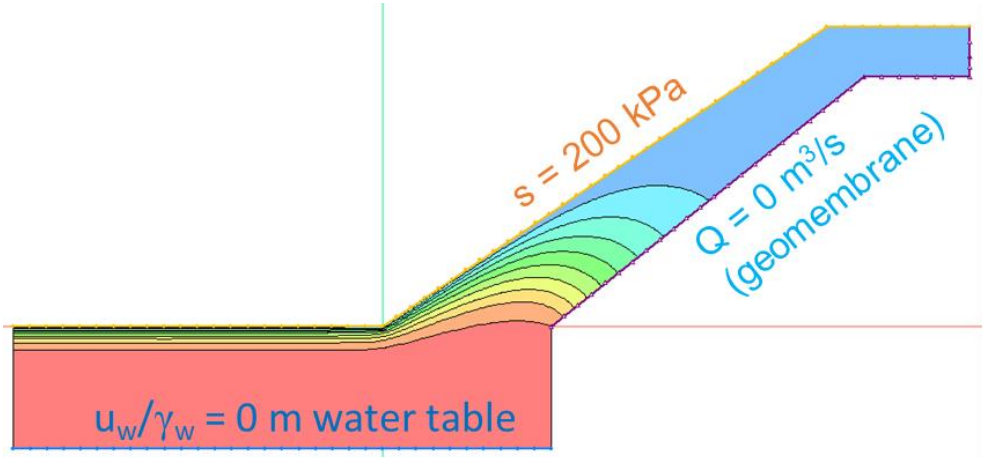

Figure 54 Initial boundary conditions imposed on the embankment slope

A water table one metre below the horizontal surface, suction equal to 200 kPa on the whole upper soil surface and an impervious material (corresponding to the geomembrane) were attributed to the geometrical model. After a first analysis in steady state conditions to allow suction development within the soil, rainfall was applied as a zero-water-pressure boundary conditions on the whole upper surface (Figure 55). A transient analysis in SEEP/W was carried out, jointly with a stability analysis in SLOPE/W, after several time steps.

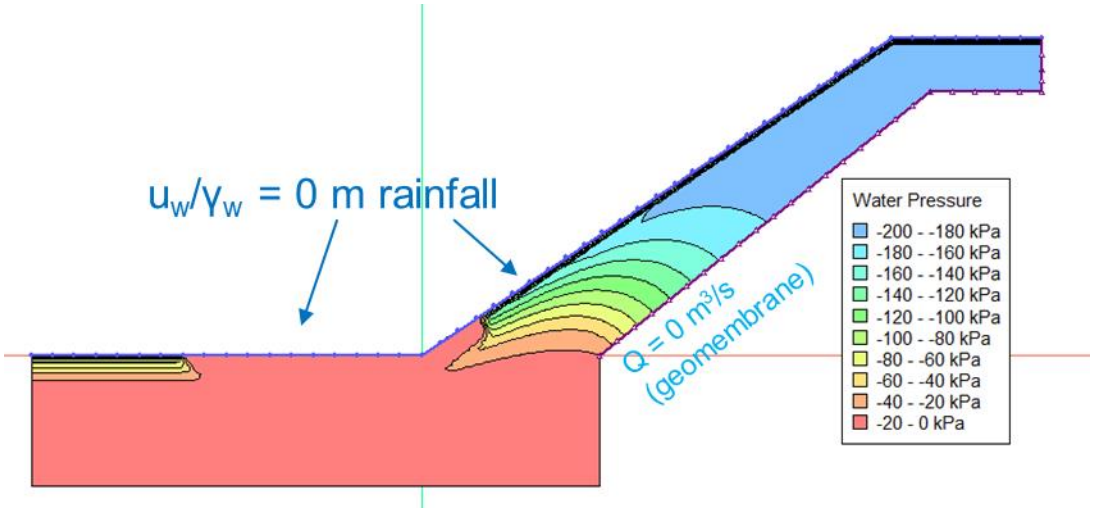

Figure 55 Boundary conditions during transient analysis to simulate rainfall

As expected, at a given simulation time, soil with a highest quantity of roots was found at lower values of suction, with respect to the bare soil, due to the increase in permeability imposed (Figure 56).

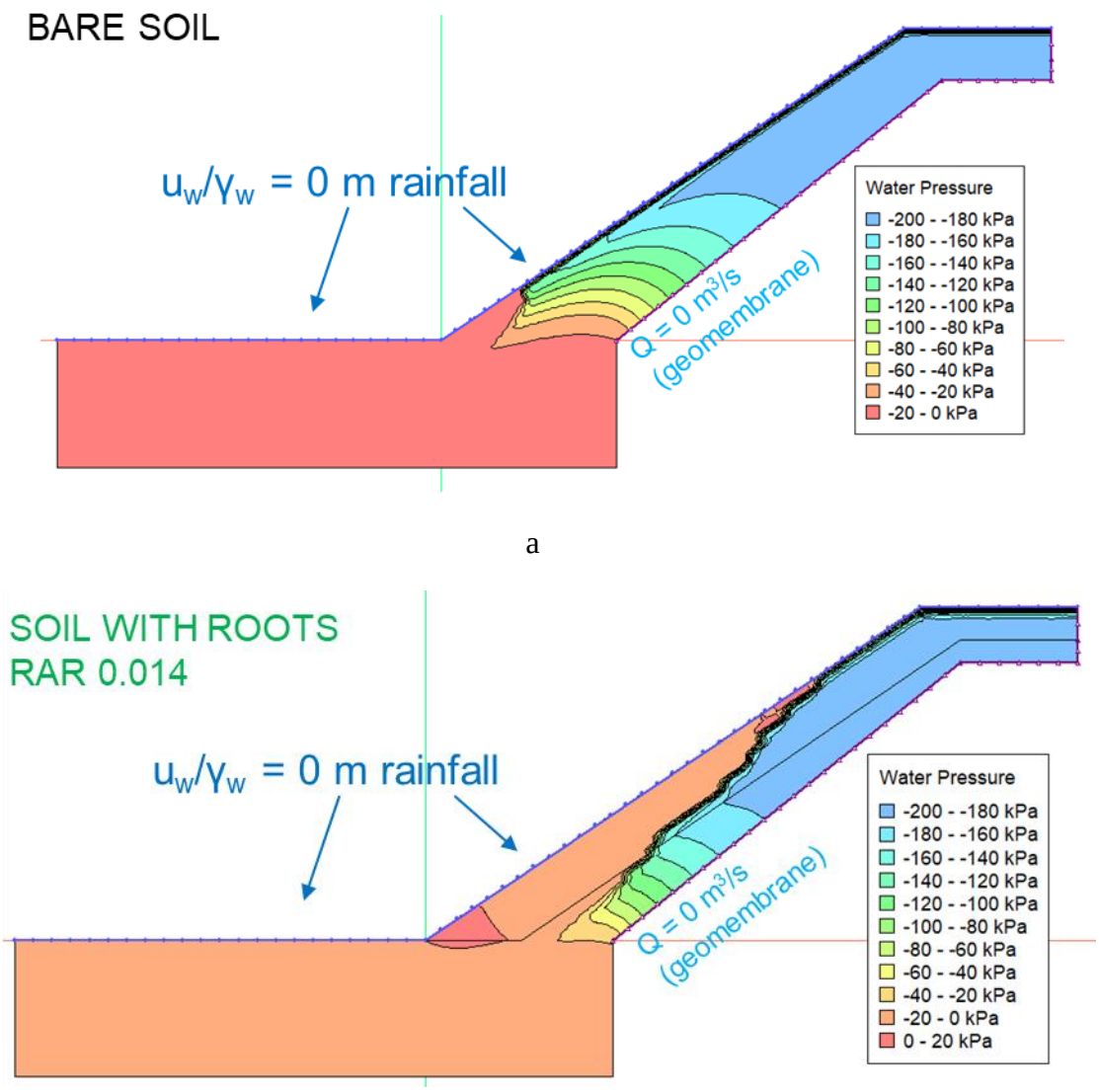

Figure 56 Comparison between: a) bare slope and b) vegetated slope with a high roots quantity after the same rainfall period.

The minimum value of the slope safety factor was evaluated at different hydraulic states, starting from the partially saturated one and until failure occurred within the bare soil (Figure 57).

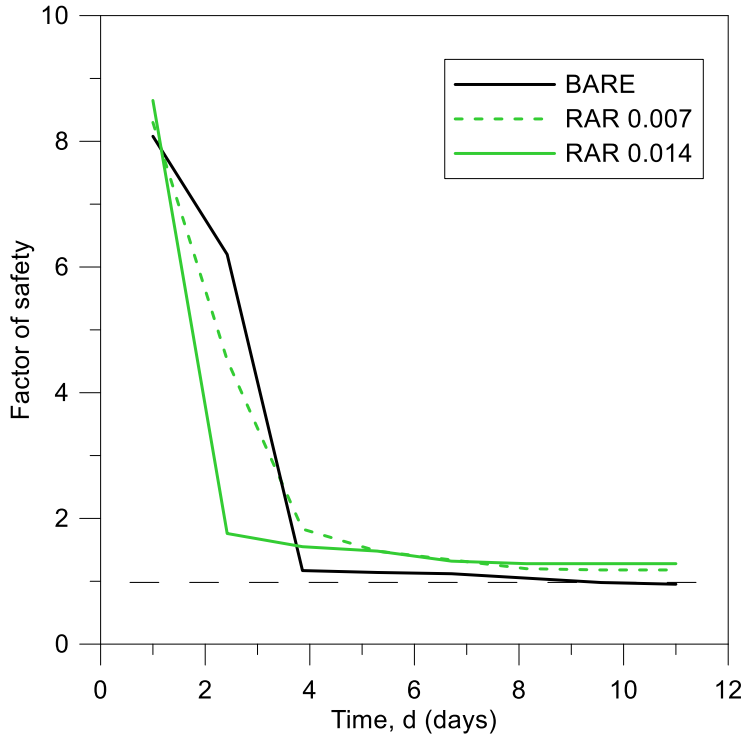

Figure 57 Evolution of the minimum safety factor for bare and vegetated slopes, during a rainfall

By comparing results of bare and root-permeated soil slope it was possible to trace the quicker drop in the value of the safety factor in the case of vegetated soil. This was due to the quicker evolution of interstitial pressure generated by the highest permeability imposed to vegetated slopes. As a result, the safety factor for the vegetated soil was, in an early stage of the rainfall event, lower than that for bare soil. Finally, vegetated slopes remained safe, with a safety factor higher than the unity even when the slopes were under hydraulic stationary conditions. The bare slope finally failed.

Roots were proved to be mechanically beneficial for a slope, but more attention has to be paid to their hydraulic negative effects on slope stability.

References

Fraccica, A., Romero, E., & Fourcaud, T. (2019). Multi-scale effects on the hydraulic behaviour of a root-permeated and compacted soil. In A. Tarantino & E. Ibraim (Eds.), *IS-Glasgow* (p. 12014). https://doi.org/doi.org/10.1051/e3sconf/20199212014

Fredlund, D. G., & Rahardjo, H. (1993). *Soil Mechanics for Unsaturated Soils*. https://doi.org/https://doi.org/10.1002/9780470172759

Fredlund, D. G., & Xing, A. (1994). Equations for the soil-water characteristic curve. *Canadian Geotechnical Journal*, *31*, 521–532. https://doi.org/http://dx.doi.org/10.1139/t94-061

6. Conclusions

During the thesis, a complete geotechnical characterization of a partially saturated compacted silty sand with roots was carried out. Moreover, some techniques coming from agronomic engineering were used to geometrically and mechanically characterize the plant roots carefully retrieved from tested soil samples. Experimental results allowed achieving an important advance in the state-of-the-art knowledge of the following aspects: a) combined effects of suction and roots on soil hydro-mechanical response, b) relationship between effects produced by roots on soil at the microscale and behaviour observed at the macroscopic level, and c) implementation of the main roots features within constitutive laws for partially saturated soils, to predict vegetated hydraulic soil response.
In the following sections, a more detailed explanation of the conclusions drawn from each specific topic dealt with in the different chapters of the thesis.

6.1 Preparation and testing protocol of samples

A protocol has been followed and systematically adopted both to generate plant growth within compacted large-size samples and to test bare and vegetated soil starting from the same initial conditions. Soil samples were always lightly compacted at the same state and maximum vertical stress (e, w, s, $\sigma_{v,max}$) to facilitate the comparison of different laboratory tests, as well as to represent the initial conditions of a large-scale on-site experiment (instrumented vegetated embankment). After compaction, plants were let grow in the soil, paying particular attention to seeding density and plant spacing: these parameters are influencing roots competition and development and are, at the same time, representative of the number of seeds used on-site for the plant cover of the above-mentioned large-scale experiment. The soil was then wetted to favour roots development, and then tested following a drying path to the target initial state. Advanced techniques were also used to characterize roots geometrical and mechanical properties, allowing to better interpret experimental geomechanics results. Comparisons and cross-validation of the obtained observations have underlined the importance of having a systematic procedure for samples preparation.

6.2 Roots effects on soil micro-structure

Two advanced and complementary techniques (mercury intrusion porosimetry and X-ray micro-tomography) were adopted to quantitatively analyse the effects produced by the growth of different

amounts of roots on the pore size distributions of the soil. Two main phenomena have been observed: clogging of small pores (pore size aprox.: 2 μm) due to root hairs and mucilage, and pore size (pore size aprox.: 200 μm) and volume enlargement (fissuring) induced by roots growth and physiology. The evolution of these phenomena was followed at different hydraulic states. It was observed that, for the same number of roots, the volume of fissures tends to increase for the drier conditions. This volume increase was formalised and linked to roots volume by implementing this plant trait in a well-established equation for partially saturated double-porosity soil.

6.3 Geotechnical characterization of a vegetated soil

A complete geotechnical characterization of the vegetated lightly compacted soil has been carried out. Different plants growing periods were considered for preparing and running experiments. Roots enhanced soil water permeability while decreased retention properties: results appeared to be linked to the number of roots found in the tested samples, but they were hardly explainable, at the phenomenological scale. However, they were consistent with the observations gathered at soil micro-scale: fissures and interfaces generated by roots contributed to enhance soil permeability and to decrease suction generated by capillary effects. More complex chemical interactions, linked to roots mucilage and reduction of water surface tension in the rhizosphere contributed to developing, in the vegetated soil, suctions smaller than those measured in the bare soil, at the same water content. Large size equipment (triaxial cells, oedometer, direct shear box, tensile test prototype) were used to study the changes in soil mechanical response generated by roots. It was observed that roots were enhancing soil yielding stress, thanks to different roots failure mechanisms: pull-out and breakage. The former more likely to happen within a moist soil, the latter within a dry soil. These different mechanisms were responsible for different soil stress-strain response, depending on soil hydraulic state. Soil structure had an influence on soil mechanical behaviour too: fissures generated by roots contributed to produce larger compression volumetric strains in soil during the shearing stage. Moreover, the partial loss of contact between soil and roots, generated by fissures, reduced the reinforcing capacity of the roots themselves (loss of the frictional component developing during roots pull-out and exploitation of the mere roots tensile strength). This last roots/suction coupled effect has influenced particularly the results of direct tensile tests, from which apparent cohesion was estimated using Mohr-Coulomb's failure criterion. Roots produced a greater beneficial effect, in terms of cohesion, when the soil was moist. After drying, roots reinforcement has been slightly counterbalanced by fissures opening.

6.4 Constitutive model to predict a vegetated soil retention curve

Information gathered at soil microscale was used to adapt a well-established model, to predict the change in fissures volume as a function of root length density and suction changes. Constitutive expressions were incorporated into a model developed in literature to predict retention curve for double-porosity soils. The resulting framework was validated with retention curves obtained in literature, for different samples and different roots quantities. Statistical analyses confirmed the good quality of the model in predicting results obtained at the macroscopic level. It is believed that the model predicting fissures may be easily extendible to other plant species since it is depending on a root trait (root length density), which is indicating the quantity of soil-roots interfaces generated. These interfaces are supposed to have a direct effect on fissure volume in soil.

6.5 Simulation of the HM response of a vegetated slope submitted to water content changes

Data coming from the hydro-mechanical characterization carried out in the thesis was used to simulate the response of bare and vegetated slopes during a wetting event. Responses of soil after different plants growing times were also simulated. In vegetated soil, especially in the one with the higher roots normalized volume, a drastic drop in the slope safety factor was observed at the first stages of the hydraulic event. In the same period, the minimum safety factor of the bare slope remained higher. At complete saturation, bare slope failed (FS<1) while vegetated soil remained safe. This response was generated by the complex hydro-mechanical behaviour that roots generated in the soil, as observed in the laboratory. The increase of permeability produced by roots, facilitated and accelerated the increase of pore water pressures within the slope and, consequently, the decrease of soil effective stresses and shear strength. Engineers and scientists must be aware of these possible responses when designing earthworks and investigating roots reinforcement.

6.6 Applications to engineering problems

In view of the potential use of plants in an engineering project and as ground improvement technique, from this thesis work, it can be deduced that:

- Although plants create a certain mechanical reinforcement on the ground, roots may cause fissures – mainly on drying – that reduce the whole reinforcement efficiency and affect the hydraulic behaviour of soil, with negative effects on the development of pore water pressures.

- it is advisable to achieve higher levels of compaction in the soil of the work, such as to increase the value of energy needed by roots to create fissures in the matrix; nevertheless, the pore size of the compacted material should be adequate for the development of roots (macro-pores within a size range of 200-300 μm) .
- It is advisable the use of plant species which develop fine and thin roots, with diameters that generally remain constant in size throughout their life and development. This aspect, coupled with a good compaction level, may induce roots to mainly "steal voids" either than creating fissures.
- The process of occupying/clogging voids by roots and their mucilage should be then "engineered" to maximize roots reinforcement potential while not degrading soil hydraulic properties too much.
- Special maintenance is recommended for works already covered by vegetation: a geometrical and mechanical characterization of the involved plant roots is fundamental to interpret the overall soil hydro-mechanical behaviour. In the case that pore water pressure and/or settlements observed in the structure are higher than expected, it is reasonable to attribute these effects to root growth and to act accordingly.

6.7 Thesis contribution

The results of the investigation will contribute to the database of partially saturated soils characterization, both for the bare and the vegetated conditions. Specifically, the results highlighted the main positive and negative aspects of the use of plants in geotechnical engineering works. The thesis will be used as a basis for future lines of research in the development of hydro-mechanical constitutive models and the modelling of compacted soils with different quantities and types of roots. Results may be useful in the assessment of slopes stability with vegetated soil subjected to ground-atmosphere interactions, in projects involving the use of materials in which root develop (road and canal embankments, flood protection embankments, ...), as well as in the choice of adequate parameters to assign to vegetated partitions in regional-scale early warning systems for landslides.
Finally, the thesis provides a systematic methodology to perform a complete hydro-mechanical geotechnical characterization of a soil with roots.

6.8 Future lines of research

Some points still missing to fully characterize roots effects on the hydro-mechanical behaviour of compacted silty soils are:

- the effects of different initial compaction maximum stress and state on roots development and consequent changes of soil response: higher or lower water content, higher or lower initial dry density.
- the effects of different hydro-mechanical paths on soil shear strength and plant physiology: drying and wetting cycles, different mechanical impedance on roots development.
- the effects of different plants on soil hydro-mechanical response: volume of fissures generated, hydraulic conductivity, shear strength response, volume change behaviour.
- assessing the anisotropy of soil hydro-mechanical response due to roots growth and structural changes generated.
- simulating the coupled hydro-mechanical behaviour of vegetated soil during laboratory/field experiments using advanced techniques (DEM/FEM analyses) and including roots stress-strain behaviour.